Drilled Shaft Socket Connections for Precast Columns in Seismic Regions

Hung Viet Tran

A thesis
submitted in partial fulfillment of the
requirements for the degree of

Master of Science in Civil Engineering

University of Washington

2012

Committee:

John F. Stanton

Marc O. Eberhard

Peter Mackenzie-Helnwein

Program Authorized to Offer Degree:
Civil and Environmental Engineering

Table of Contents

ii

List of Figures

iv

v

List of Tables

Notation

A_{tr}	=	area of shaft transverse reinforcement or spiral (in.^{2})
A_l	=	total area of longitudinal column reinforcement (in.^{2})
$A_{l,sh}$	=	total area of longitudinal shaft reinforcement (in.^{2})
c	=	depth to the neutral axis
D	=	diameter of shaft spiral (in.)
d	=	distance from the extreme compression fiber to the extreme tension longitudinal reinforcement
e	=	distance from the inner bar to the outer bar
E_s	=	modulus of elasticity of reinforcement (ksi)
f_r	=	concrete modulus of rupture (ksi)
f_s	=	tensile stress in reinforcement (ksi)
f_{yt}	=	specified minimum yield strength of shaft transverse reinforcement (ksi)
f_{ul}	=	specified minimum tensile strength of column longitudinal reinforcement (ksi), 90 ksi for A615 and 80 ksi for A706
l_{ns}	=	total noncontact lap splice length
l_s	=	Class C tension lap splice length of the column longitudinal reinforcement (in.)
L_{tr}	=	distance between the outer bars
R	=	radius of shaft spiral (in.)
s_{tr}	=	spacing of shaft transverse reinforcement (in.)
VOL_s	=	total volume of steel, including both longitudinal and transverse in the splice.
ϵ_s	=	tensile strain in reinforcement (ksi)
θ	=	inclination angle of the strut (degree or rad)
Φ	=	curvature (1/in.)

1   INTRODUCTION

1.1   The need for Rapid Construction

Bridge substructures are most commonly constructed of cast-in-place (CIP) concrete. Despite having some clear advantages (e.g., ease of transportation and to making continuous connections), CIP concrete has two main drawbacks: long on-site construction times and large labor requirements in the field, which can result in high construction costs. Using cast-in-place construction for bridge replacement is particularly disruptive when it exacerbates traffic congestion. Therefore, there is an urgent need to develop methods for accelerating bridge construction.

Using precast bridge elements is one solution for reducing on-site construction time, field labor requirements, and traffic delays. Although large substructures (and even full bridges) can be constructed off site, precast elements are usually limited to beams and columns to make fabrication and transportation easier. The quality of the individual precast elements cast in a factory often exceeds the quality of elements cast in the field. However, maintaining quality in the on-site connections between these precast elements is more difficult. Achieving good connections is particularly challenging in seismically hazardous areas, like the Pacific Northwest, in which the largest forces are developed at the beam-to-column or column-to-footing connections. Therefore, it is vital to develop economical connections that are strong enough to resist seismic excitation, and easy to construct with high quality.

1.2   Socket Connection Concept

A lot of research has been performed on precast bridge connections, but mainly for applications in which the seismic demands are low (e.g., Matsumoto et al. 2001, FHWA 2004). Less research has been performed for applications in seismically active regions. Hieber et al. (2005a) summarize the state of the art in this area in 2005. Since then, Hieber et al. (2005b) performed numerical analyses of precast piers, and Wacker et al. (2005) developed displacement and force-based design procedures.

1

In 2008, Pang et al. proposed using "Large-Bar" connections to connect beams and columns. They proposed to connect the elements with a small number of large bars that would fit into large ducts. Steuck et al. (2008, 2009) showed that bars as large as #18 could be anchored within the typical depth of a cap beam. Cohagen et al. (2008) later proposed using un-bonded post-tension strands to help re-center the column after the earthquake. In 2011, Matsumoto et al. summarized the development of a precast concrete bent-cap system for seismic regions. Haraldsson et al. (2011) developed the concept of using a socket connection to connect the base of a precast column with a cast-in-place spread footing.

This thesis adapts the column-to-foundation socket concept to connections between a precast column and cast-in-place drilled shaft, which has a lot of benefit in bridge construction in urban areas. In this connection, the bottom of the precast column is roughened, where it will be embedded in the drilled shaft.

The construction stages, shown in Figure 1-1, are as follows:

1. Drill the shaft excavation, position the reinforcing cage, and place the concrete.
2. Position and brace the precast column
3. Cast the transition
4. Position precast cross beam with ducts and grout to protruding column bars.

2

1. Dig and cast drilled shaft

2. Position and brace precast column

3. Cast transition

4. Position precast cross beam with ducts and grout to protruding column bars
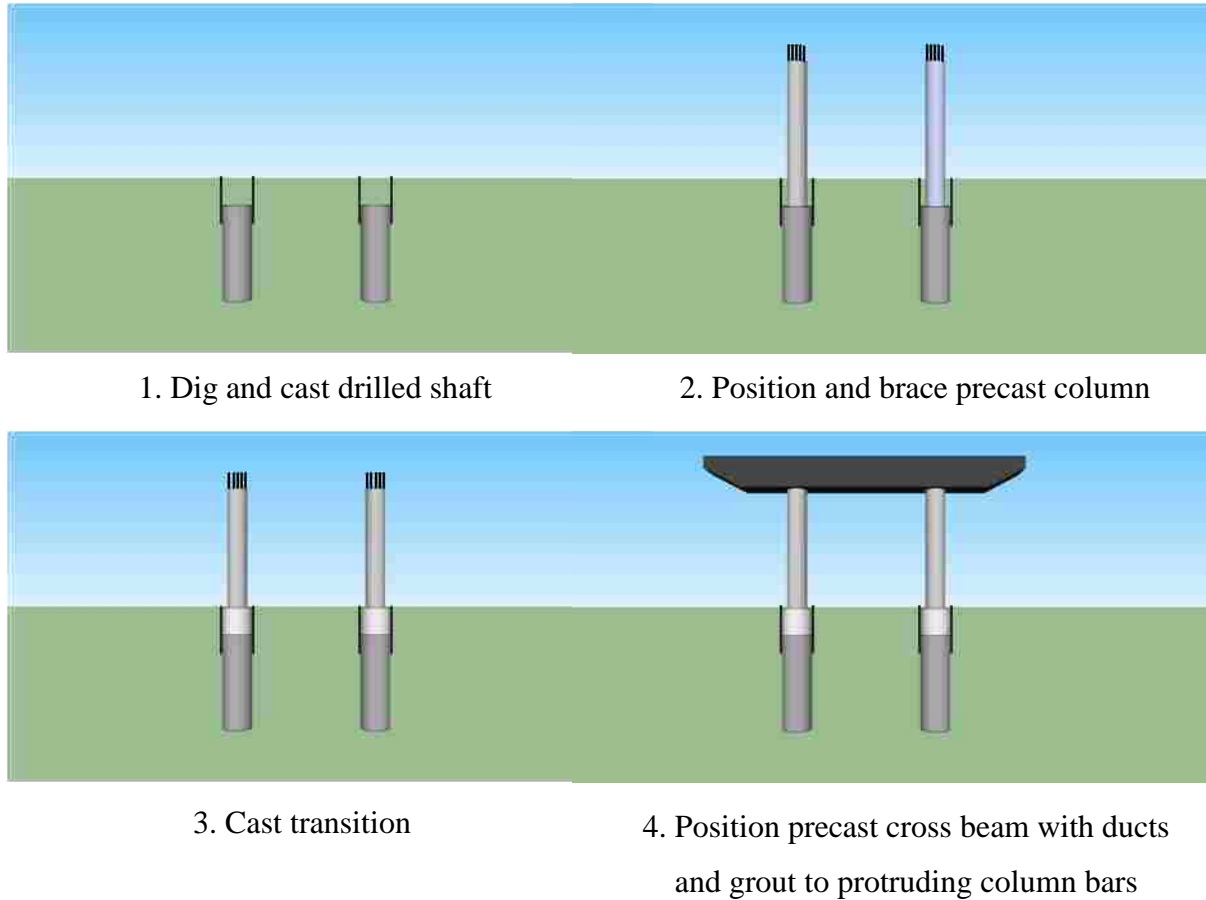
Figure 1-1. Precast bridge bent construction stages

1.3 Research Objectives and Scope

The objective of this research is to evaluate the behavior of precast column-to-drilled shaft connections. Particular emphasis is placed on inelastic behavior under cyclic excitations which may occur during a severe earthquake. Experimental and analytical studies of the behavior of the connection are described. The behavior is discussed with respect to quasi-static hysteretic behavior under cyclic loads.

The specific questions that this research is designed to answer as follow:

1. Does the column-to-drilled shaft connection behave like a non-contact lap splice as assumed in *Washington State Department of Transportation Bridge Design Manual 2012 [WSDOT BDM]*?

www.manaraa.com

2. Does the WSDOT BDM design formula for proportioning transverse reinforcement of the shaft transition result in acceptable seismic response?

3. Does the 3-wraps of spiral at the end of the shaft work like anchorage or undergo large lateral force transmitted by column?

Two scaled (1/3.6) tests were performed. One specimen was designed to satisfy the current design specifications for cast-in-place systems (*AASHTO Load Resistant Factor Design 2009 [AASHTO LRFD 2009]*, *AASHTO Guide Specification for LRFD Seismic Design 2009 [AASHTO GS 2009]*, *Washington State Department of Transportation Bridge Design Manual 2012 [WSDOT BDM 2012]*). The second specimen was designed the same as the first one, except that the spiral in the shaft was reduced by half with the intention that specimen would fail in the shaft.

Chapter 2 describes the development and design of the test specimens. Chapter 3 describes the experimental program. Damage progression is summarized in Chapter 4, and the measured responses are reported in Chapter 5. The analysis and proposed models are presented in Chapter 6, and Chapter 7 gives a summary, conclusion, and recommendation for future research.

2   DESIGN OF TEST SPECIMENS

Two drilled shaft-column connection specimens (DS-1 and DS-2) were designed, constructed and tested at the University of Washington. The design and construction of the specimens are described in this chapter.

The prototype and test specimen were designed according to the *AASHTO Load Resistant Factor Design 2009, AASHTO Guide Specifications for LRFD Seismic Design 2009, and WSDOT Bridge Design Manual (2012).* The detailed design drawings are shown in Appendix A.

2.1 Configuration of Test Specimens

The two specimens each consisted of a precast column, embedded in a cast-in-place drilled shaft, which in turn was anchored to the testing rig by a cast-in-place base. For both specimens, these three components had the following geometries:

- PRECAST COLUMN: The cantilever-precast columns had a diameter of 20 in. and a span of 60 in., resulting in a shear span-to-depth ratio of 3.
- DRILLED SHAFT: The cast-in-place drilled shaft had a diameter of 30-in. and length of 31-in., which slightly exceeded the length of the transition region (28 in.)
- BASE: The drilled shaft was embedded in a 74"×48"×24" cast-in-place base to anchor the specimen to the base of the testing rig.

The test specimen dimension and reinforcement were scaled (1/3.6) from a prototype as shown in Table 2-1. The diameter of the prototype column and shaft were chosen as 6 ft. and 9 ft. respectively to make the transition region more critical. The scale factor was chosen as 3.6 to match the 20-in diameter of column specimens tested by previous researchers (e.g., Haraldsson et al. 2011, and Janes et al. 2011).

The only difference between Specimen DS-1 and Specimen DS-2 was that the amount of spiral in the column-to-shaft transition region was reduced by half in DS-2.

Table 2-1. Prototype and Specimen Design Dimensions

	Prototype	Specimen
		(*Scale factor: 1/3.6*)
Column diameter	6 ft	20 in
Shaft diameter	9 ft	30 in
Column cover	2 in	0.6 in
Shaft cover	6 in	1.7 in

2.2 Design of Prototype and Test Columns

The test column was designed to have a reinforcement ratio of 1%, which was provided using 10#5 bars. The transverse reinforcement ratio was chosen as 0.82% to be consistent with previous tests done at the University of Washington (Pang et al. 2008, Cohagen et al. 2008, Haraldsson et al. 2011, and Janes et al. 2011). Thus, the transverse reinforcement was 3-gauge (0.244-in. diameter) spirals at a pitch of 1.25 in. All reinforcement was assumed to be ASTM A706, and the nominal concrete strength was assumed to be 6 ksi.

The flexural strength of column in specimens was found by performing moment-curvature analysis using Mphi18 program by John Stanton – University of Washington. Steel properties were modeled according to AASHTO Guide Specifications and the confined concrete properties were modeled using Kent and Park's model (Kent and Park 1971). However, the values of the confined concrete strength, the strain at peak stress and the ultimate compression strain were generated from the properties of the confinement reinforcement using Mander's formula (Mander et al. 1988; Priestley et al. 1996), rather than using the values recommended by Kent and Park. Details of moment-curvature analysis are shown in Chapter 6. The constant axial load applied in the column was 10% the axial load capacity of column ($0.1 P_o$=159 kips). Using the above moment-curvature program, the ultimate moment capacity of column cross section was $M_u = 3507$ kip-in.

The embedment part of the column (28 in.) had an octagonal shape, and was circumscribed inside the circular section of the upper part of column. The outside surface was intentionally roughened with a saw-tooth detail similar to the one required by WSDOT BDM for prestressed

girders. The dimension of the saw-tooth detail was used in the shear-friction design procedure proposed by AASHTO LRFD. All dimensions designed for the prototype were scaled down to specimen dimensions.

The ends of the longitudinal column reinforcement were terminated with rebar end anchors (Lenton Terminators), instead of using the more conventional detail of bending the longitudinal bars outwards into the foundation. This kind of anchor not only helped to reduce the development length of longitudinal reinforcement, but also made the connection betweeb precast column and cast-in-place drilled shaft more constructible.

2.3 Design of Specimen Column-to-Drilled Shaft Connection

The embedded length of the column in the drilled shaft (28 in.) was based on the scaled-down non-contact lap splice length of the shaft prototype according to WSDOT BDM 7.4.4. This length calculation was proposed by McLean et al. 1997. The embedded length equal to $l_{ns} = l_s + e$, where:

- l_{ns} =length of noncontact lap splice
- l_s = lap splice length required by AASHTO LRFD 5.11.5.3 or
- $l_s = 1.7l_d$ (for a Class C lap splice) where l_d is the development length of the larger bar
- e = distance between the shaft and column longitudinal reinforcement

The shaft longitudinal reinforcement was designed to form a plastic hinge in the column. Therefore, the yield moment of the shaft had to be larger than the moment at the base of the shaft (5319 kip-in.) due to the over-strength moment and shear from the column above. Calculation showed that using 30 bundles with 2#3 per bundle for the longitudinal shaft reinforcement in the test specimens would satisfy the requirement.

The shaft spirals were designed as non-contact lap splices according to WSDOT BDM 7.4.4 and 7.8.2. Accordingly, the spacing for spiral was given as:

$$s_{tr} = \frac{2\pi A_{sp} f_{ytr} l_s}{k A_l f_{ul}}$$

7

In addition, the spirals within non-contact lap splice zone should not be less than #6 @ 6 in. pitch in the prototype. However, the spacing should not exceed 9".

To satisfy all these requirements, #6 spirals @ 8" pitch was used in prototype which would be a bundle of 2 gauge-9 wire (0.148-in. diameter) @ 3-in. pitch. However, in DS-2 specimen, to increase the likelihood of failure in the connection, the amount of spiral was reduced by half to 1 gauge-9 wire @ 3-in. pitch.

Table 2-2. Shaft reinforcement

Item	Prototype	DS-1	DS-2
Longitudinal reinforcement	2#11/ bundle, total 30 bundles	2#3/ bundle, total 30 bundles	2#3/ bundle, total 30 bundles
Spiral	#6 @ 8 in. pitch	2 gauge-9 wire @ 3 in. pitch	1 gauge-9 wire @ 3 in. pitch

WSDOT BDM 7.4.5 requires three turns of wire at the end to terminate the spiral. This is an anchorage requirement. However, in case of column-shaft connection, it was believed that the extra turns also provided extra strength at the top of the transition region.

The bottom of the shaft connected with a 74"×48"×24" cast-in-place footing to attach the specimen to the testing rig. The longitudinal bars of the drilled shaft were hooked at the bottom mat of footing as shown in Figure 2-1.

8

a). Column reinforcement

b).Shaft-Footing reinforcement

Figure 2-1 (a).Column reinforcement – (b).Shaft-Footing reinforcement

a). Precast Column

b). Column-Shaft connection

Figure 2-2. Specimen

9

3   EXPERIMENTAL PROGRAM

Quasi-static, cyclic tests were performed to evaluate the seismic performance of two column-to-drilled-shaft connections (DS-1 and DS-2). In such testing, deformations are applied at a rate much lower than would be applied during an earthquake,

This chapter describes the test setup, displacement history, instrumentation and data acquisition. The two drilled-shaft tests were part of a larger research program whose aim was to develop a family of connections for rapid construction of bridges. Therefore, the experimental program for these tests was similar the one conducted by Haraldsson et al. (2011) and Janes et al. (2011) on spread footings.

3.1   Test Setup

The two specimens were tested by using the self-reacting rig shown in Figure 3-1. The rig included a base, two vertical columns, a horizontal beam, two diagonal braces and a servo-controlled actuator.

- The base consisted of two blocks of concrete, attached to two W24x94 beams, one on each side of the blocks. These components were post-tensioned together by four, threaded Williams bars placed in plastic tubes through the blocks and beams.

- Two vertical W24x94 columns were welded at the end of the two base beams.

- A horizontal W14x14 beam was bolted to the two vertical columns at the same level as the lateral load.

- The two vertical beams of the frame were stiffened on each side with a diagonal HSS 6x6x3/8.

-The lateral loads were applied to the column with a servo-controlled actuator with a capacity of 220 kips. One end of the actuator was attached to the column, and the other end was connected to the horizontal beam.

The specimens were positioned in the rig, leveled with shims, and then attached to the base with Hydro-stone. To prevent the specimen from overturning under cyclic excitations, four threaded 1.25-in. diameter Williams bars were placed in plastic tubes through the footing of specimens and threaded into nut cast into the concrete block of the rig's base. The top nuts on these bolts were tightened to 125 kips to hold the footing of the specimens down to the base.

The column axial load was provided by the 2.4-million lbs. Baldwin Universal Testing Machine. The force was transferred to the column through a spherical bearing. The top of the bearing slid in a channel attached to the Baldwin. To minimize friction, the spherical surface of the bearing was greased, a stainless steel plate was placed in the channel, and a greased sheet of polytetraflouroethylene (PTFE) was glued to the top and the sides of the bearing.
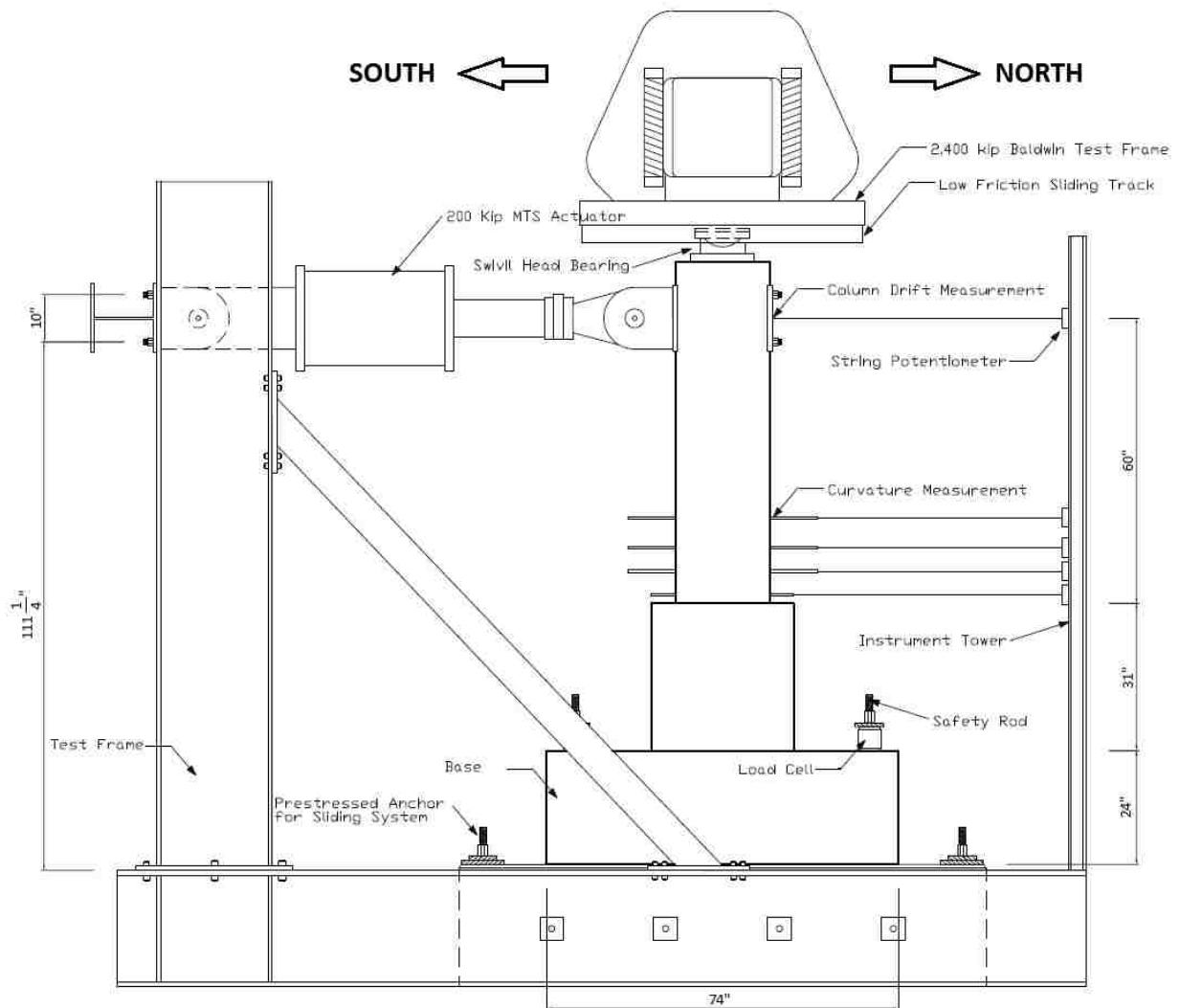
Figure 3-1. Test setup

11

3.2 Instrumentation

The axial load applied in the top of column was monitored by load cells in the Baldwin Testing Machine. The lateral load was monitored by load cells in the MTS actuator. The response of the specimen was monitored by potentiometers, linear variable differential transformers (LVDTs), a research-grade motion capture system (Optotrak Certus brand), and strain gauges.

The horizontal displacement of the column at the elevation of the lateral load (60 in. above the column-shaft interface) was monitored in two ways. On the north side, the displacement of the column was monitored with a string potentiometer attached to a steel reference column, which was unloaded, as shown in Figure 3-2. In addition, the actuator displacement was monitored using the LVDT built into the actuator, and the displacement of the loading frame with respect to another unloaded frame was monitored by another LVDT (on the South side). Thus, a second measure of the absolute displacement of the column was calculated as the sum of displacement of the actuator (MTS LVTD in Figure 3-2) and the deformation of test rig. These two ways of measuring the top displacement yielded nearly identical results, as shown in Figure 3-3.

The horizontal displacements of column and transition region were monitored by string potentiometers. Four string potentiometers were connected to the end of the four north curvature rods to measure the displacement of column at these positions. The relative displacements between the footing of specimens and concrete blocks, and between the concrete blocks and ground were captured by potentiometers (Duncan brand). Four potentiometers (numbers 18, 19, 20, 21) were used to capture uplift and slip relative displacement between footing and concrete block in North and South side. Another four potentiometers (numbers 22, 23, 24, 25) were used to captured uplift and slip relative displacement between concrete block and ground in North and South side. The positions of these potentiometers are shown in Figure 3-2.

To determine relative rotations of column for four segments at the base of the column, eight potentiometers (numbers 1→8) were set up in the north and south sides to measure the relative displacement of threaded rods (called curvature rods). The relative rotation calculation is provided in the next chapter. The rods were located 2 in., 7 in., 12 in., and 18 in. above the

12

interface. Detailed installation is illustrated in Figure 3-2. To determine absolute rotations of column, four inclinometers (number 14→17) were attached on the East side of column at 10 in, 18 in., 30 in. and 40 in. above the interface.
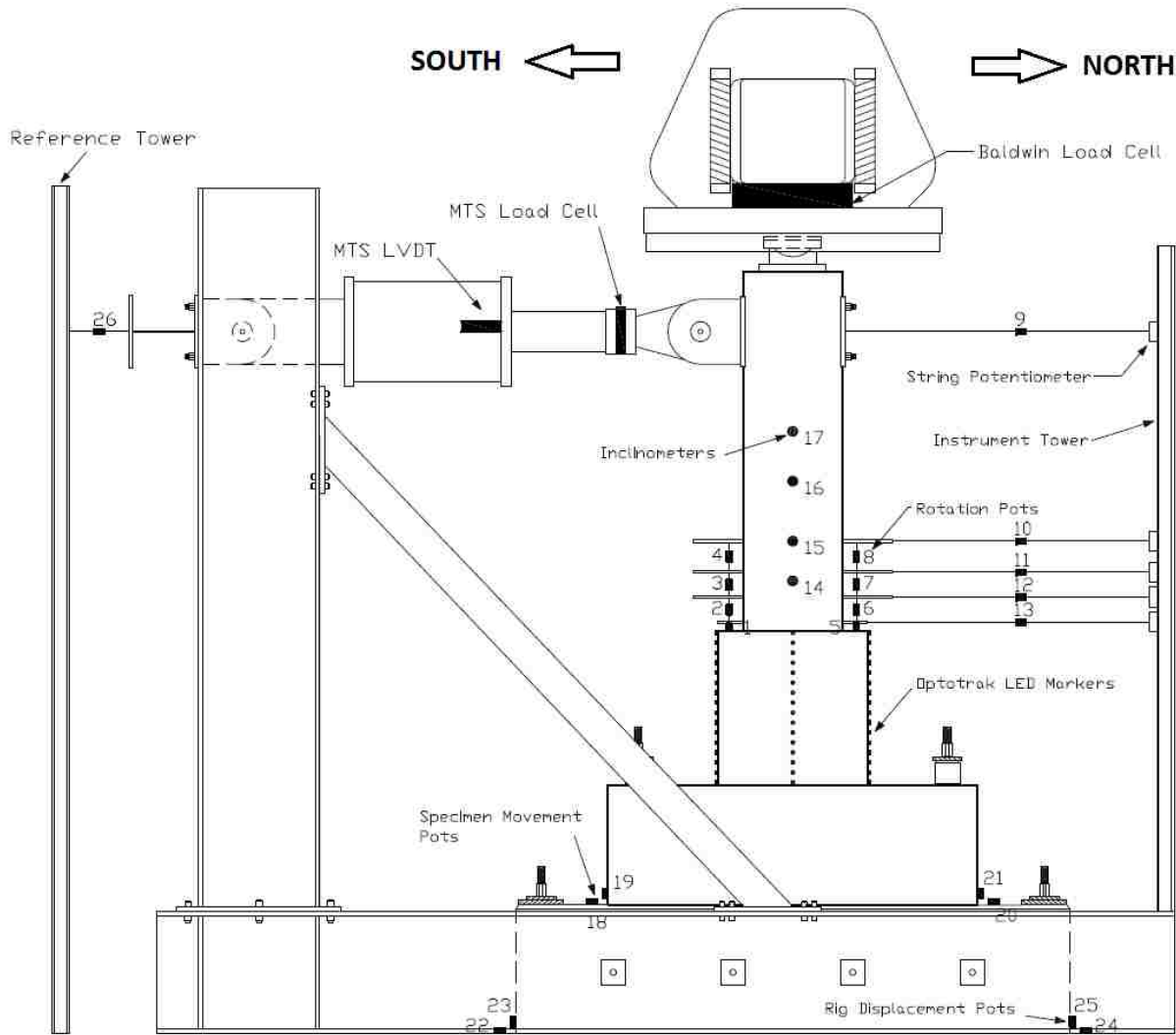
Figure 3-2. Locations of external instruments

Strain gauges were attached to some key shaft and column longitudinal reinforcing bars, and in shaft spirals in the transition area of column and shaft as shown in Figure 3-4. The gages on the longitudinal bars and spiral were installed at three levels: top, middle, and bottom of the transition to capture strain data, which help to understand the mechanism, force distribution, and behavior of the connection. All strain gauges were supplied by Texas Instruments, type FLA-6-

13

11-5LT. This kind of strain gauges was used to reduce the effect of temperature variations on the recorded data.
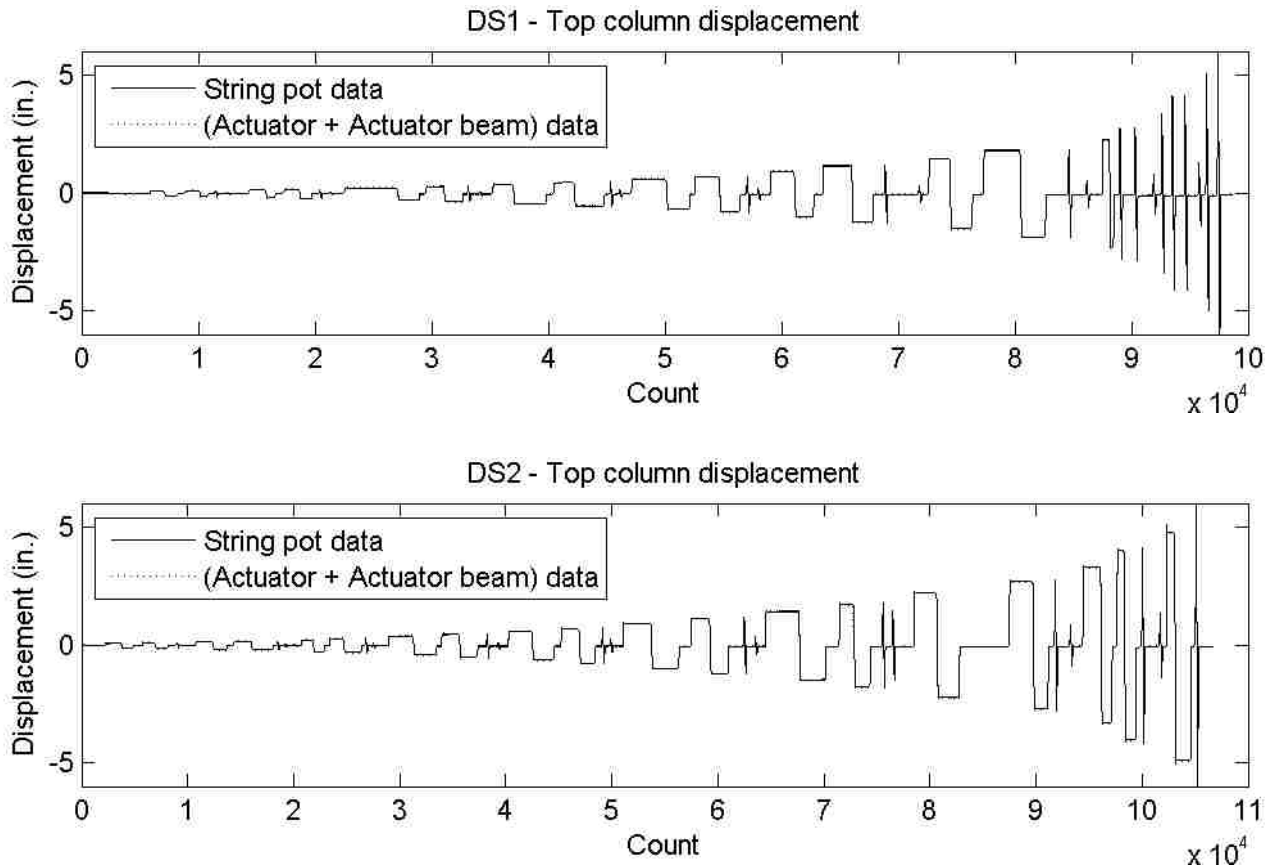
Figure 3-3. Top column displacement comparison for (a) DS1 and (b) DS2

Markers of the research-grade motion capture system were attached to the column and shaft surface in the north, west and south sides to measure displacement (see Figure 3-2). Another four markers were attached close to the north curvature rods' positions to compare the data of string pots and the motion capture system. In Specimen DS-2, more markers were set up in the column to determine the rotation of column to compare with inclinometers' data. As shown in Chapter 5, the research-grade motion capture system and the potentiometers provided consistent results.

Data was recorded with a sampling rate 4Hz using LabVIEW (Laboratory Virtual Instrument Engineering Workbench) from National Instruments.

14
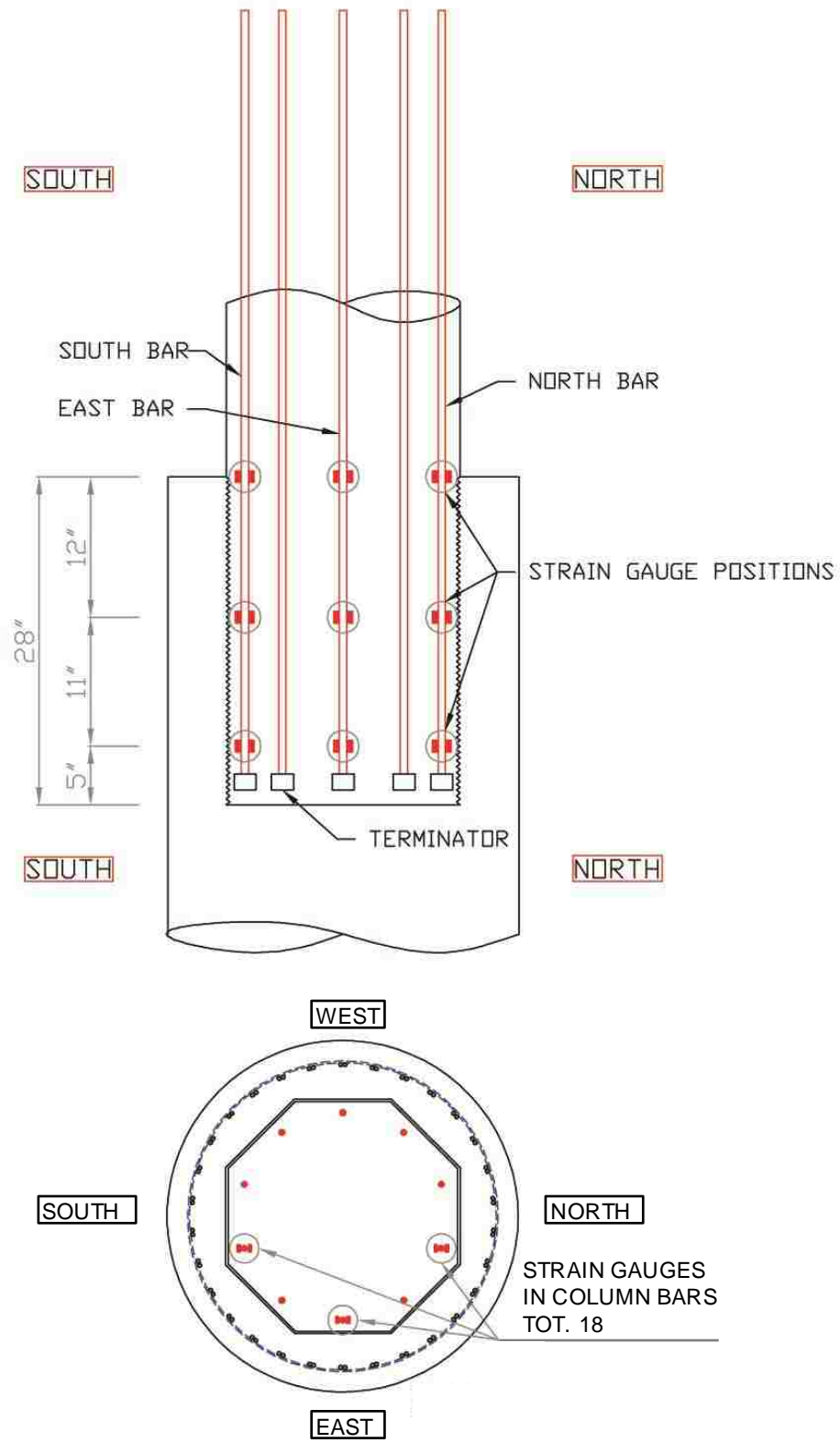
(a) Location of gauges in the column

15
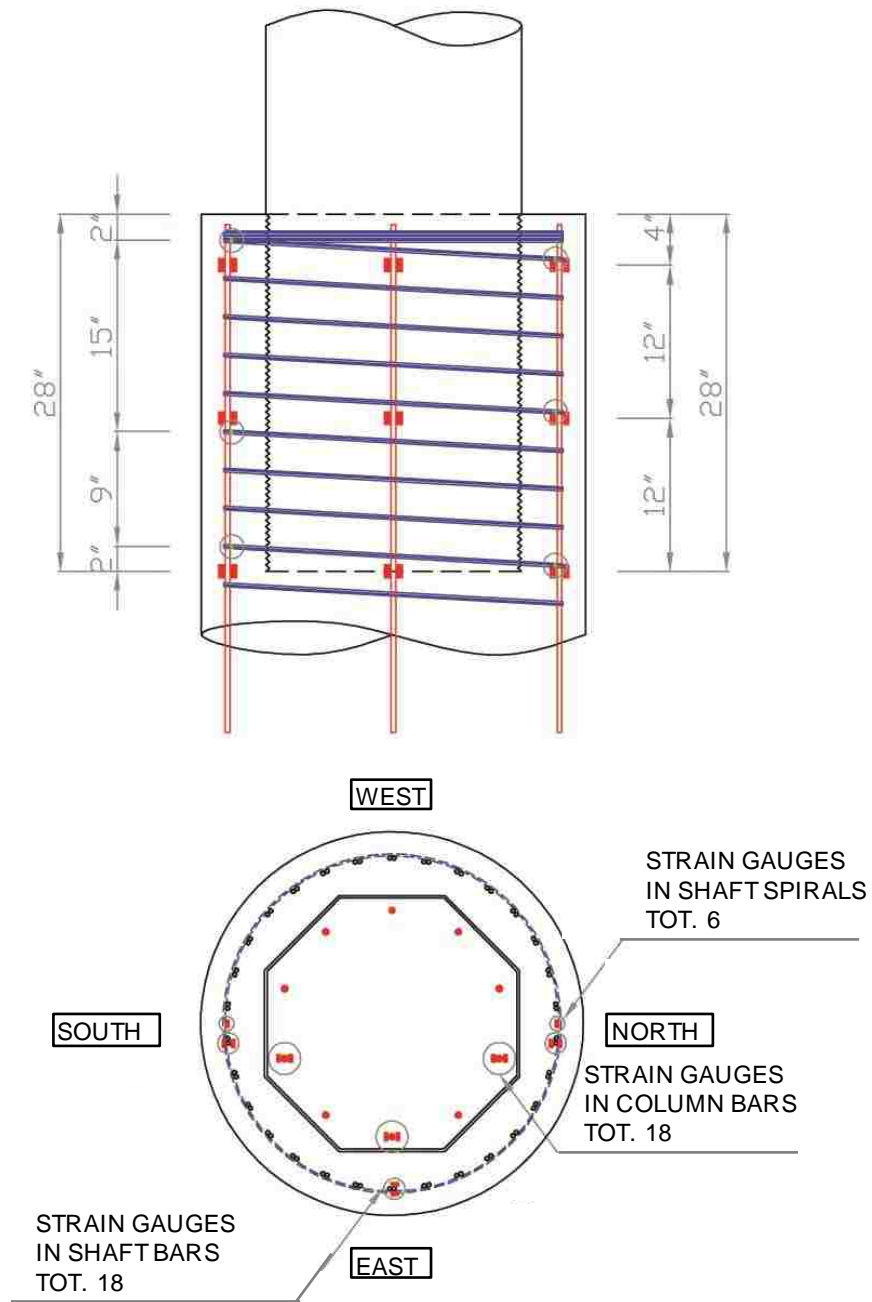
(b) Location of gauges in the shaft

Figure 3-4. Locations of strain gauges

3.3   Displacement History

First, the axial load applied in the column was increased to an unfactored dead load value of 159 kips. This axial load was kept constant until the end of testing. Later, the specimen was

subjected to displacement controlled cyclic excitation. The displacement history was the same as in previous test in the Rapid Construction project at the University of Washington (Pang et al. 2008, Cohagen et al. 2008, Haraldsson et al. 2011, Janes et al. 2011). This displacement history was a modification of a loading history for precast structural walls recommended in NEHRP (Building Seismic Safety Council).

The displacement history included of sets of 4 cycles. The peak amplitudes of the cycle in a set were 1.2A, 1.4A, 1.4A, and 0.33A respectively, where A is the maximum peak amplitude in the previous set. The small amplitude cycle was intended to evaluate the residual small-displacement stiffness in the specimen after the maximum peak amplitude cycle of each set. In all cycles, the actuator moved from zero displacement to the peak cycle displacement in 20 seconds. As in Haraldson's (2010) and Janes' (2011) report, the positive and negative peak displacement were called "peak" and "valley". After peak loading was to the south reinforcing bars of column in specimen DS-1 broke and spirals of the shaft in specimen DS-2 broke, the testing stopped. The target displacement history is provided in Figure 3-5 and Table 3-1.
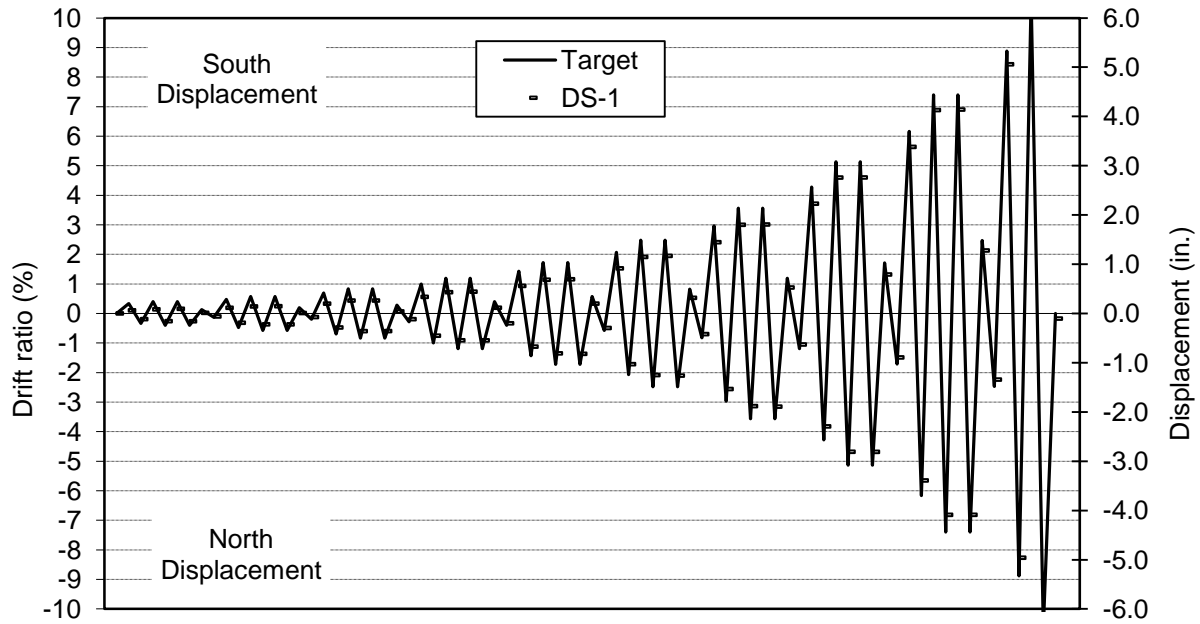
a) Specimen DS-1
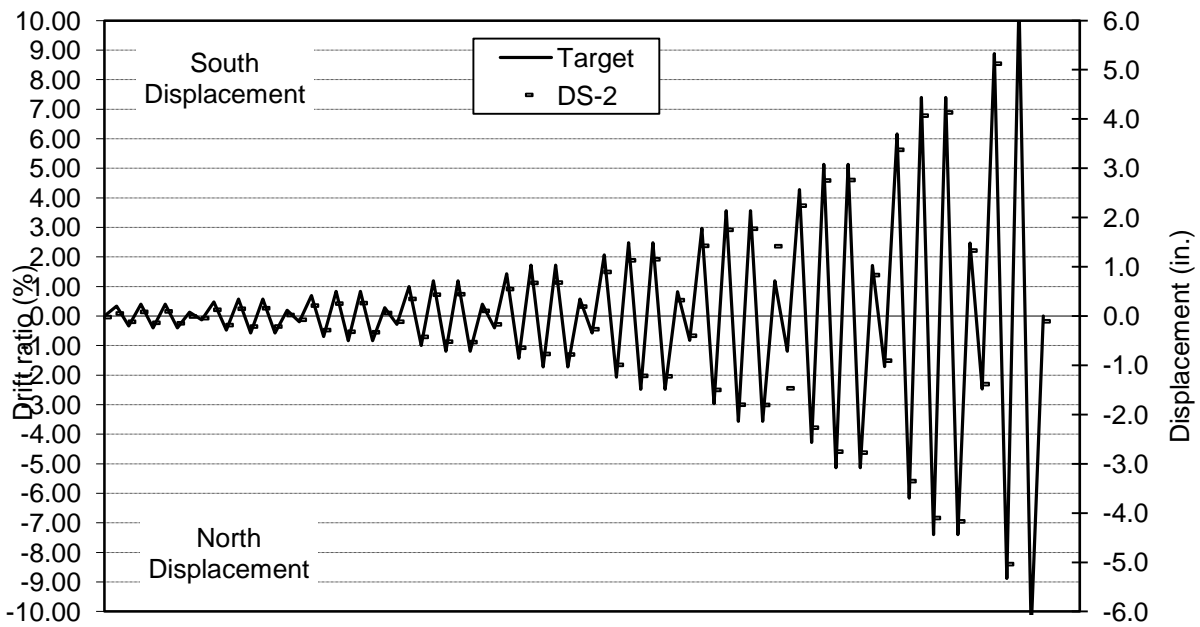
b) Specimen DS-2

Figure 3-5. Lateral loading displacement history

18

Table 3-1. Target displacement history

Set	Cycle	Drift Ratio (%)	Displ. (in.)		DS-1 Displ. (in.)	DS-2 Displ. (in.)
1	1	±0.33	±0.20	P	0.06	0.05
				V	-0.12	-0.12
	2	±0.40	±0.24	P	0.08	0.09
				V	-0.16	-0.14
	3	±0.40	±0.24	P	0.09	0.10
				V	-0.16	-0.15
	4	±0.13	±0.08	P	0.01	-0.01
				V	-0.06	-0.04
2	1	±0.48	±0.29	P	0.11	0.13
				V	-0.19	-0.18
	2	±0.58	±0.35	P	0.14	0.15
				V	-0.22	-0.21
	3	±0.58	±0.35	P	0.15	0.16
				V	-0.22	-0.21
	4	±0.19	±0.12	P	0.01	0.02
				V	-0.07	-0.07
3	1	±0.69	±0.41	P	0.20	0.21
				V	-0.29	-0.28
	2	±0.83	±0.50	P	0.26	0.25
				V	-0.36	-0.32
	3	±0.83	±0.50	P	0.26	0.26
				V	-0.36	-0.33
	4	±0.28	±0.17	P	0.04	0.06
				V	-0.12	-0.11
4	1	±1.00	±0.60	P	0.34	0.35
				V	-0.45	-0.42
	2	±1.19	±0.72	P	0.43	0.43
				V	-0.55	-0.52
	3	±1.19	±0.72	P	0.44	0.44
				V	-0.55	-0.53
	4	±0.40	±0.24	P	0.12	0.11
				V	-0.20	-0.17
5	1	±1.43	±0.86	P	0.56	0.55
				V	-0.67	-0.64
	2	±1.72	±1.03	P	0.68	0.67
				V	-0.81	-0.77
	3	±1.72	±1.03	P	0.69	0.68
				V	-0.82	-0.78
	4	±0.57	±0.34	P	0.20	0.19
				V	-0.30	-0.27

Set	Cycle	Drift Ratio (%)	Displ. (in.)		DS-1 Displ. (in.)	DS-2 Displ. (in.)
6	1	±2.06	±1.24	P	0.91	0.90
				V	-1.03	-0.99
	2	±2.48	±1.49	P	1.15	1.13
				V	-1.25	-1.21
	3	±2.48	±1.49	P	1.17	1.15
				V	-1.26	-1.22
	4	±0.83	±0.50	P	0.32	0.32
				V	-0.42	-0.40
7	1	±2.97	±1.78	P	1.45	1.43
				V	-1.53	-1.50
	2	±3.57	±2.14	P	1.80	1.75
				V	-1.88	-1.80
	3	±3.57	±2.14	P	1.81	1.77
				V	-1.89	-1.80
	4	±1.19	±0.71	P	0.53	1.42
				V	-0.63	-1.47
8	1	±4.28	±2.57	P	2.23	2.24
				V	-2.29	-2.27
	2	±5.14	±3.08	P	2.76	2.75
				V	-2.81	-2.75
	3	±5.14	±3.08	P	2.76	2.76
				V	-2.81	-2.77
	4	±1.71	±1.03	P	0.79	0.83
				V	-0.89	-0.90
9	1	±6.16	±3.70	P	3.38	3.38
				V	-3.39	-3.35
	2	±7.40	±4.44	P	4.13	4.07
				V	-4.09	-4.10
	3	±7.40	±4.44	P	4.14	4.13
				V	-4.09	-4.17
	4	±2.47	±1.48	P	1.28	1.33
				V	-1.34	-1.38
10	1	±8.87	±5.32	P	5.06	5.12
				V	-4.96	-5.04
	2	±10.65	±6.39	P	6.30	6.20
				V	-6.01	-6.03
	3	±10.65	±6.39	P		
				V		
	4	±3.55	±2.13	P		
				V		

4 DAMAGE PROGRESSION

This chapter defines the damage states and describes the damage progression. The progression of damage throughout the test was recorded with detailed sketches, measurements of crack propagation, crack widths, and photos (see Appendix C).

4.1 Definitions of Damage States

The performance of each specimen was related to key damage states, as defined in the UW/PEER Structural Performance Database (Berry et al. 2003) and defined in Table 4-1. These states provided a convenient basis for comparing the progression of damage in the specimens.

Table 4-1. List of Damage States

Damage Event	Description
First significant horizontal crack	Crack width $\geq$ 0.5 mm
First significant diagonal crack	Diagonal crack extends 1/4 of column diameter. Crack width $\geq$ 0.5mm
First open residual crack	Residual crack width $\geq$ 0.25 mm
First yield of longitudinal reinforcement	First strain gauge that reaches yield strain (0.00212)
First yield of transverse reinforcement	First strain gauge that reaches yield strain (0.00212)
First spalling in footing	Observed spalling on surface
First spalling in column	Observed flaking, minor spalling
Significant spalling in column	Spalled height $\geq$ 1/4 of column diameter
Fully spalled	Spalling height no longer increases with increasing deformation
Exposure of longitudinal reinforcement	First observation of column longitudinal reinforcement.

Buckling of longitudinal reinforcement	First observation of column longitudinal bar buckling.
Large cracks in concrete core	Crack width $\geq$ 2.0 mm
Fracture of transverse reinforcement	Observation or sound
Fracture of longitudinal reinforcement	Observation or sound
Loss of axial capacity	Instability of member

4.2 Damage Progression

On the day before testing, pre-test cycles were performed to verify that the instruments were working correctly. The columns were loaded axially up to 90 kips and were cycled at +/- 0.035% lateral drift. No cracks were detected.

On the day of testing, each column was loaded vertically to 159 kips, which corresponded to the scaled-down, unfactored dead load on the bridge column. That vertical load was kept constant throughout the test.

The lateral excitation history consisted of sets of four cycles and was controlled in terms of lateral displacement. The amplitudes of the cycles were described in Chapter 3. The positive loading direction (with a maximum at "peak") was defined by the actuator being in tension and displacements to the south. Each new set of cycles started in the positive direction. In the negative direction, the extreme displacement is referred to as the "valley".

The continuity of the loading differed among the cycles of each set. In the first two cycles of each set, cycling was interrupted at extreme displacements ("peak" and "valley") to allow inspection of cracks. At zero displacement, between cycles, the biggest residual crack width was measured. In the second two cycles, the loading was continuous with no interruptions and no cracks were inspected or marked.

Both Specimen DS-1 and DS-2 tests were subjected to a total of 38 cycles (up to cycle 10-2). The results are shown in Figure 4-1 and Table 4-2, where they are compared with the results of spread footing specimens SF-1 and SF-2 of Haraldsson et al. (2011), and SF-3 of Janes et al.

21

(2011). It should be noted that, for many damage states, close correlation between the drilled shaft and spread footing specimens should not be expected because the two systems behaved rather differently. For example, in the drilled shafts, the drift ratio was computed by dividing the total displacement at the load point by the height (60 in.) of the column alone, regardless of any lateral deformation over the height of the shaft. The same definition of drift ratio was used in the spread footing connections, but in them, there was no lateral deformation of the footing.

The details of the damage progression for specimens DS-1 and DS-2 are also shown in Figure 4-1. In the initial cycles, up to about 0.7% drift ratio, the cracks in both specimens were fine and closed almost completely at zero displacement between cycles. At about 0.7% drift ratio, the longitudinal steel in the column yielded and the first significant horizontal cracks appeared. Those cracks did not close completely when the load dropped to zero.

After the longitudinal column reinforcement yielded, the behaviors of specimens DS-1 and DS-2 differed significantly. In DS-1, the damage was concentrated in the column, and the specimen eventually failed by fracture of the longitudinal steel in the plastic hinge region of the column, in what might be thought of as a typical column failure. The longitudinal bars buckled, causing a kink in the spiral steel, which initiated its fracture. After the spiral fractured, the longitudinal bars straightened and re-buckled with each load cycle and eventually fractured due to the low-cycle fatigue caused by the alternate bending and straightening. The longitudinal steel in the shaft never yielded, and the transverse steel in the shaft yielded but never fractured. This behavior, characterized by concentration of damage in the column, was similar to that of specimens SF-1 and SF-2.

In Specimen DS-2, the amount of spiral steel in the shaft was only half that in Specimen DS-1. It is therefore not surprising that, in it, the transverse reinforcement in the shaft yielded earlier than in DS-2, and subsequently fractured. The behavior of the specimen was characterized by very large cracks opening in the shaft, which suffered extensive shear deformations as a result. Failure was initiated by fracture of the spiral steel in the shaft, starting at the top and progressing downwards. The damage to the shaft caused the load to drop even though the drift was increasing. The longitudinal bars in the column did not buckle, and by observation, it was known that the spirals in the column never fractured.

22

Table 4-4-2. Damage Milestone for all five specimens

Damage Event	Specimen DS-1						Specimen DS-2						Specimen SF-1			Specimen SF-2			Specimen SF-3		
	Shaft			Column			Shaft			Column											
	Set	Cycle	Drift (%)	Set	Cycle	Drift (%)	Set	Cycle	Drift (%)	Set	Cycle	Drift (%)	Set	Cycle	Drift (%)	Set	Cycle	Drift (%)	Set	Cycle	Drift (%)
First significant horizontal crack	4	2	0.72	4	1	0.56	4	2	0.72	4	2	0.72	4	1	0.69	3	2	0.56	3	1	0.49
First significant diagonal crack	6	1	1.52/ -1.72	5	2	1.13/ -1.35	6	1	1.49/ -1.65	6	1	1.49/ -1.65	6	1	1.68/ -1.80	6	1	1.74	6	1	1.71
First open residual crack	5	3	1.16/ -1.37	5	2	1.13/ -1.35	6	2	1.89/ -2.02	6	2	1.89/ -2.02	6	1	1.68/ -1.80	4	3	0.88/ -0.95	5	1	1.13/ -1.23
First yield of longitudinal reinforcement	N/A	N/A	N/A	4	2	0.72	N/A	N/A	N/A	4	1	0.58	3	1	-0.55	3	2	0.47	3	1	-0.51
First yield of transverse reinforcement	8	1	3.71/ -3.82	N/A	N/A	N/A	6	3	1.92/ -2.03	N/A	N/A	N/A	9	1	0.33	9	2	-5.41	8	2	-4.77
First spalling in footing	6	1	1.52/ -1.72	N/A	N/A	N/A	7	1	2.38/ -2.50	N/A	N/A	N/A	N/A	N/A	N/A	N/A	N/A	N/A	9	2	7.11/ -6.92
First spalling in column	N/A	N/A	N/A	5	2	1.13/ -1.35	N/A	N/A	N/A	N/A	N/A	N/A	5	1	1.07/ -1.21	5	1	1.10/ -1.19	5	3	1.41/ -1.49

Significant spalling in column	N/A	N/A	N/A	7	2	3.00/ -3.14	N/A	N/A	N/A	N/A	N/A	N/A	6	2	-2.25	7	1	2.64	6	2	2.13/ -2.21
Full spalling in column	N/A	N/A	N/A	9	2	6.88/ -6.82	N/A	N/A	N/A	N/A	N/A	N/A	9	3	7.08/ -6.90	8	1	3.98	9	1	5.84/ -5.76
Exposure of longitudinal reinforcement	N/A	N/A	N/A	9	3	6.90/ -6.81	9	3	6.89/ -6.95	N/A	N/A	N/A	9	1	-5.68	9	2	-6.85	9	3	7.15/ -6.93
Buckling of longitudinal reinforcement	N/A	N/A	N/A	9	3	6.90/ -6.81	N/A	N/A	N/A	N/A	N/A	N/A	9	2	7.09/ -6.88	9	3	7.19/ -6.88	9	3	7.15/ -6.93
Large cracks in concrete core	N/A	N/A	N/A	7	2	3.00/ -3.14	7	1	2.38/ -2.50	6	1	1.49/ -1.65	10	2	10.61	10	2	-9.95	10	2	10.58/ -9.97
Fracture of transverse reinforcement	N/A	N/A	N/A	10	1	8.43	8	2	4.59	N/A	N/A	N/A	9	2	-6.88	10	1	-8.29	10	1	8.72
Fracture of longitudinal reinforcement	N/A	N/A	N/A	10	2	10.49	N/A	N/A	N/A	N/A	N/A	N/A	10	2	10.61	10	2	10.65	N/A	N/A	N/A
Loss of axial capacity	N/A	N/A	N/A	N/A	N/A	N/A	N/A	N/A	N/A	N/A	N/A	N/A	N/A	N/A	N/A	N/A	N/A	N/A	10	3	10.7

24

In the drilled shaft specimens, shear sliding between the precast column and cast-in-place shaft was an important behavioral mechanism. No instrumental measurements could be made, so visual observations provided the only available evidence, and they could be made primarily after the test was complete. Figure 4-3 shows Specimen DS-1 after the test. The damage to the shaft exists mainly in the small region of top cover concrete above the ends of the vertical bars. In the remainder of the shaft, the column is still held firmly by friction. Figure 4-4 shows Specimen DS-2 after testing. There, the shaft has been pried open by the lateral movements of the column so the column could be lifted freely out of the shaft with no frictional resistance. The prying action on the shaft yielded the transverse steel in it and led to the large deformations.
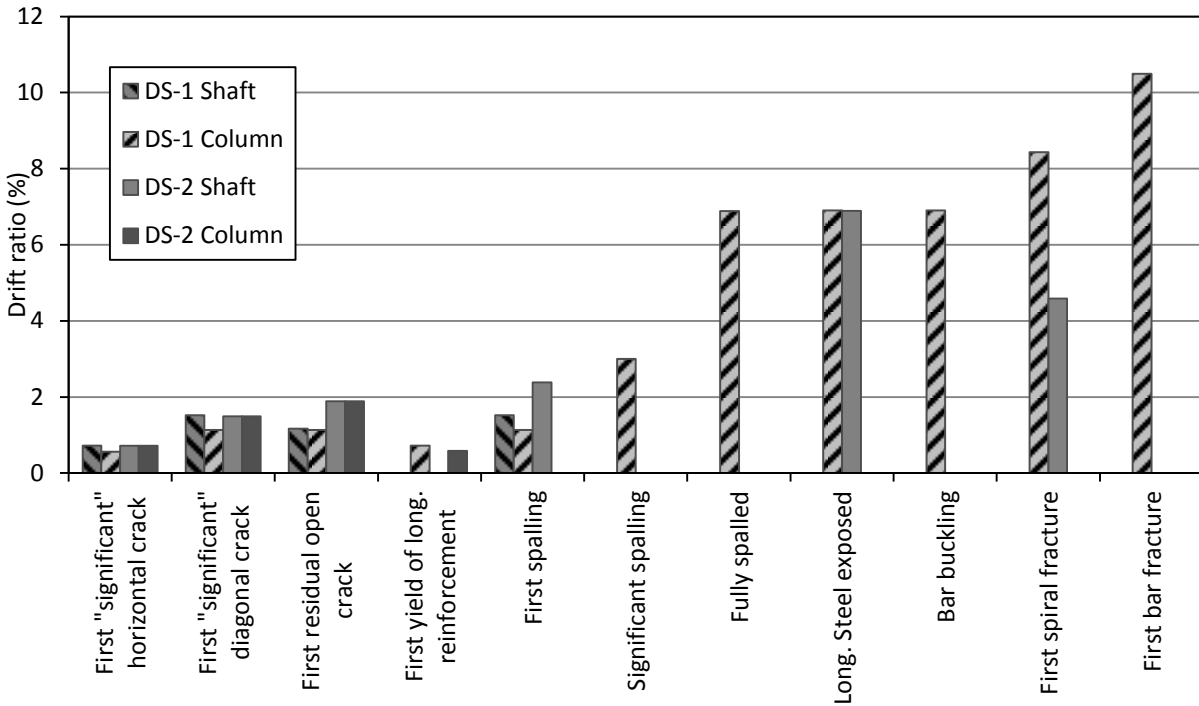
Figure 4-1. Comparison of specimens' drift ratios for the major damage states
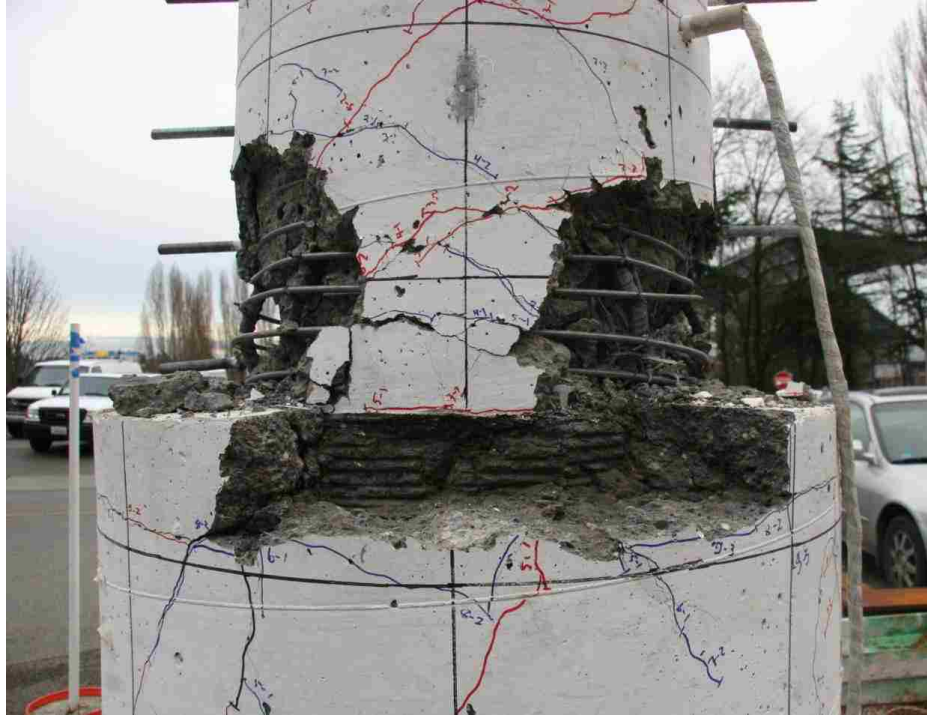
Figure 4-2. Specimen DS-1 after testing

Figure 4-3. Specimen DS-2 after testing

26

5   MEASURED RESPONSE

This chapter reports the response of the specimens DS-1 and DS-2 measured by the instruments.

5.1   Moment-Drift Response

The moment-drift response is similar to the load-displacement response, but it differs slightly, because the moment includes components from both the vertical and lateral loads, whereas the load-displacement response includes only the horizontal load.

The moment at the base of column is given by:

$$M_c = h_1.V - F_{fric}.h_2 + (\Delta_2 - \Delta_3).P \tag{5-1}$$

where:

M_c = the column moment at the base.

h_1 = height from the column-shaft interface to the line of action of the lateral load.

h_2 = is the height from the interface to the top of column where the axial load, P, is applied by the Baldwin Universal Testing Machine.

V = applied lateral load.

F_{fric} = the friction force between the bearing and the sliding channel, and the greased steel-to-steel spherical element on bearing.

Δ_1 = the lateral displacement at the location of the lateral load.

Δ_2 = the lateral displacement at the top of column.

Δ_3 = the lateral displacement at the top of transition, was taken approximately as lateral displacement at the first curvature rod (2 inches above the top of transition).

These parameters are illustrated in Figure 5-1.

27

In the absence of a measured value for Δ_2, it was approximated by assuming the column rotated as a rigid body about its base, in which case:

$$(\Delta_2 - \Delta_3) \approx (\Delta_1 - \Delta_3).\frac{h_2}{h_1}$$
(5-2)

and

$$M_c = h_1.V - F_{fric}.h_2 + (\Delta_1 - \Delta_3).\frac{h_2}{h_1}.P$$
(5-3)

It should be noted that the vertical load, P, contributed about one third of the total moment at the maximum drift, and less than that at smaller drifts. Thus, any relative error in the approximation of Δ_2 creates a smaller relative error in the moment calculation.
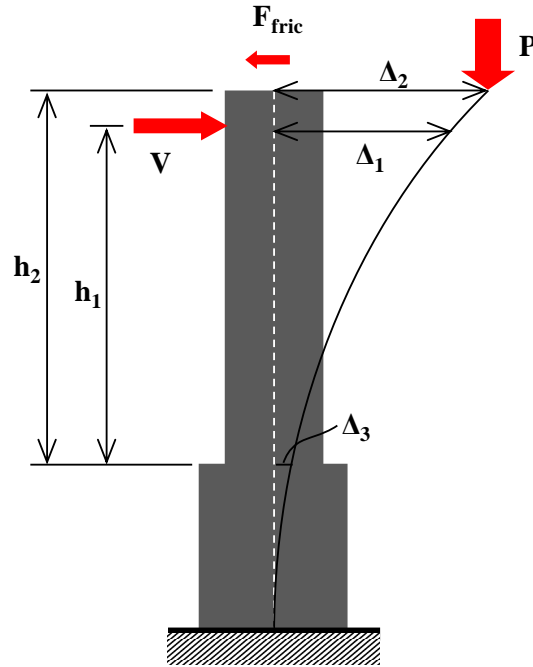

Figure 5-1. Displacements and Forces on test specimen

Figure 5-2 shows the moment vs. drift ratio response of the test specimens DS-1 and DS-2. Because the columns used in these DS specimens were nominally identical to those used in spread footings SF-1 and SF-2 by Haraldsson et al. (2011) and SF-3 by Janes et al. (2011), results from those tests are shown for comparison. The measured response of specimen DS-1 was similar to those of specimens SF-1, and SF-2. In all three cases, failure occurred by plastic hinging in the column while the connection region in the foundation remained largely undamaged. However, in
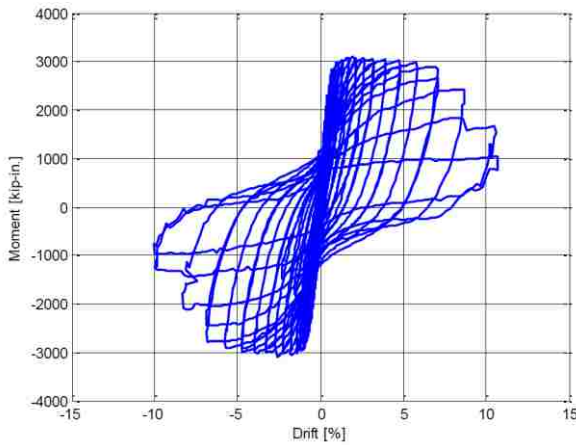
specimens DS-2 and SF-3, failure occurred in the connection region after some damage had first occurred in the column. This difference is apparent in the figures for those specimens, in which the strength decays with increasing drift more rapidly than is the case in SF-1, SF-2 and DS-1.
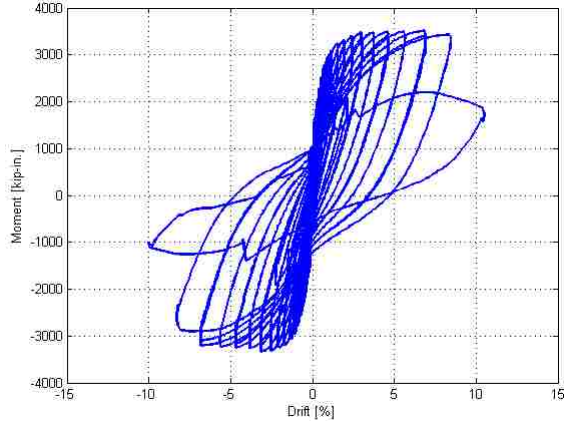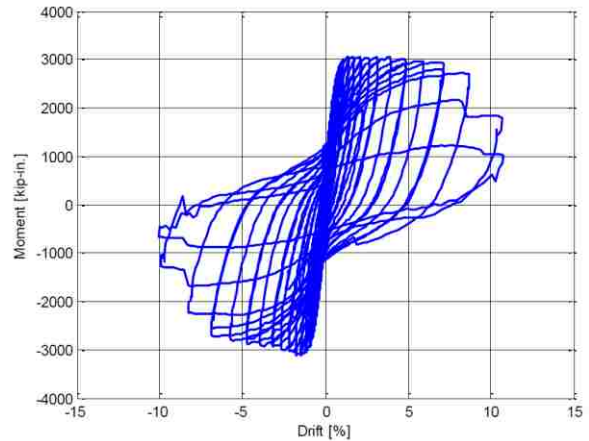

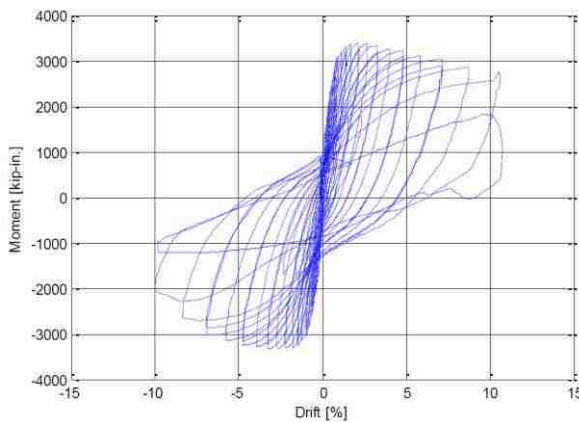a). Specimen DS-1 moment-drift response
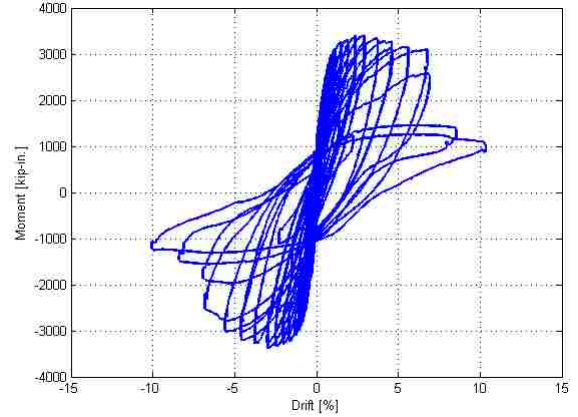
b). Specimen DS-2 moment-drift response

c). Specimen SF-1 moment-drift response

d). Specimen SF-2 moment-drift response

e). Specimen SF-3 moment-drift response

Figure 5-2. Moment vs. Drift Ratio response

29

In all cases, the peak moment occurred at about (2.5%-3.0%) drift ratio, and the moment first dropped below 80% of the peak value at about 8% drift, except in DS-2 occurred at about 7% drift; the response was very ductile. The similarity between the peak strengths in specimens SF-1, SF-2 and DS-1 was expected because the columns were nominally identical and the specimen strength was controlled by the column response. (The primary differences was the concrete strengths).

As shown in Table 5-1, the maximum moments at the interface were approximately 3,400 kip-in. in both specimens DS-1 and DS-2. The stiffness of the columns was measured at the force corresponding to the first yield of column reinforcement. It shows that DS-1 had nearly the same stiffness as DS-2.

Table 5-1. Moment and drift ratio at maximum and 80 percent of maximum resistance

Points of Interest	DS-1		DS-2	
	North Direction	South Direction	North Direction	South Direction
Secant Stiffness at Initial Yield Moment (kip/in.)	109	126	101	122
Maximum Column Interface Moment (kip-in.)	-3,290	3,476	-3373	3,393
Drift Ratio at Maximum Column Interface Moment (%)	-3.09	6.83	-2.96	2.90
80% of Maximum Column Interface Moment (kip-in.)	-2,657	2,811	-2,293	2,337
Drift Ratio at 80% of Maximum Interface Column Moment (%)	-8.27	8.15	-5.95	6.84

The columns were also stiffer in the South direction of loading, which was the direction in which they were first loaded. This behavior was observed for both specimens. The exact reason for this behavior is unknown, but it appears to be related to the level of cracking, which is likely to have been larger in the direction of second loading.

30

The failure is commonly defined at the point where the maximum moment is 80% of peak moment. In Specimen DS-1, it occurred after 8.0% drift ratio and corresponded to the onset of buckling of the column longitudinal reinforcement. However, in Specimen DS-2, it occurred at about 6.0% drift when vertical and diagonal cracks had propagated throughout the transition region, and the spirals were at incipient fracture.

The lateral load, V, used in equations (5-1) and (5-3) was corrected for friction in the sliding bearing using the recommendation proposed by Brown et al. (2008). The test-setup in the Baldwin Universal Testing Machine (see Figure 3-1) created frictional resistance in the system by two mechanisms: rotation between the greased steel-to-steel spherical element in the swivel head bearing, and sliding between the bearing's top flat plate and the channel attached to the Baldwin head. The friction component in the channel was minimized by placing a silicon-greased Teflon sheet on the bearing where it slid against smooth stainless steel plates in the channel. This correction has been done previously in research on Accelerated Bridge Construction (ABC) at the University of Washington. The rotational element in the bearing was also greased, but because it consists of two mating steel surfaces, the friction there is necessarily higher.

The correction model consists of a bilinear spring with a spring stiffness, k, of 60 kips/in., and has a maximum friction force, $F_{max\ friction}$, of $\mu_{eff}.P$ where μ_{eff} is a calculated coefficient of friction and was taken as 0.016 (Brown et al. 2008), and P is the target axial load (160 kips). Therefore, the estimated maximum resistance of approximately 2.56 kips. This is approximately 5 percent of the maximum applied lateral load in both tests.
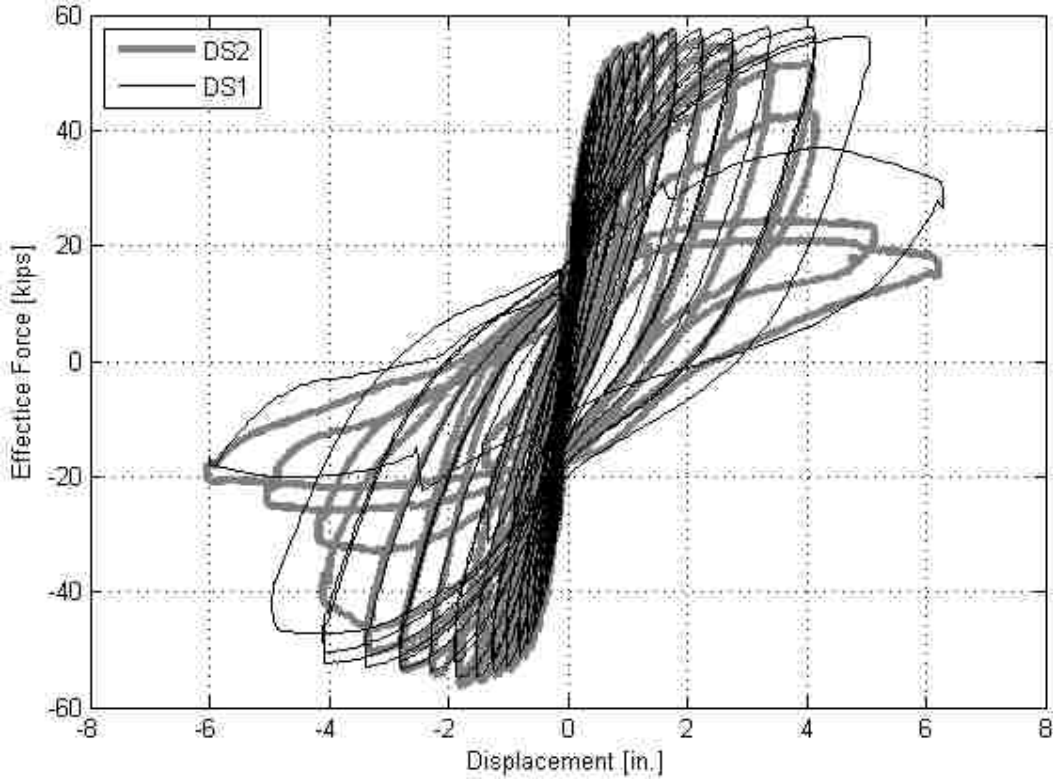
5.2 Effective force

The effective force acting on the specimens was calculated by dividing the moment at the interface by the height from the interface to the line of action of the lateral load. Equation (5-3) is divided by h_1 to obtain Equation (5-4):

$$F_{eff} = V - F_{fric}.\frac{h_2}{h_1} + (\Delta_1 - \Delta_3).\frac{h_2}{h_1^2}.P \qquad (5\text{-}4)$$

31

In Figure 5-3, the effective force is plotted against displacement for both specimens. The shapes of the curves are identical to the moment-drift responses, but they are expressed in terms of the effective force and displacement.

Figure 5-3. Effective force-Displacement response

Table 5-2 summarizes the values of 100% and 80% of the maximum effective force (MEF) and the corresponding displacements.

Table 5-2. Effective force and displacement at maximum and 80 percent maximum of resistance

Points of Interest	DS-1		DS-2	
	North Direction	South Direction	North Direction	South Direction
Maximum Effective Force (kips)	-54.8	57.9	-56.21	56.5
MEF Displacement (in.)	-1.85	4.10	-1.80	1.74
80% of Maximum Effective Force (kips)	-43.8	46.3	-45.0	45.2
80% of MEF Displacement (in.)	-4.96	4.89	-3.57	4.02

32

5.3 **Curvature**

Average curvatures were computed from the measured displacement data at selected locations along the columns and shafts. They are reported here to show the distribution of bending deformations and to evaluate the contribution of bending to the total displacement.

In the columns, the curvatures were computed from local rotations, and near the bottom of the column, these were established by measuring the differential displacement on either side of the column of rods that were embedded horizontally into the concrete (see Figure 5-4). These were referred to as "curvature rods". Higher up the column, where no curvature rods existed, the rotations were obtained from inclinometers attached to the column face.
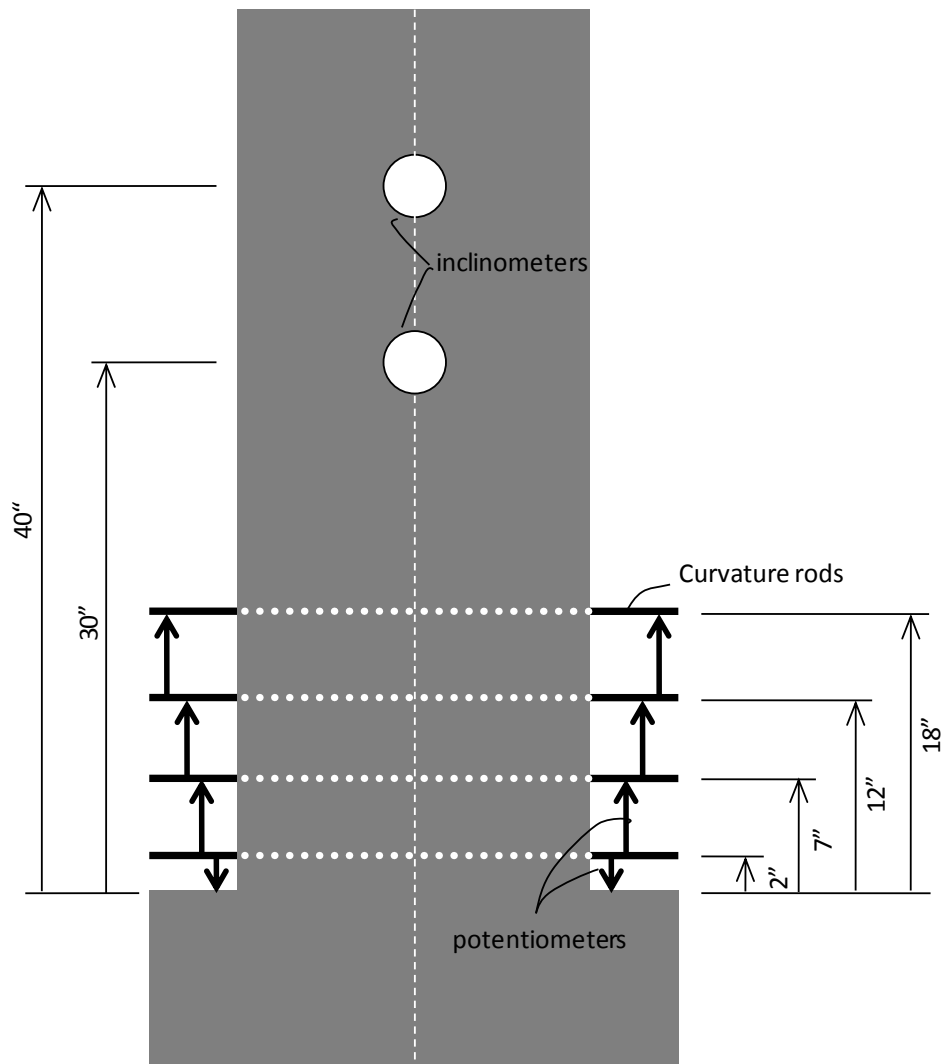
Figure 5-4. Detailed Curvature Rods Setup

These methods were also used by Haraldsson (2011) and Janes (2011). Curvature rods were embedded in the column about 2 in., 7 in., 12 in., and 18 in. above the interface. The average curvatures between rods were plotted at the mid-point of those segments. The curvatures were calculated using Equation (5-5):

$$\varphi_i = \left(\frac{\delta_{i,N} - \delta_{i,S}}{L_i} \right) / H_i \tag{5-5}$$

where

φ_i = the calculated average curvature.

$\delta_{i,N}$ and $\delta_{i,S}$ = the relative displacement between rods on the North side and South side at particular height above the interface.

L_i = the horizontal length between North and South potentiometers.

H_i = the height of each segment.

Above the rod position, the column average curvatures were obtained by the column average rotation difference between two inclinometers.

The shaft average curvatures were determined from the shaft rotation at selected locations (measured by the motion capture system). At each level, one marker was attached on each of the North, South, and West sides of the shaft. The rotations of the shaft were taken as the rotation of the plane defined by these three points.
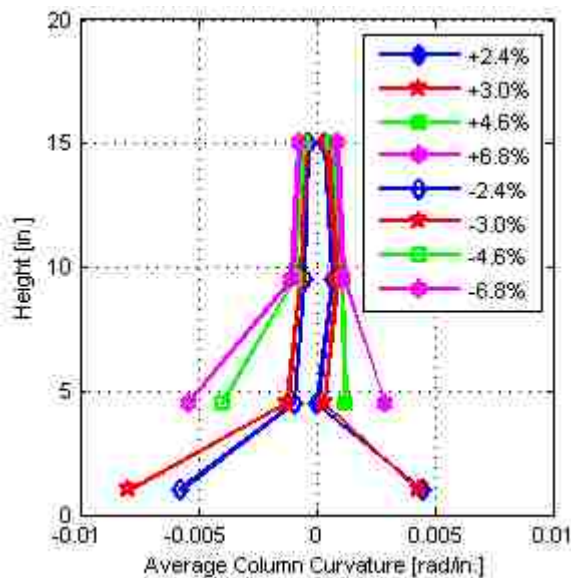
Figure 5-5 shows the average column curvature versus height for selected drift ratios. The height was relative to the column-shaft interface.
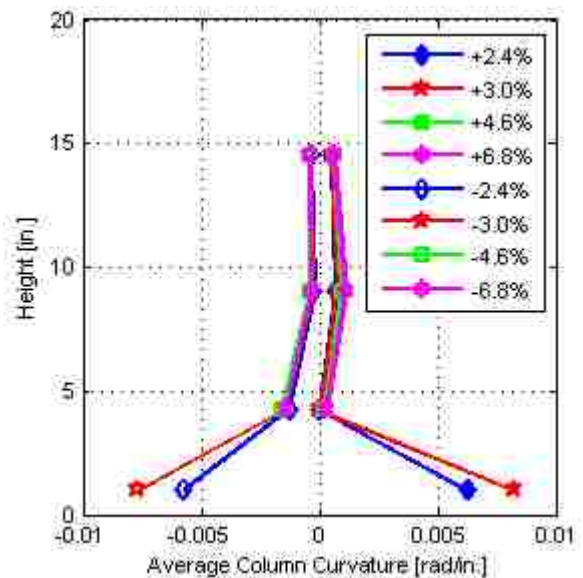
34
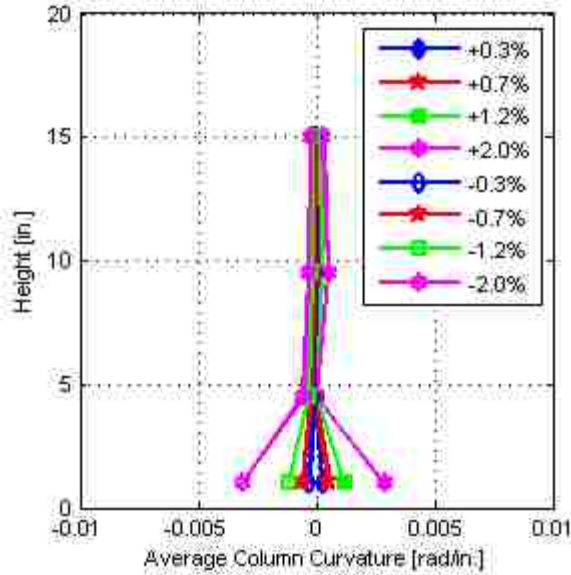
a). Specimen DS-1 (small drift)
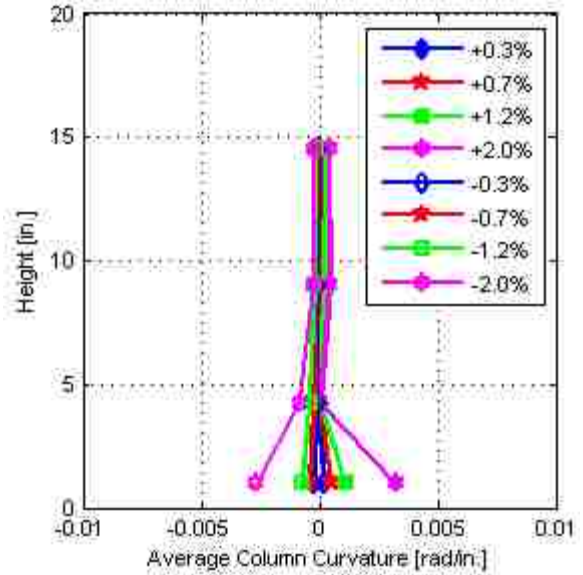
b). Specimen DS-2 (small drift)

c). Specimen DS-1 (large drift)

b). Specimen DS-2 (large drift)

Figure 5-5. Average Column Curvature (specimen DS-1 and DS-2)

The curvatures were plotted up to 6.8% drift. The curvature data at higher drift were not reliable because the spalling of concrete in the column in specimen DS-1 and in the top surface of the shaft in specimen DS-2 affected the potentiometers. The column curvature distribution was similar in both specimens until 3.0% drift. These curvatures were similar because, up to that drift, the majority of the displacement was in both cases provided by the column. The deformation was distributed over the column height with the largest values at the bottom. The

35

latter were caused by the formation of a significant crack at the column-shaft interface, which dominated the displacement measured by the potentiometers. The segment length at the bottom was also short (2"), and the average rotation measured included column rotation and bending rotation, thus, the computed curvature was relatively high. The concept of curvature is based on the existence of a continuous deformation field. In a cracked, discontinuous, medium, such as the concrete in the columns and shafts, the calculated curvature is not unique and depends on both the segment size and the locations of the cracks relative to the segment boundaries. Nonetheless, the distribution of computed curvature gives an overall sense of the distribution of bending deformations.
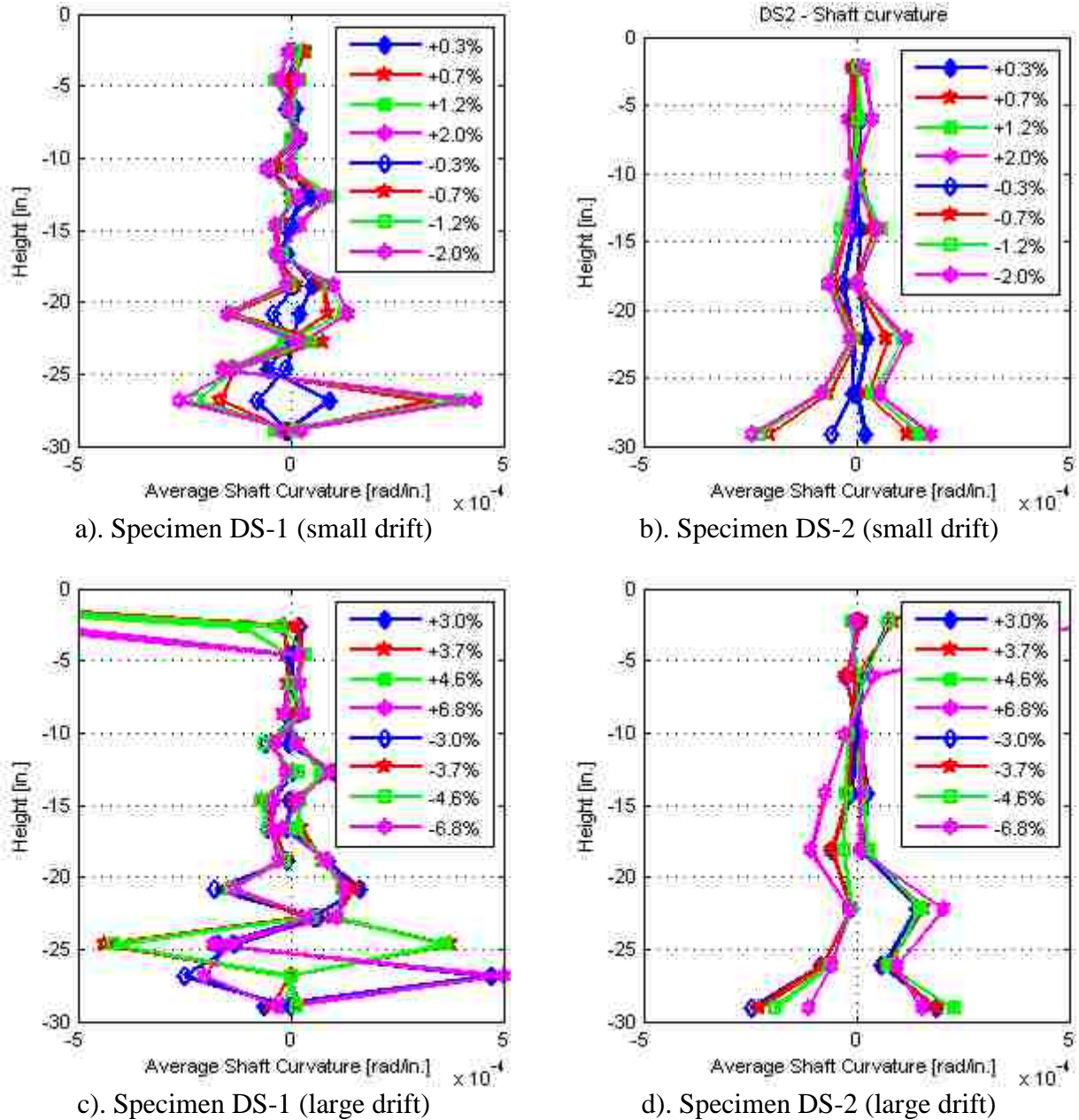
At higher drift ratios (after 3.0% drift), because of the onset of spalling at the top of transition, the strain values at the bottom segment measured by potentiometers were unreliable, and were not plotted in the figures. The column curvature distribution differed between the two specimens. In DS-1, the average curvature at 5in. above the interface increased rapidly while it did not change in DS-2. That was consistent with the damage progression in two test when spalling occured in DS-1 and did not happened in DS-2. The bond stress between column and shaft started degrading, and the shaft in Specimen DS-2 started to deform significantly. Thus, at any given drift, the column curvature was smaller in Specimen DS-2 than in Specimen DS-1.

In DS-2 specimen, the method using three "Optotrak" markers to measure rotation was performed in the column to compare with the result of using curvature rods. The column average curvature versus height for selected drift ratios were provided in Figure 5-6. The result of column curvature distribution were quite similar by using "Optotrak" markers and curvature rods. The different curvatures at the bottom segment were unknown but this values were unreliable as explained above. In the next section, the comparision of rotation of column show that using "Optotrak" also had the similar result with using inclinometer. Therefore, the motion capture system is recommended to use because of its multipurpose.

a). Specimen DS-2 (small drift) b). Specimen DS-2 (small drift)
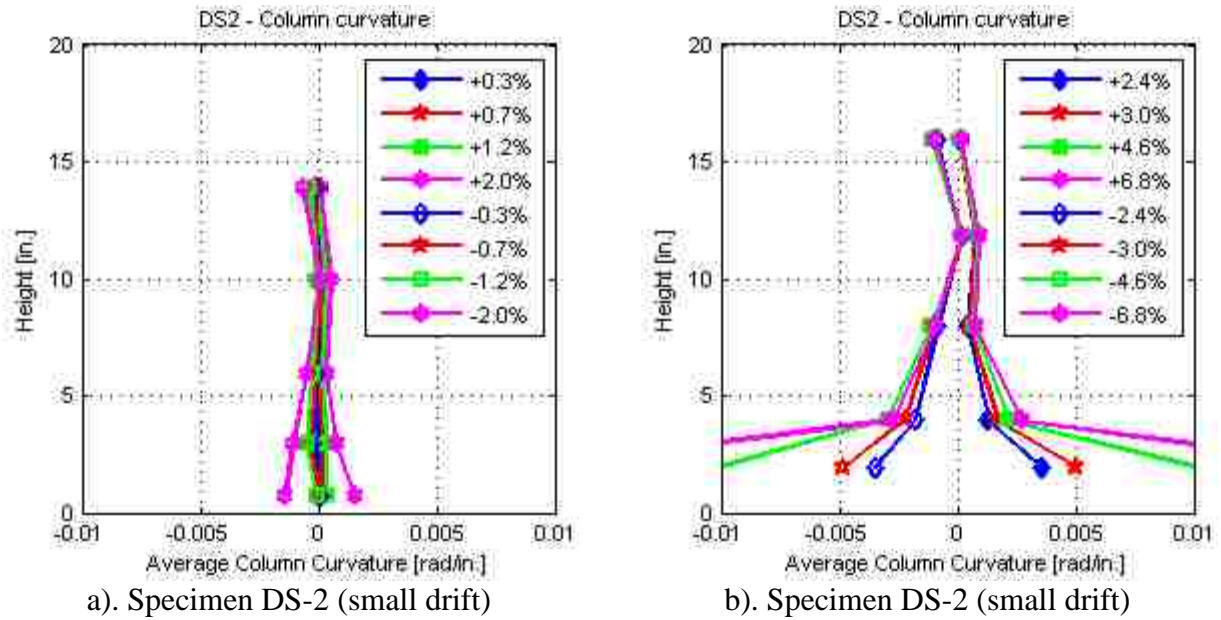
Figure 5-6. Average Column Curvature (measured by Optotrak) – Specimen DS-2

The average shaft curvature versus height for selected drift ratios is shown in Figure 5-7. The curvatures in the shafts were also distributed non-uniformly, with the largest values at the base. That distribution reflects the existence of a flexural crack at the base. Each of the peaks of curvature corresponds to a horizontal crack position. Note that the scales on the column and shaft plots are different, and that the shaft curvatures were smaller by about an order of magnitude than the column curvatures.

37

a). Specimen DS-1 (small drift)   b). Specimen DS-2 (small drift)

c). Specimen DS-1 (large drift)   d). Specimen DS-2 (large drift)

Figure 5-7. Average Shaft Curvature (Specimen DS-1 and DS-2)

5.4   Displacement

In the test specimens, the horizontal displacement at the top of the column depended on the deformations of the individual elements. To simplify discussion, those deformations are broken down into the following components, which are illustrated in Figure 5-8:

38

1. *Shaft bending deformations.* These are the curvatures of the shaft, and depend on the elongation of one vertical face and the shortening of the opposite one. Curvature was measured by the three "Optotrak" markers attached to the shaft at the same level, using the motion capture system. At each level, one "Optotrak" marker was attached on each of the North, South, and West sides of the shaft. The rotations of the shaft were taken as the rotation of the plane defined by these three points. Then, the average curvature of segment was calculated by dividing the difference of rotation at adjacent level to segment's height.

2. *Shaft shear deformations.* These derformations consist of pure shear deformations of the shaft. They were obtained by subtracting from the total horizontal displacements the shaft bending displacements. The total displacements were obtained from the horizontal displacements measured by the motion capture system (and verified by the string potentiometers). The bending displacements were obtained by integrating the rotations obtained from (1) above.

3. *Column base rotations.* The column can rotate as a rigid body, due to damage in the transition region of the shaft. These rotations were obtained from the bottom inclinometer attached to the column, and from the group of three "Optotrak" markers attached to the bottom of column (2 in. above the interface).

4. *Column bending deformations.* These deformation consist of the curvatures of the column. Rotations were measured at discrete locations up the column and average curvature was computed from the difference between rotations at adjacent locations. The rotations were obtained using the inclinometers, curvature rods instruments in specimen DS-1, and they were also compared with "Optotrak" data, in Specimen DS-2.

5. *Column shear deformations.* These consist of the pure shear deformations of the column. They were very small in both cases, and were estimated from subtracting the total displacement to the displacement of components (1), (2), (3), and (4). This value would include error in this computation.

The displacements were calculated at the top of column (60 in. above the interface). The shaft bending diplacements were calculated by numerical integration of the shaft curvature. The shaft shear displacement were calculated by shaft displacement (measured by "Optotrak") subtracted the shaft bending diplacement at the interface position (top of the shaft). The column

39

rotation displacement were calculated by the product of column height and the difference between the rotation of column at 10 in. above the interface (measured by inclinometer) and the rotation of shaft at the interface (measured by Optotrak). The column bending displacement were calculated by numerical integration of the column curvature. The column shear displacement and error of instruments were calculated by displacement at the top of column (measured by string pot) subtracted the displacement of shaft bending, shaft shear, column rotation, and column bending.

Vertical displacements were measured only by the Optottrek system. No values are presented here.
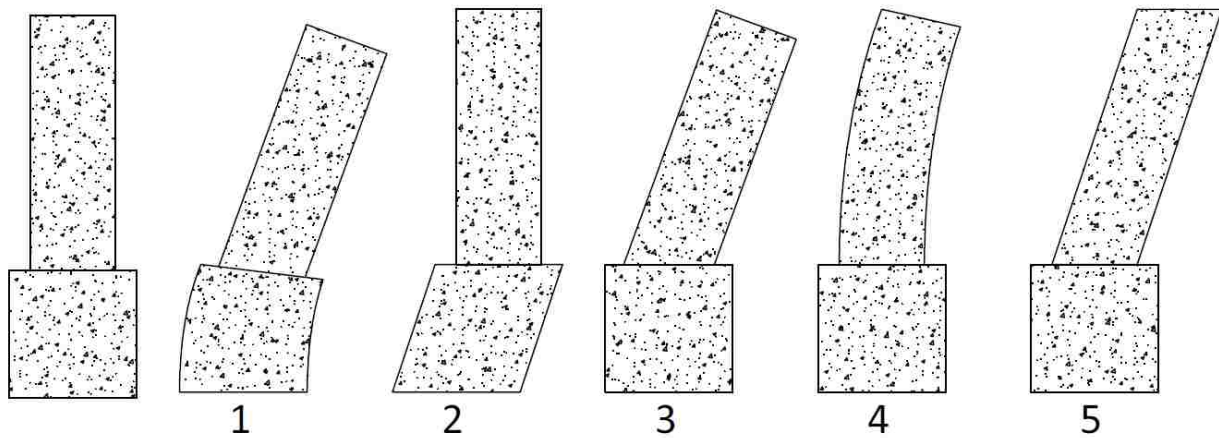
Figure 5-8. Displacement types

The method of measuring rotation of specimens using groups of three Optotrak marker was compared with the results of inclinometers to show the accuracy of this method. The comparision is shown in Figure 5-9 and Figure 5-10 with the results were measured in specimen DS-2. The comparision show that the result of method using Optotrak were similar to inclinometers' result.
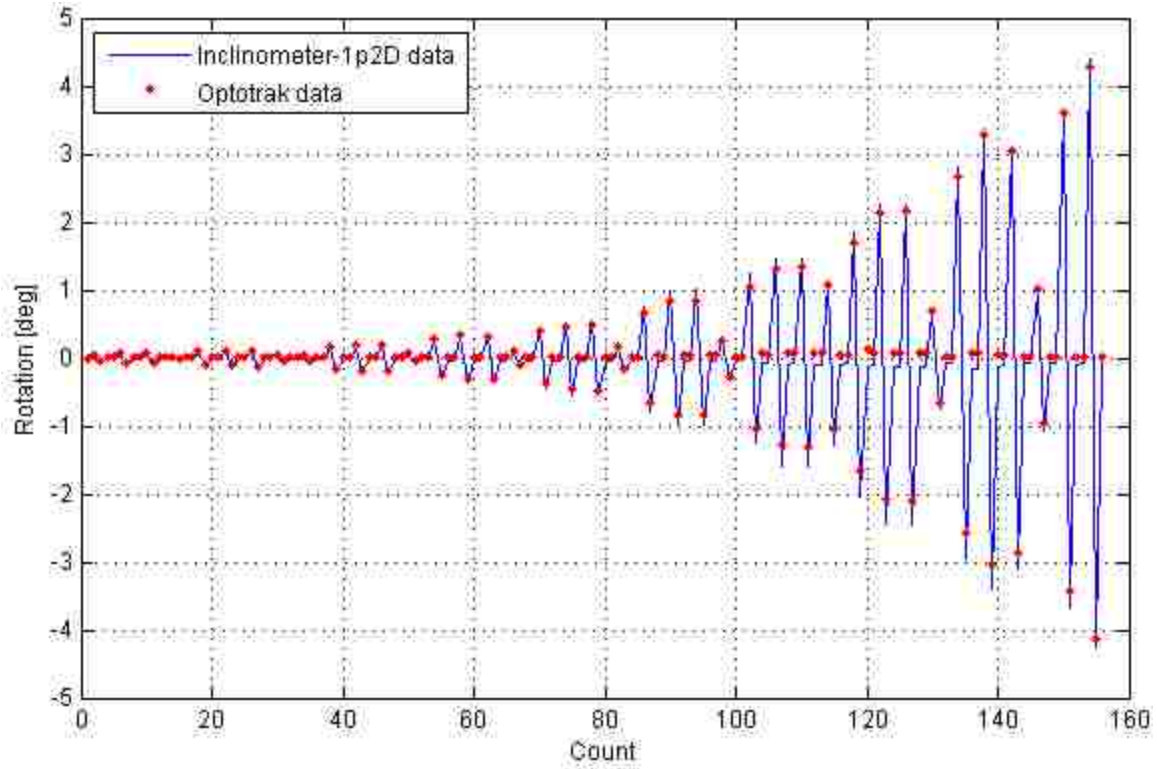
Figure 5-9. Rotation Comparison at 10'' above the interface position (Specimen DS-2)
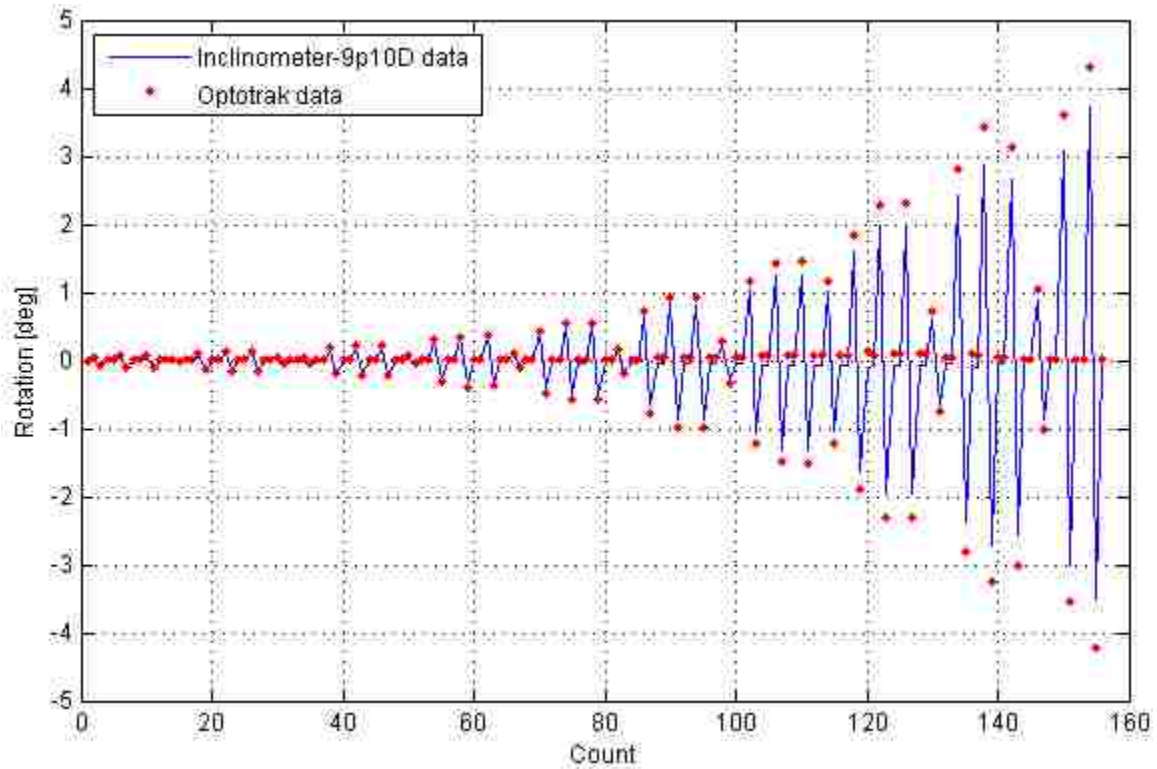
Figure 5-10. Rotation Comparison at 18'' above the interface position (Specimen DS-2)

41

The displacement profiles of the shaft and column are plotted for specimens DS-1 and DS-2 in Figure 5-11 and Figure 5-12 respectively. The vertical axis represents distance above the base of the shaft, while the horizontal axis is the displacement in inches. Note that the shaft was 30 inches high, and the height of the column, measured from the top of the shaft to the loading point, was 60 inches.

Profiles are given for the peak displacement in each cycle set, up to 3.0% drift. Separate curves are given for the positive and negative directions. For each load level, two curves are presented. The solid line represents the total displacement, while the dashed line represents the sum of the displacements due to components 1, 2 and 3 (shaft bending, shaft shear and column base rotation). Components 1 and 2 may be thought of as shaft contributions to the overall displacement. Component 3, column base rotation, may be thought as column boundary condition contributions which is nearly zero in the column-spread footing socket connection of Haraldsson et al. (2011). The difference between the dashed and solid lines for any load level therefore represent the displacement due to column bending and shear, or the column contributions to the total displacement. The column shear component was in all cases small compared with the column bending component.

Up to 0.7% drift, the displacement profiles of specimens DS-1 and DS-2 were similar. The angle of dotted lines at the interface position corresponded to the appearance of column base rotation. Thus, the column base rotations were nearly zero because there was no angle at the interface position in dotted lines.

However, after 0.7% drift, the behaviors of specimens DS-1 and DS-2 were different. Overall, the majority of the displacement in Specimen DS-1 arose from column deformations, because a plastic hinge started to form in the column. By contrast, in specimen DS-2, the column deformations were small and the column base rotations deformations dominated the behavior of specimen.

The details of the response were as follows. In specimen DS-1, the column bending deformation kept increasing with each cycle up to 3.0% drift. This was suggested by the rapid increasing of distance between solid lines and dotted lines at the top position at the same drift. On the other hand, in specimen DS-2, the column bending deformation decreased after 0.7% drift and was very small at 3.0% drift. The majority of the total displacement was attributable to

42

column base rotation, which was 0.012 rad (1.2% drift) in DS-1 and 0.007 rad (0.7% drift) in DS-2. However in DS-2 specimen, the percentage of column base rotation contributed to total deformation was higher than in DS-1 specimen.
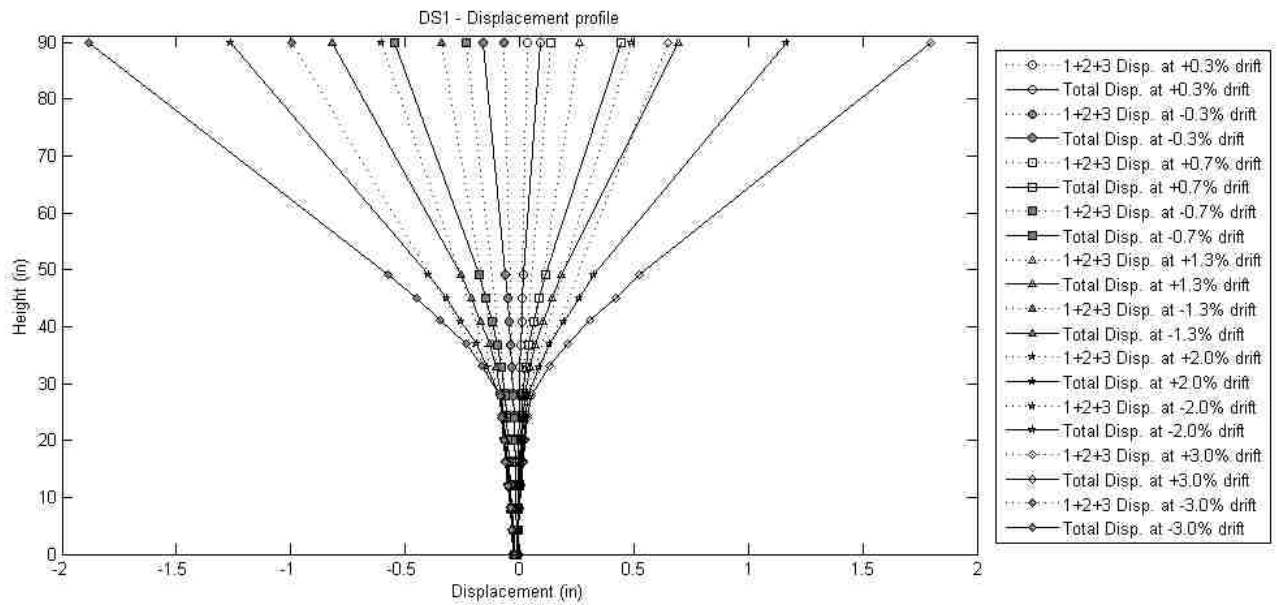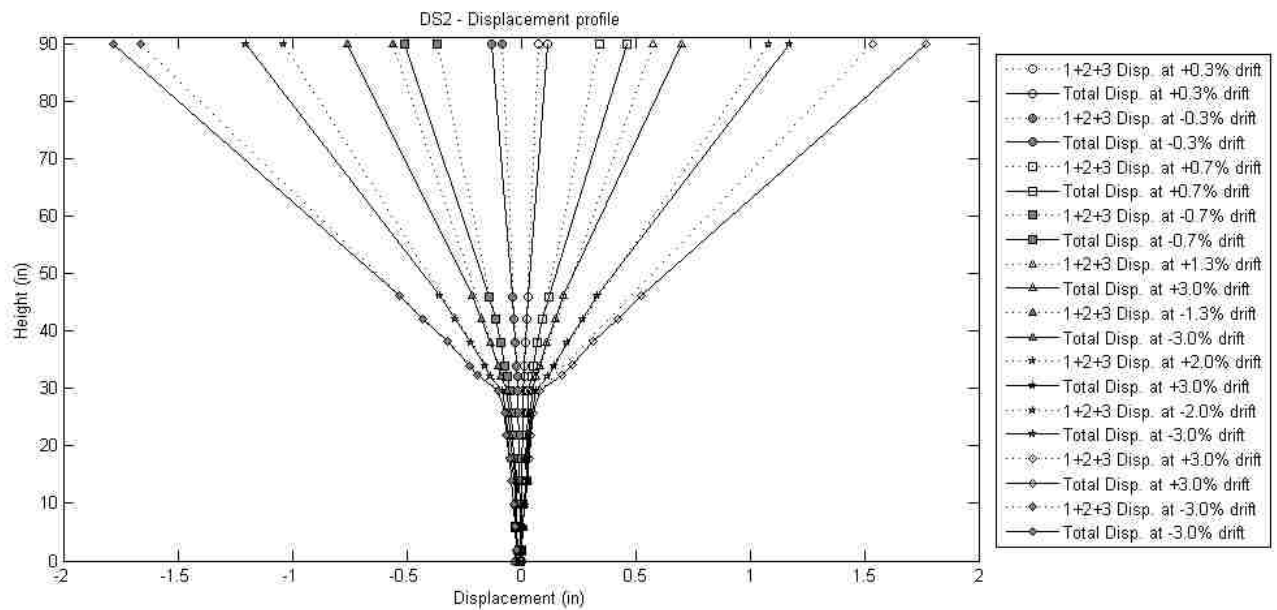

Figure 5-11. Specimen DS-1 - Displacement profile

Figure 5-12. Specimen DS-2 - Displacement profile

43

The contribution of displacement types were shown in Figure 5-13 and Figure 5-14. In specimen DS-2, after set 8-cycle 1 (near 7% drift), big vertical cracks appeared in the shaft. Thus, the data of "Optotrak" marker attached in the shaft were not reliable for calculating the curvature of the shaft. Therefore, the displacement of the shaft bending, column shear and error were not reliable after 7% drift.

a). Specimen DS-1   b). Specimen DS-2
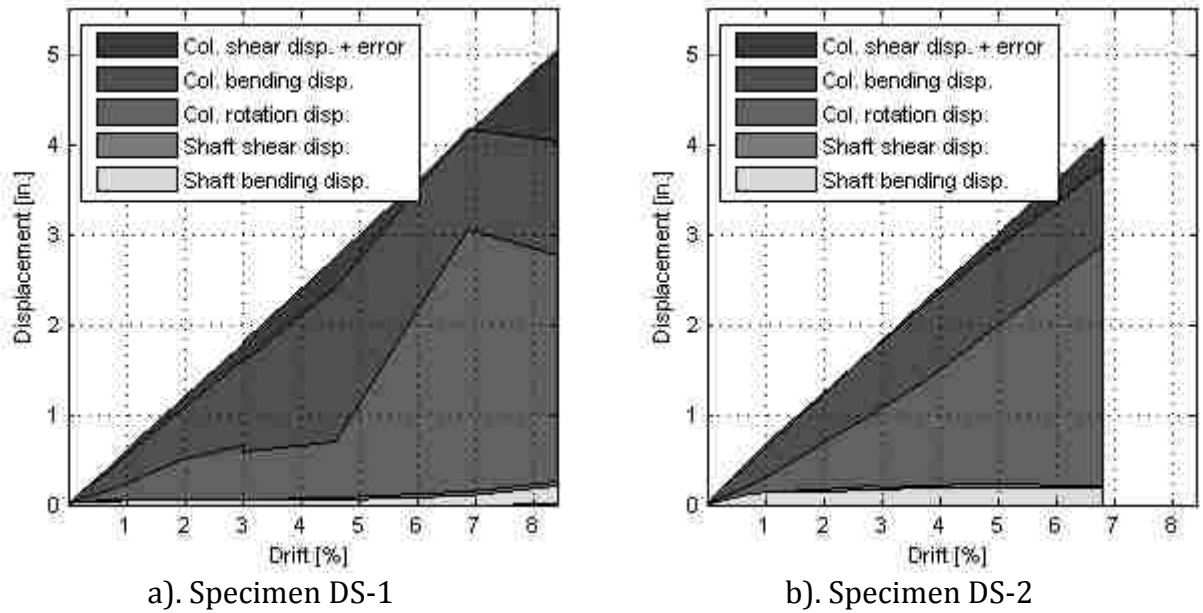
Figure 5-13. Displacement-Drift response (specimens DS-1 and DS-2)

a). Specimen DS-1   b). Specimen DS-2
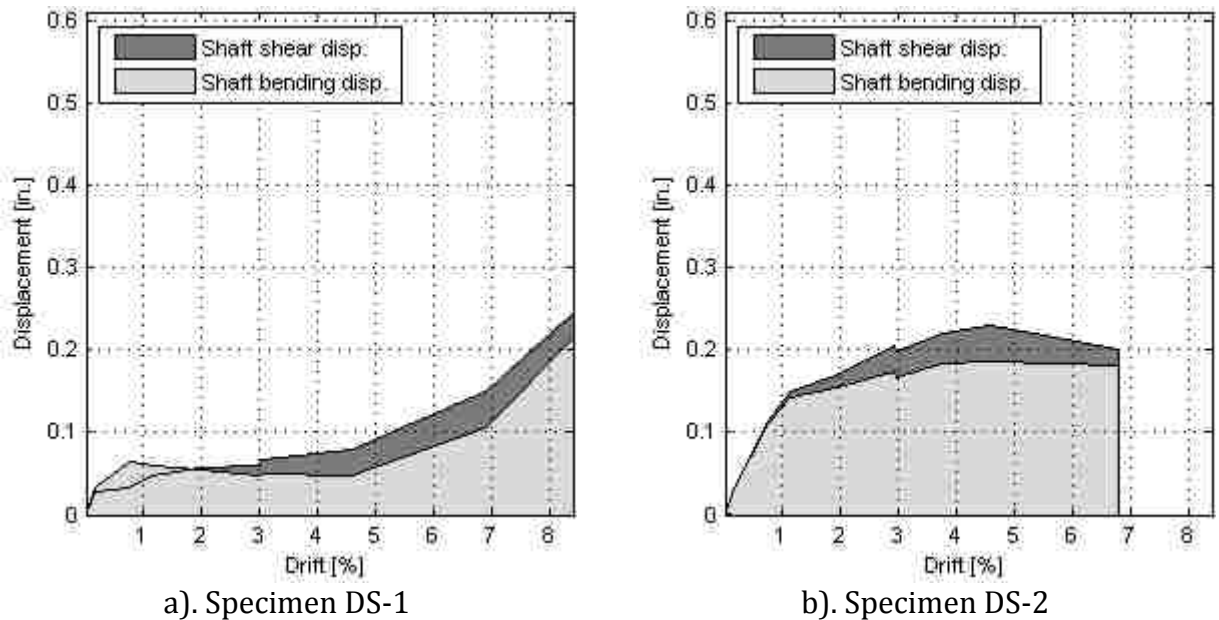
Figure 5-14. Displacement-Drift response of shaft (Specimens DS-1 and DS-2)

44

As shown in figures, the column bending deformations were higher in DS-1 than in DS-2 before reduce at 7% drift. At this time, the column rebar were buckling and the concrete were crushed. In DS-2 specimen, the column bending deformation were smaller and most of displacement at the top of column were the column rotation displacement. In the shaft, the shaft shear deformation were similar in DS-1 and DS-2 specimen. However, the shaft bending in DS-2 specimen were higher than in DS-1 specimen.

5.5 Strains in Column Reinforcing Bars

The longitudinal reinforcing bars in the column were gauged as described in Figure 5-15. Because they were configured symmetrically, only the East reinforcing bars were gauged. In both specimens, gauges were attached on the reinforcing bars in pairs at three locations: 0 in., 12 in. and 23 in. below the interface of the shaft and column.
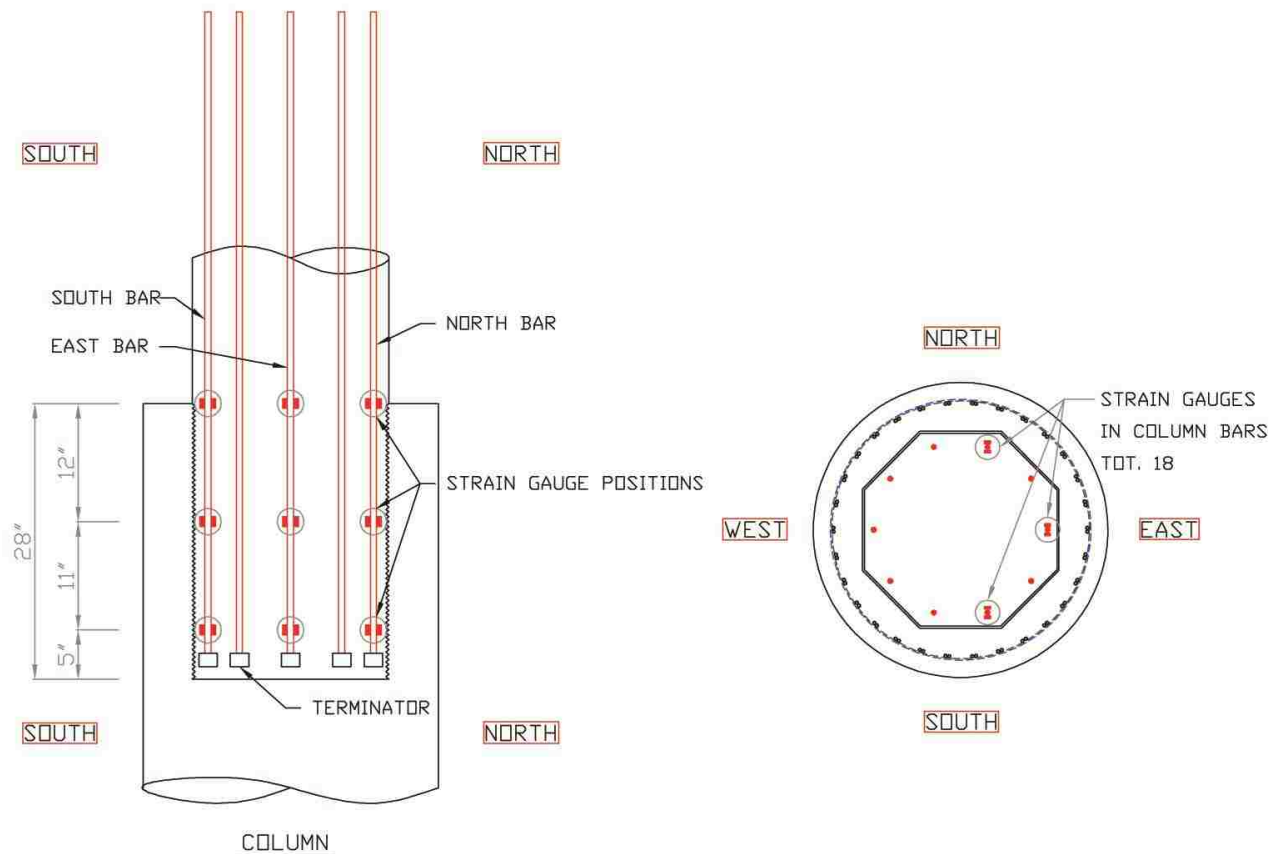
Figure 5-15. Column strain gauge positions

Figure 5-16 shows the axial strain distributions (obtained by averaging the readings from each pair of gauges) over the height of the North, South and East reinforcing bars at various drifts for specimen DS-1 and DS-2. The strains were plotted up to 3% drift. Both specimens show similar strains profiles before yielding in the reinforcing bars. The plots show that the reinforcing bars in North and South experienced alternate tension and compression as they were loaded cyclically, and they started to yield in tension at the column-shaft interface at 0.7% drift. The East reinforcing bars of specimens DS-1 and DS-2 were located at the mid-depth of the column, so they experienced almost equal tension strains when the column was displaced to the North and South. They started to yield in tension at 1.2% drift.

At a location 12 in. below the interface, the bars started to yield at 2.0% drift in the North and South reinforcing bars, and at 3.0% drift in the East reinforcing bars in both specimens. After 3.0% drift, the tension strains began to exceed the measurement range of the data acquisition system, whichwas from -0.011 to +0.011 in/in. For real strains outside this range, the recorded value was +/- 0.011 in/in. When the real strain came back within the readable range, the correct value was again recorded.
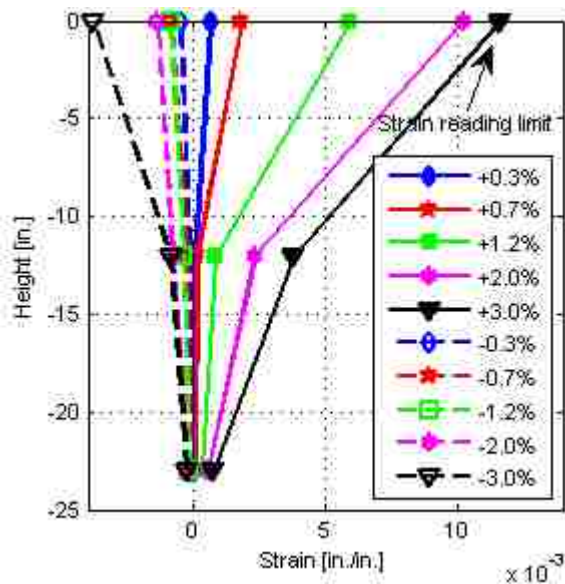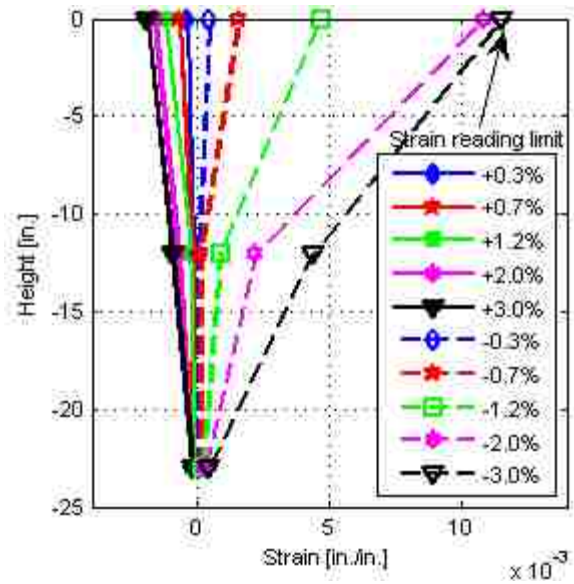

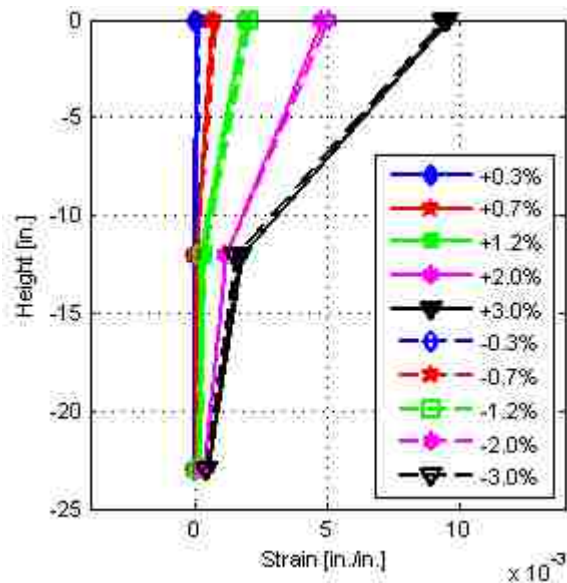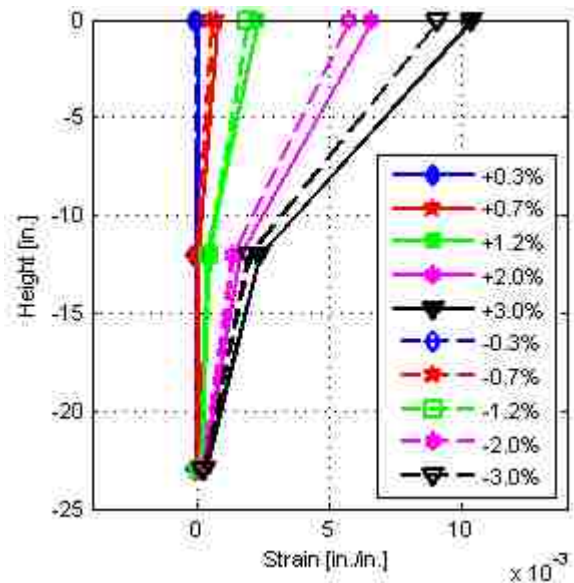a). DS-1 - North reinforcing bar of column.   b). DS-2 - North reinforcing bar of column.
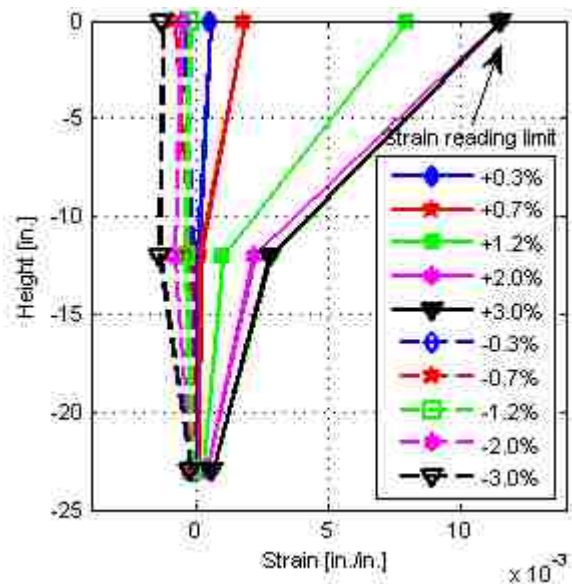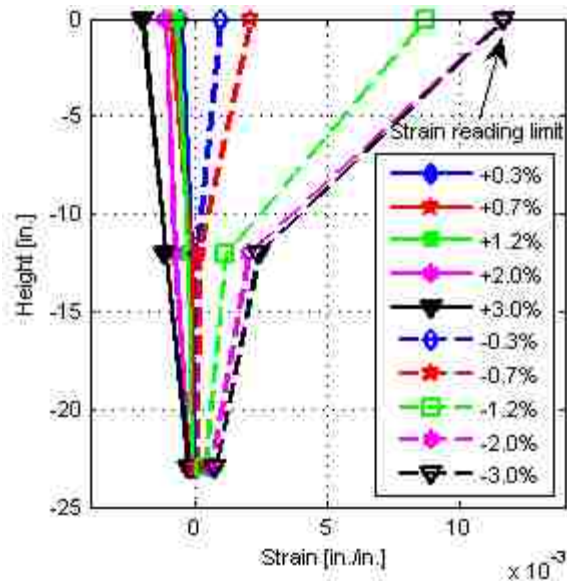
c). DS-1 - South reinforcing bar of column.

d). DS-2 - South reinforcing bar of column.

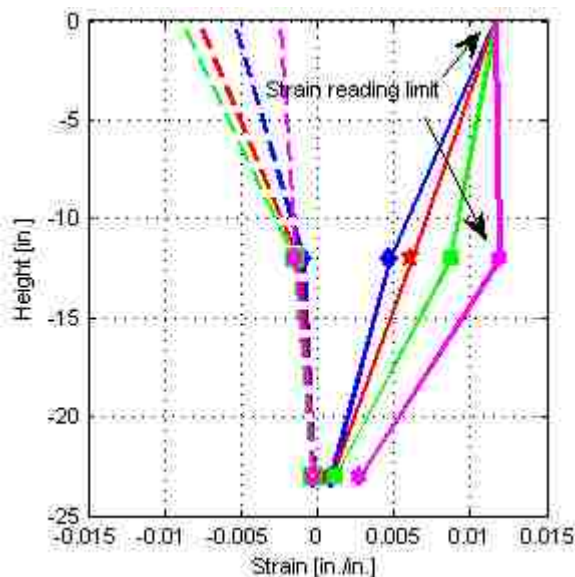e). DS-1 - East reinforcing bar of column.

f). DS-2 - East reinforcing bar of column.

Figure 5-16. Strain profiles in reinforcing bars of the column (until 3% drift)

The axial strains distributions after 3% drift are plotted in Figure 5-17. For the reasons given above, the recorded values are limited to the range +/- 0.11 in/in. They were plotted up to 8.4% drift when the spiral in the column broke. At the next cycle, 10% drift, the reinforcing bars in the column broke. so no strain is presented.

47

The plots show that after 3% drift, the strain distributions of specimens DS-1 and DS-2 were different. Consider first the bar strains at the interface. In both the North and South bars in specimen DS-2 and in the South bar of specimen DS-1, the bar experienced only modest compression strain (no more than -0.003 in./in.). This suggests that the concrete in the region was reasonably intact and was still carrying most of the compression force. By contrast, the North bar in specimen DS-1 experienced large compressive strains (to -0.009 in./in.) at 6.9% drift because the concrete had suffered significant damage and most of the force was being carried by the bars. However, by 8.4% drift the column spiral has fractured and the bars had buckled, so the load they resisted and the strain they displayed were reduced.

At the bottom of the column, the bars in all cases never reached yield in tension. This suggests that the anchorage of the bars was being provided at least partly by bond. However, because the tension strain was close to yield, the anchor heads were clearly necessary. In Specimen DS-2, the South bars exhibited high compression strains at drifts of 6.9% and above. These are believed to be caused by the column rocking on its edges after the resistance of the shaft had largely been lost. This can be seen in figures of damages at the bottom of column of specimen DS-2 after testing in the Appendix C.
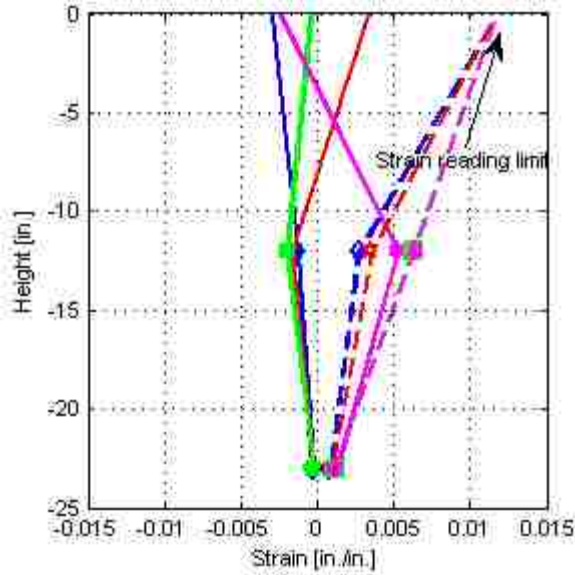

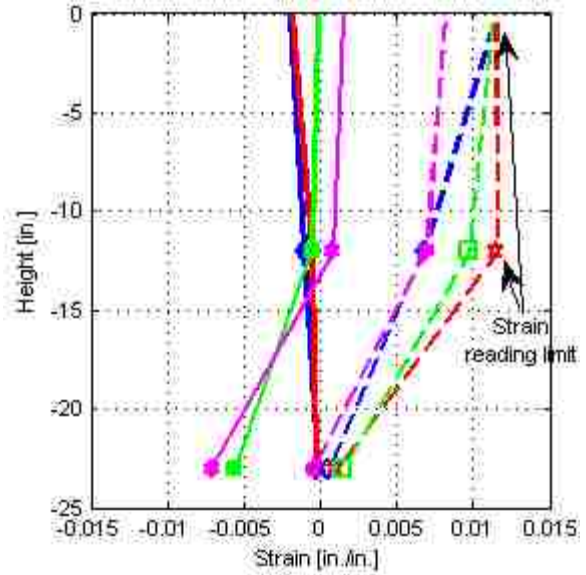a). DS-1 - North reinforcing bar of column.   b). DS-2 - North reinforcing bar of column.
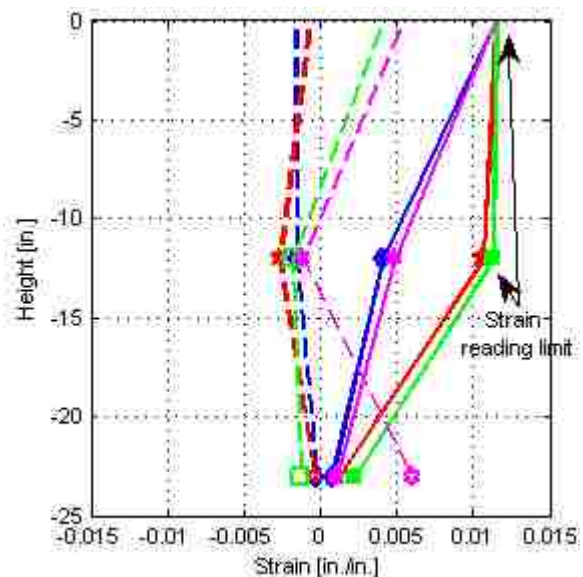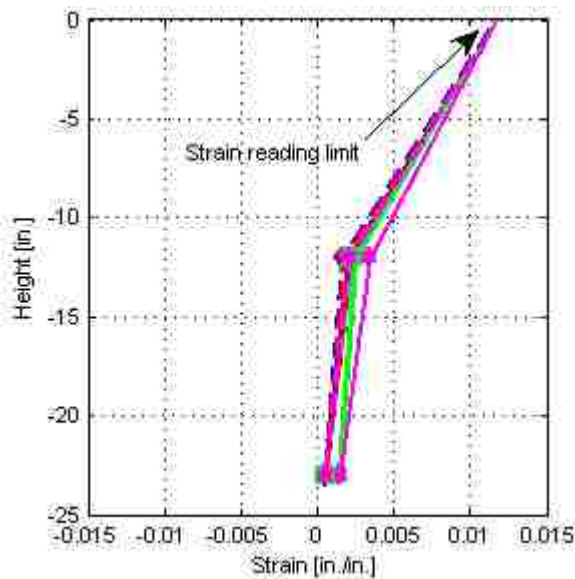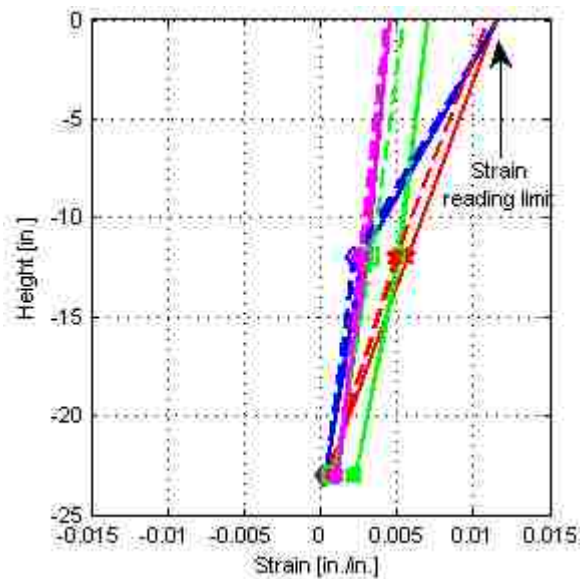
c). DS-1 - South reinforcing bar of column.

d). DS-2 - South reinforcing bar of column.

e). DS-1 - East reinforcing bar of column.

f). DS-2 - East reinforcing bar of column.

Figure 5-17. Strain profiles in reinforcing bars of column (after 3% drift)

The strain distributions in the East bars were also different between specimens DS-1 and DS-2. In specimen DS-1, the strain distribution was non-linear, suggesting that the moment decayed rapidly with depth. However, in specimen DS-2, after 4.6% drift, the strain distribution was linear. It suggests that there was no friction between the surface of column and the shaft, and that the moments were determined only by the horizntal forces at the top and vertical forces at the

49

bottom of the transition region. It is also noticeable that the strains decreased after 4.6% drift. This is explained by the drop in load then, caused by the damage to the transition region of the shaft.

Figure 5-18 shows respectively the cyclic effective Force-Strain relationships of column reinforcing bars at the interface, 12 in. and 23 in. below the interface in the specimens DS-1 and DS-2. In each plot, the cyclic Effective Force-Strain relationships were plotted for the North, South and East reinforcing bars in blue, green and purple respectively at the given depth.

At the interface, up to 0.7% drift, the relationships in the specimens DS-1 and DS-2 were similar. When the effective force reached 40 kips, the strains in North, South and East reinforcing bars were 2.25e-3, -1.0e-3 and 1.0e-3 respectively in both specimens. This illustrated that the North and South reinforcing bars reached yield point at 0.7% drift in both specimens. The relationships had a line of symmetry through effective force F_{eff} = 0. At F_{eff} = 0, all the strains in reinforcing bars were nearly zero. It suggested that the friction between the column surface and the shaft was still good. When the cyclic drift went from 0.7% to 4.6%, the relationships in DS-1 and DS-2 were different. As illustrated in Figures, the compression strain in North and South reinforcing bars in specimen DS-1 were higher than in DS-2. This indicated that at this time the column concrete in DS-1 was crushed and more compression force was being caried by the bars. This contrasts with the behavior of Specimen DS-2 where the column concrete was not crushed. During this period, the strain in the North, South and East reinforcing bars in both specimens were not only non-zero when F_{eff} = 0, but also increased after each cycle.

At 12 in. below the column-shaft interface, up to 3.0% drift the relationships in both specimens were similar. The North, South and East rebar reached yield at about 3.0% drift. It can be recognized that the friction between the column surface and the shaft were still good in both specimen because the strain values at F_{eff} = 0 were nearly zero. When the drift increased from 3.0% to 6.9% drift, the behavior in DS-1 and DS-2 were different. In DS-1, the strain values when F_{eff} = 0 were increase a little bit indicated that the friction was decreased but still good. That is because when the tension reinforcing bar strain dropped from two times of yield strain (0.004 in/in) to zero, stress in that bar must be equal compression yield strength (assume -60 ksi). At the same time, the compression reinforcing bar strain increased from about -0.001 in/in to zero, stress in that bar must be equal half of compression yield strength (assume -30 ksi).

50

Therefore, when Feff = 0, the moment at this position by column reinforcing bars was not zero. Thus, friction moment must equal this value to equilibrate. The maximum values were 0.008, 0.006 and 0.002 in North, South and East reinforcing bars in respectively. The maximum effective forces remained about 60 kips. However, in DS-2, effective force decresed from about 50 kips to 35 kips. The strain value when Feff = 0 were not zero and increased after each cycle. It illustrated that the friction was lost. Therefore most of flexure transferred to column. Thus, the strain in rebar increased dramatically over the reading capacity about 12e-3.

At 23 in. below the interface, the relationships are plotted from 0% to 6.9% drift in Figures. As shown, reinforcing bars in specimen DS-1 remained elastic through the test. In specimen DS-2, they remained elastic up to 4.6% drift, during which the strain values were similar to those in specimen DS-1, but the bars yielded in tension thereafter. Yielding at the anchor head, 23 in. below the interface, implies that the bar experienced little change in force along its length, and therefore little friction between the column and shaft.
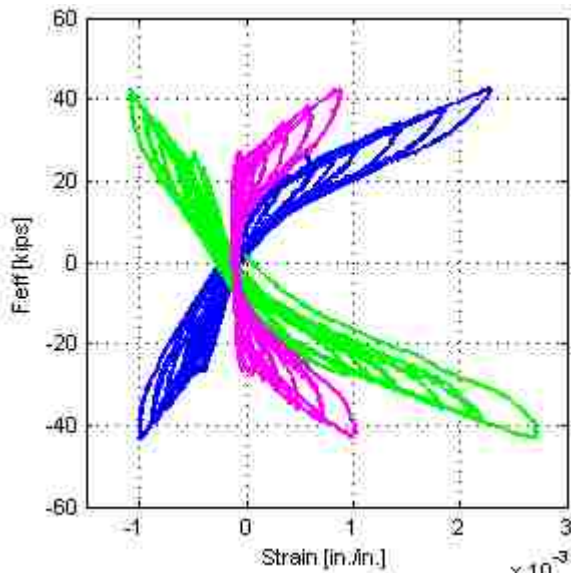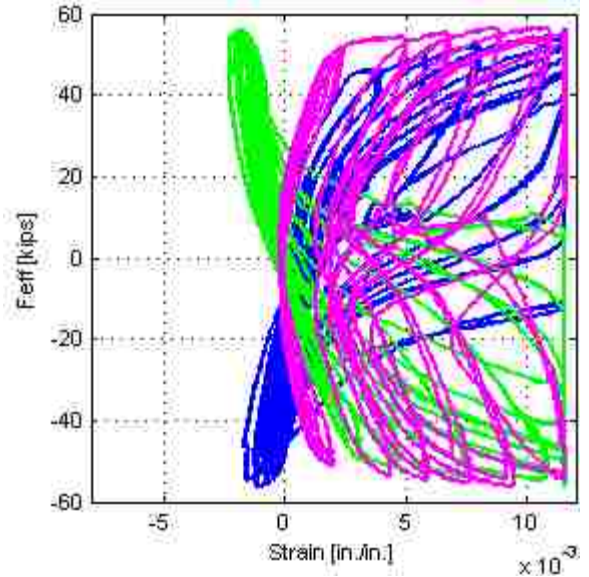

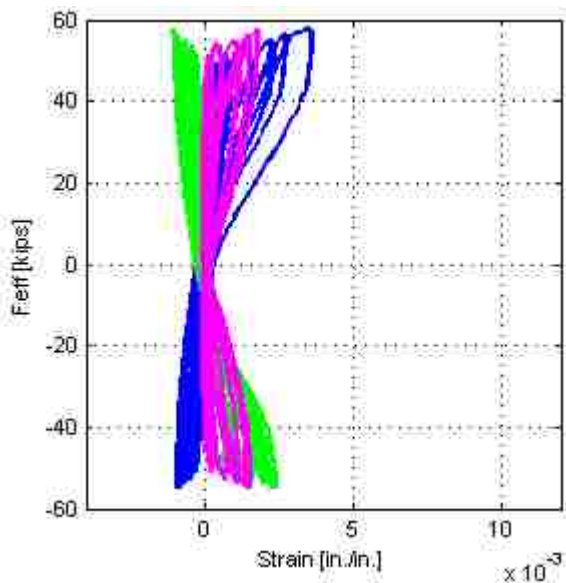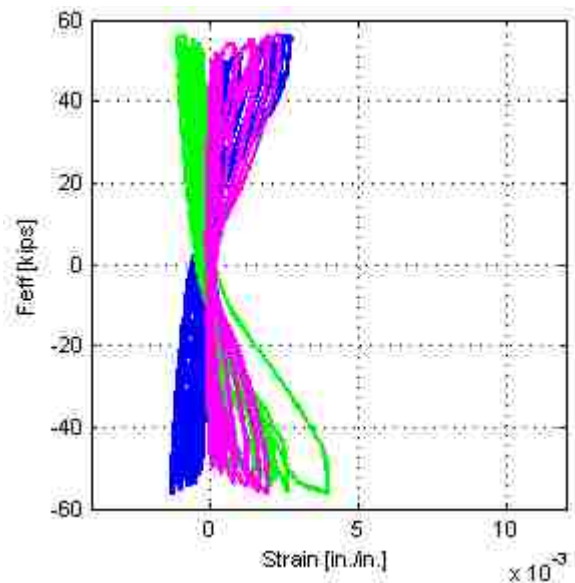a).DS-1 – Top position (until 0.7% drift)   b).DS-2 – Top position (until 0.7% drift)
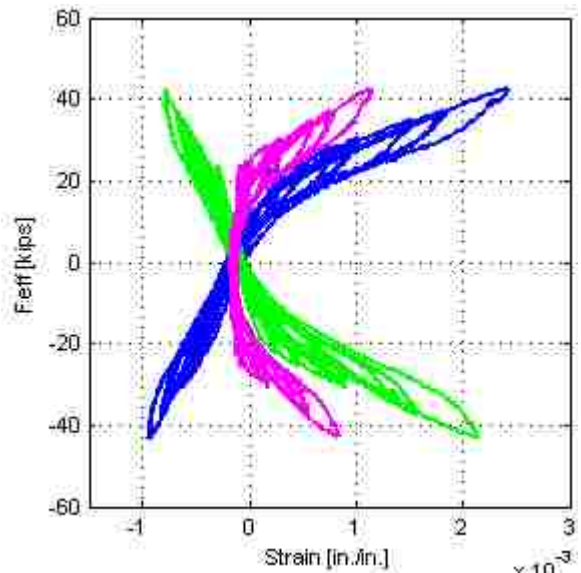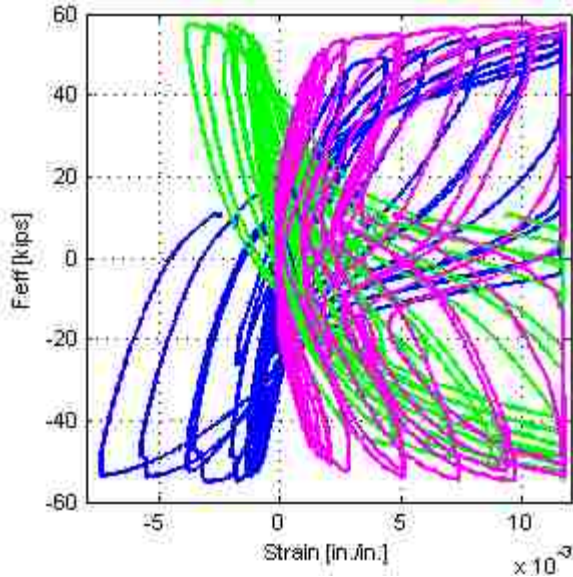
c).DS-1 – Top position (0.7%-4.6% drift)

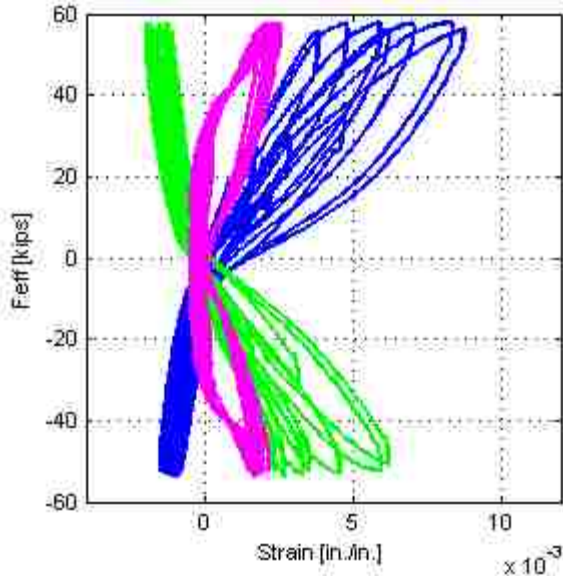d).DS-2 – Top position (0.7%-4.6% drift)

e).DS-1 – Middle position (until 3.0% drift)
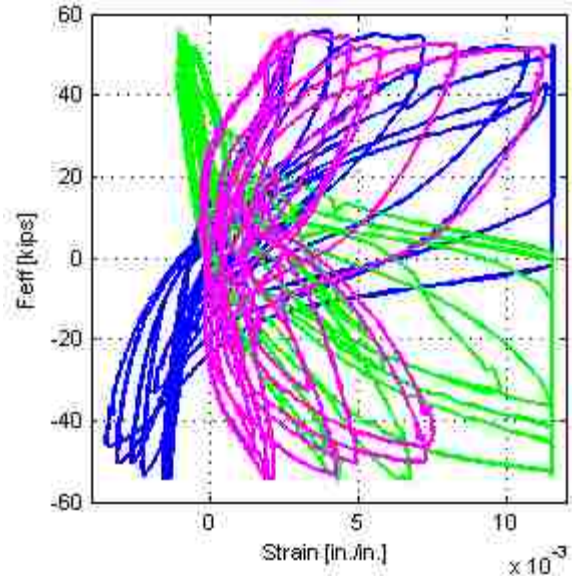

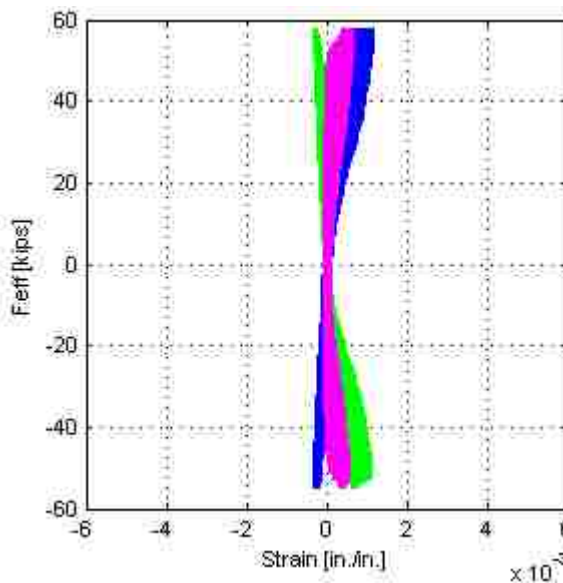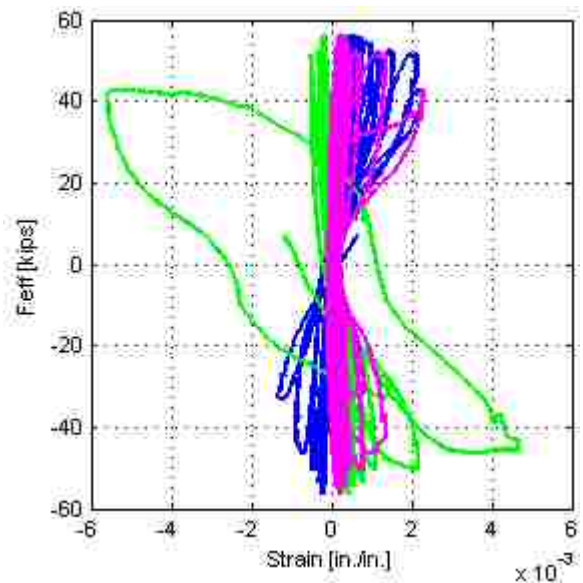f).DS-2 – Middle position (until 3.0% drift)

g).DS-1 – Middle position (3.0%-6.9% drift)   h).DS-2 – Middle position (3.0%-6.9% drift)

i).DS-1 – Bottom position (until 6.9% drift)   j).DS-2 – Bottom position (until 6.9% drift)

N-rebar   S-rebar   E-rebar

Figure 5-18. Strain-Effective force relationship of the column reinforcing bars

5.6   Strains in Shaft Reinforcing Bars

The longitudinal reinforcing bars in the shaft were gauged as shown in Figure 5-19. The symmetry of the shaft and column was utilized, thus, only the East bars were gauged. In both

53

specimens, gauges were attached on the reinforcing bars in pairs at three locations: 4 in., 16 in., and 28 in. below the shaft-column interface.
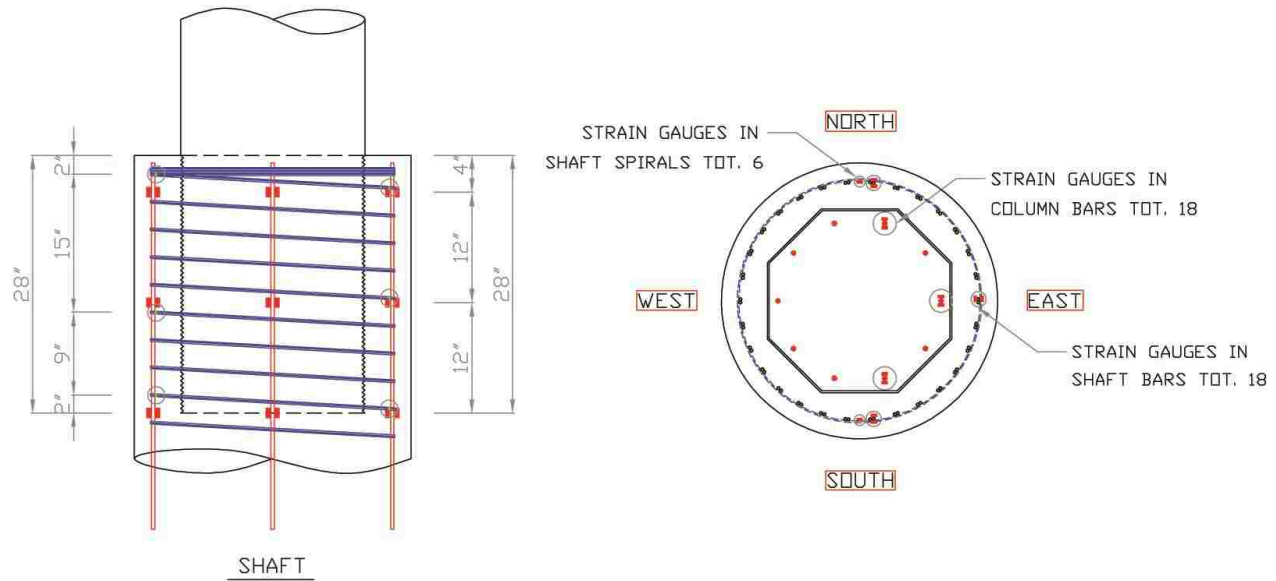

**Figure 5-19. Strain gauges position in the shaft**

The strain in shaft reinforcing bars in both specimens DS-1 and DS-2 are shown in

Figure 5-20 and

Figure 5-21. At 4 in. below the interface position, the strains recorded by the inner and outer gauges at the same position in the North bar in specimen DS-1 were similar. The strain gauge pair in the South bar in specimen DS-1 were damaged before testing. In the East bars, the two gauges gave nearly the same values until near the end of the test. The fact that the gauges gave nearly the same values implies that the bars were primarily in tension, with little bending.

However, in specimen DS-2, the values of the strain gauge pairs in the North and South bars were relatively different from count = 40000 (0.9% drift) to the end of the test. These differences in gauge readings suggest that local bending happened at these positions. As illustrated in figures, local bending caused the outside strain gauges (black line) to experience less tension and the inside strain gauges (grey line) to experience more tension. This local bending occurred after the transition region of the shaft cracked, and the spiral in it yielded. This behavior was not seen at the positions 16 in. and 28 in. below the interface in specimen DS-1 and

54

it can only be seen at the very end cycles when the spirals of the shaft were broken in Specimen DS-2.

55
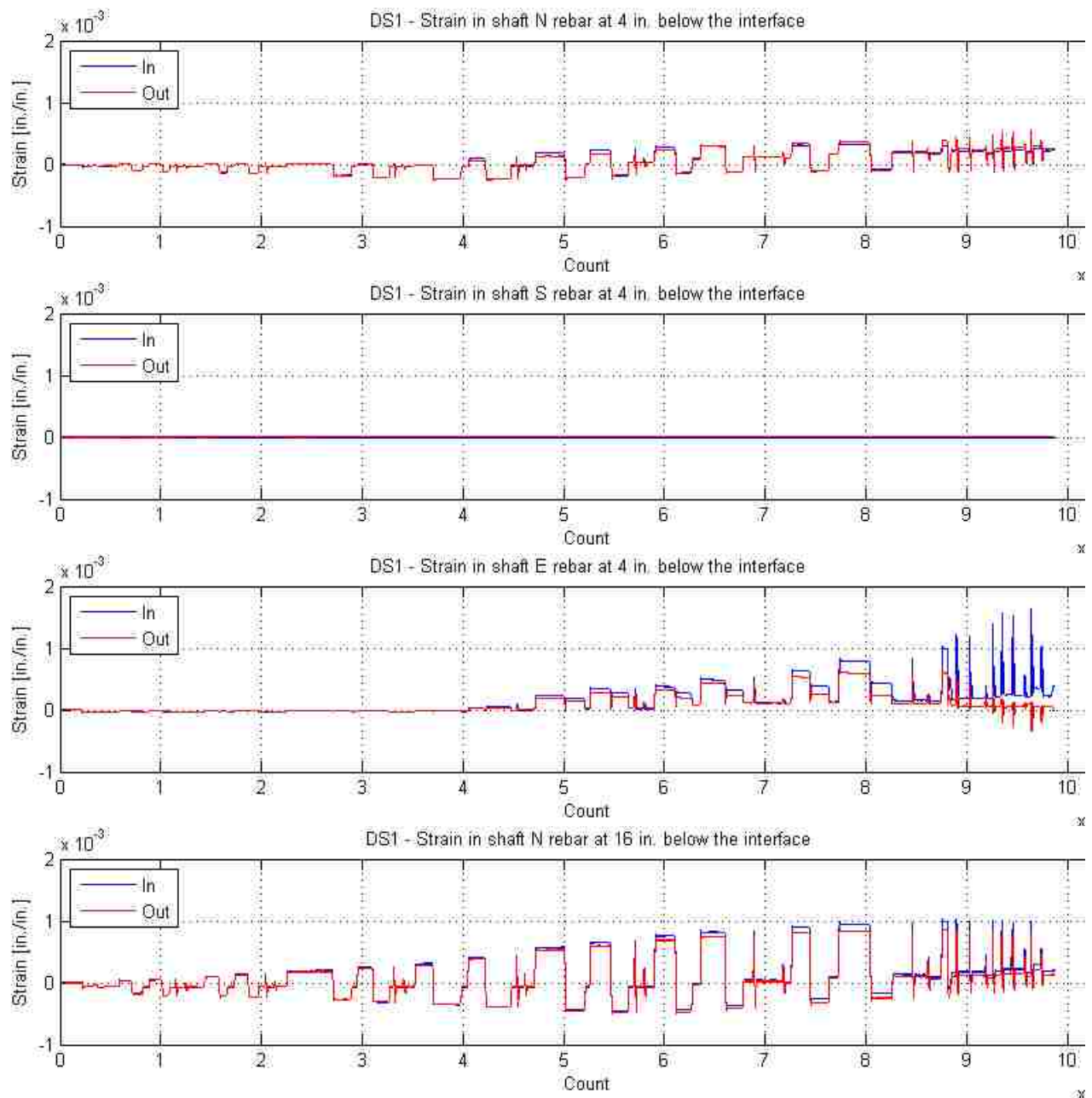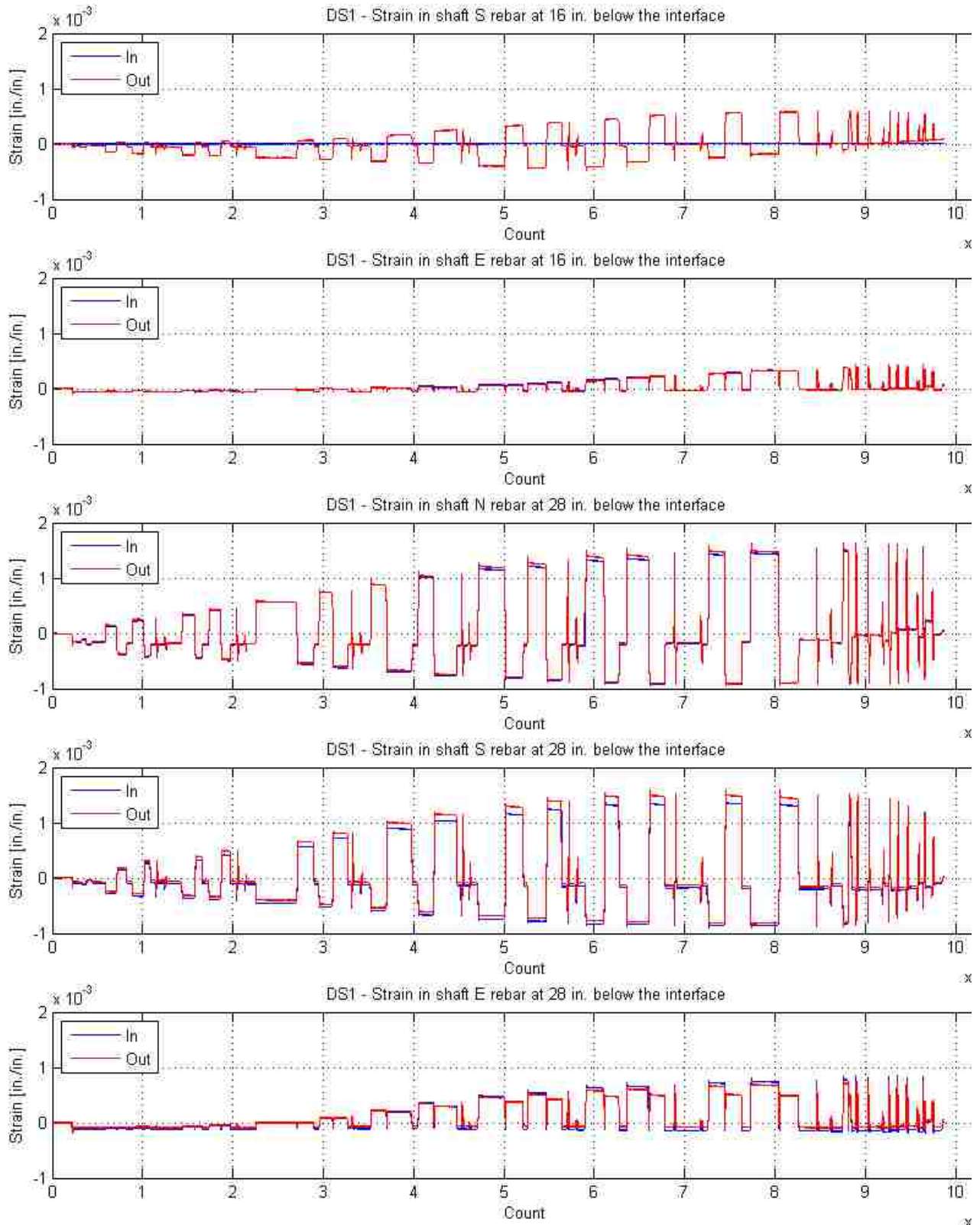
Figure 5-20. Strain in shaft reinforcing bars in specimen DS-1

DS2 - Strain in shaft N rebar at 4 in. below the interface

DS2 - Strain in shaft S rebar at 4 in. below the interface

DS2 - Strain in shaft E rebar at 4 in. below the interface

DS2 - Strain in shaft N rebar at 16 in. below the interface

DS2 - Strain in shaft S rebar at 16 in. below the interface

57
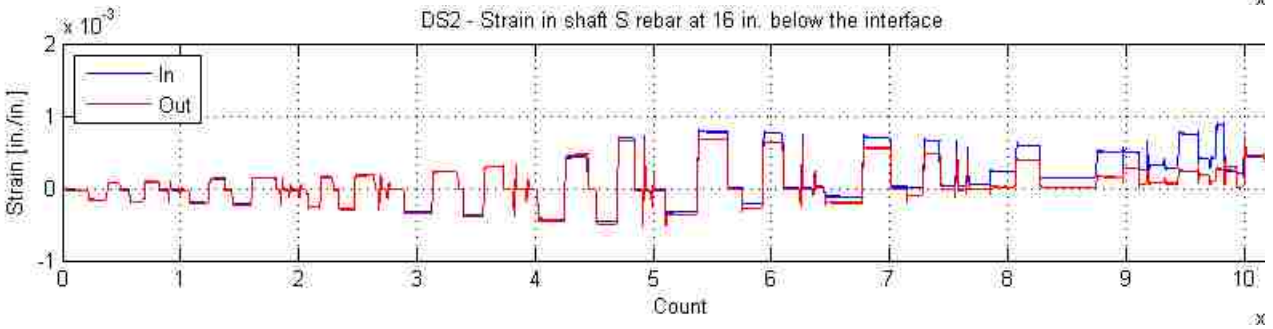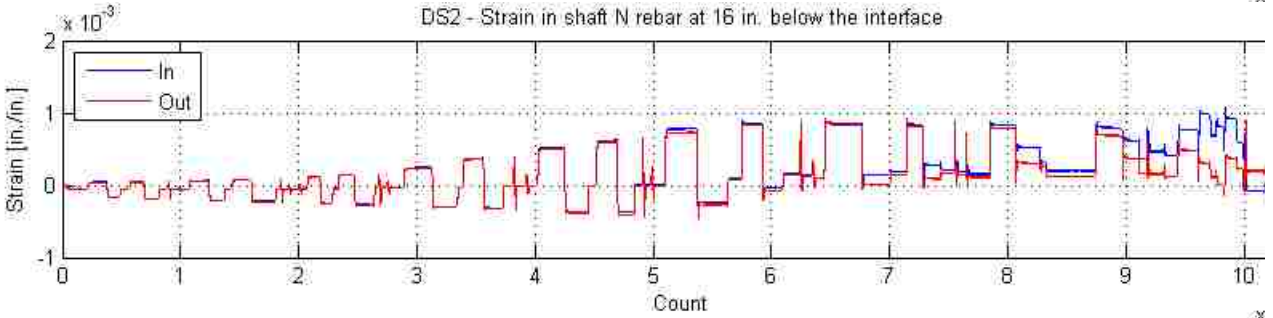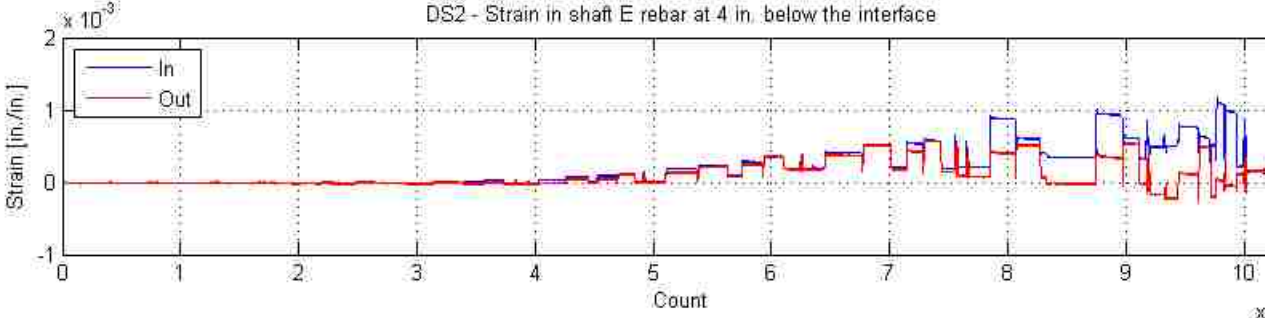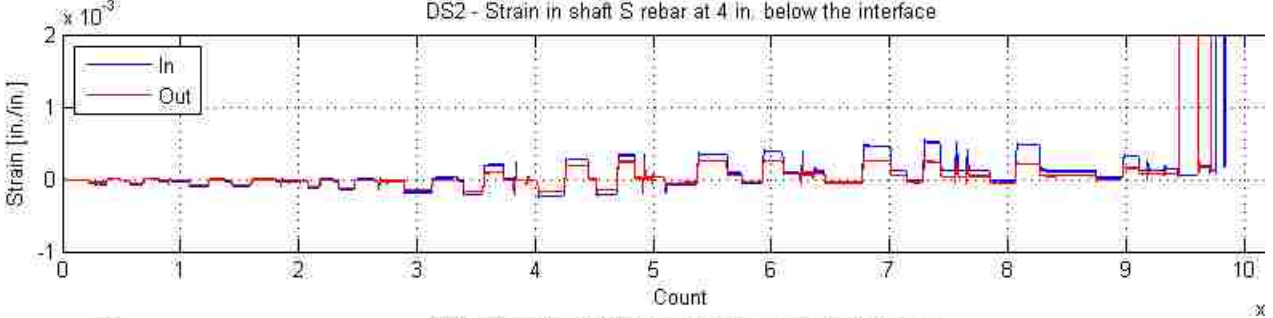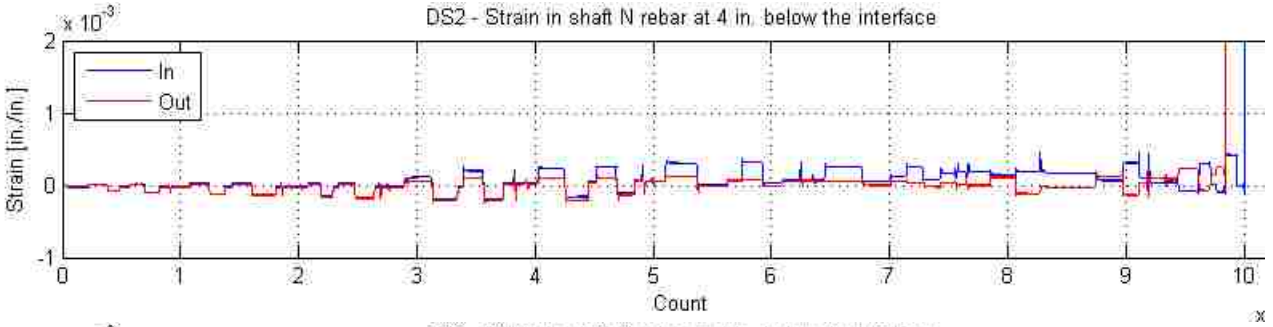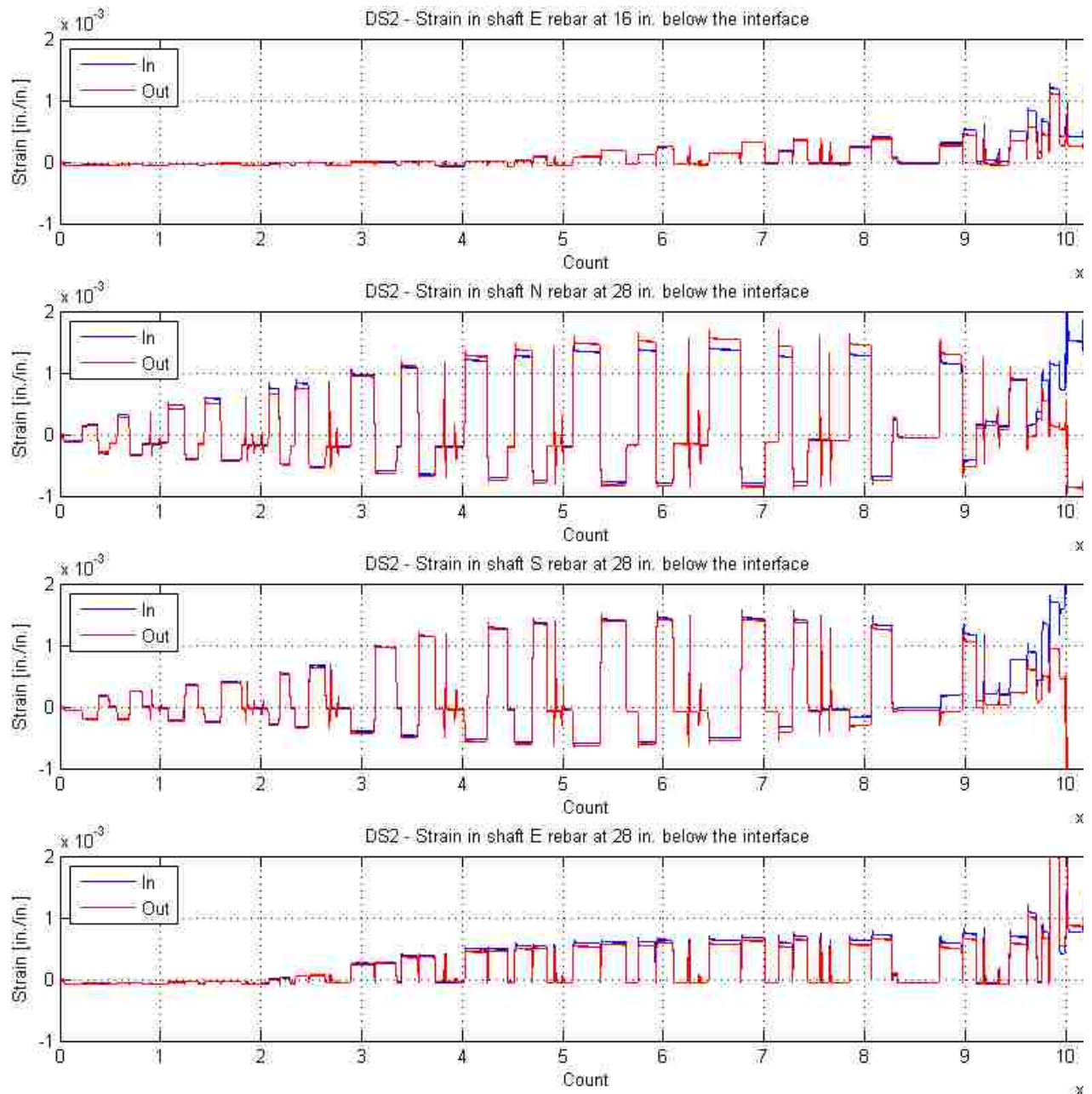
Figure 5-21. Strain in shaft reinforcing bars in specimen DS-2

The pattern of strains in the vertical bars of the shaft, 4 in. below the interface, is also consistent with the way that the shaft behaved. Before cycle 4-1 (0.7% drift, count = 29000), the shaft was essentially uncracked, so it behaved like a beam made from continuous, uncracked, material. Because the applied load consisted of both compression and bending, the vertical bar strains on the compression side were higher than the tension strains on the opposite side. However, when the shaft cracked (at cycle 4-1, 0.7% drift), the concrete could no longer resist

58

tension. Then the tension strain at the top of the shaft was higher than the comression strain on the opposite side. This change in the strain pattern, from high compression to high tension, is the one seen in the gauge records.

The strain distributions (the average of each pair of gauge readings) over the height of the North, South and East of shaft bars at various drifts for specimen DS-1 and DS-2 are shown in Figure 5-22. The strains were plotted up to 3.0% drift. Both specimens show similar strain profiles before 1.2% drift. Until 0.7% drift, tension strains at the top position (4in. below the interface) were nearly zero in both specimens. The compression strains were higher, about $200\mu\epsilon$. However, after 0.7% drift, the top of the shaft cracked vertically and diagonally, so the tension strain in the bars increased as explained above. After 1.2% drift, the strain profiles in specimens DS-1 and DS-2 were different. The tension strains increased when drift increased. However, the compression strains at 4 in. and 16 in. below the interface decreased. The compresion strain decreased gradually in specimen DS-1 and suddenly in specimen DS-2. This suggested that the friction between the column surface and the shaft reduced gradually in specimen DS-1 and was lost suddenly and almost completely in specimen DS-2 because the compression strain values dropped to nearly zero. The increasing of compression strain at 28 in. below the interface indicated that at this time, friction were still good at this position in both specimens DS-1 and DS-2.
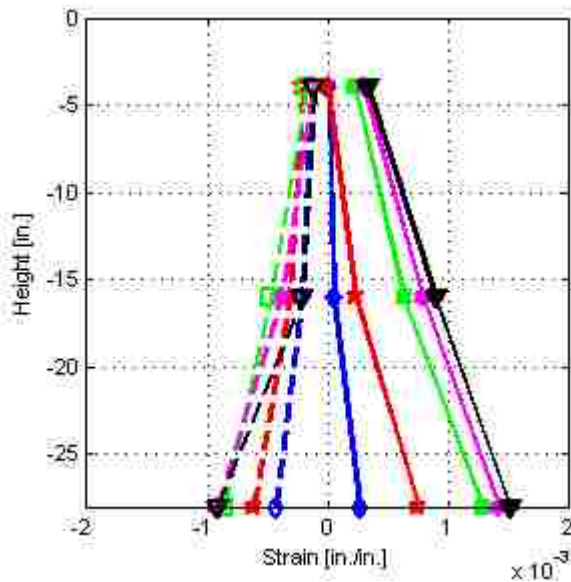
a). DS-1 – North reinforcing bar of shaft   b). DS-2 – North reinforcing bar of shaft

59
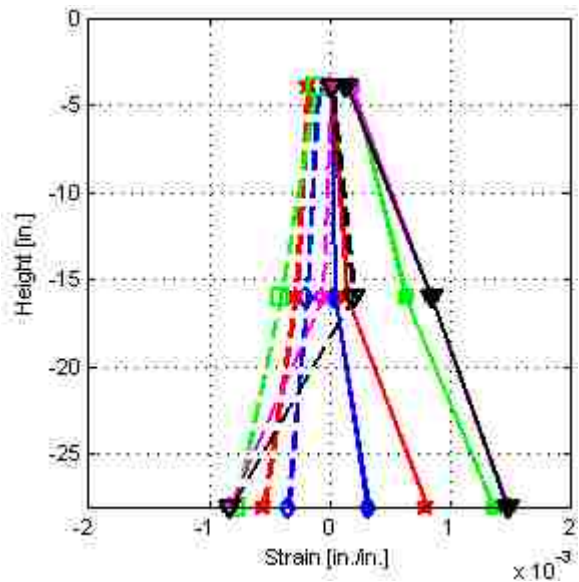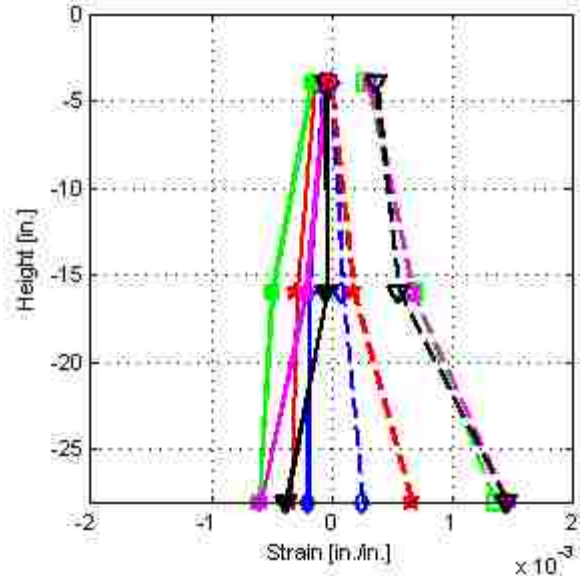
c). DS-1 – South reinforcing bar of shaft   d). DS-2 – South reinforcing bar of shaft
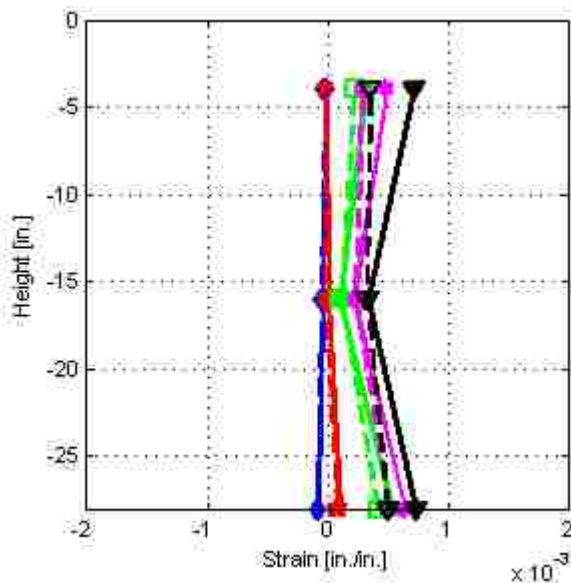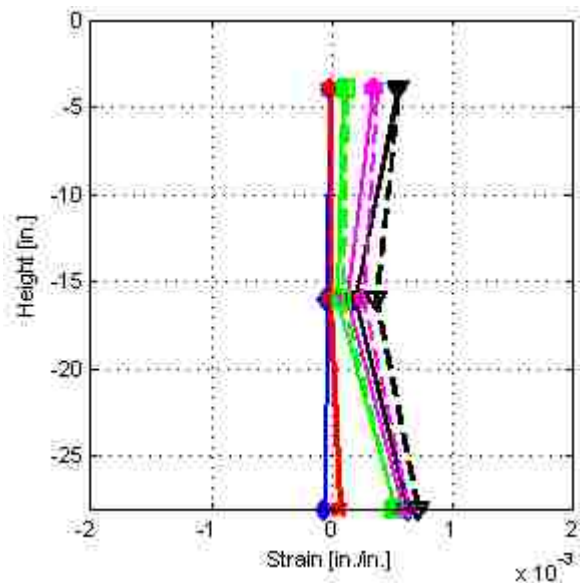
e). DS-1 – East reinforcing bar of shaft   f). DS-2 – East reinforcing bar of shaft

Figure 5-22. Strain profiles in the shaft reinforing bars

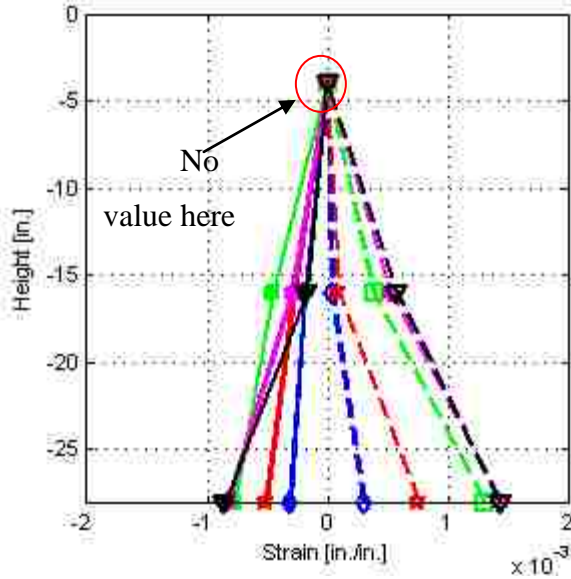Figure 5-23 shows the cyclic effective force-strain relationships of the shaft bars at 4 in., 16 in., and 28 in. below the interface, for specimens DS-1 and DS-2. In each plot, the cyclic effective force-strain relationship is plotted for the North, South and East bar in blue, green and purple. As illustrated in figures, the strain values in all gauges in the shaft reinforcing bars were

60

smaller than 0.002. This indicated that all the shaft reinforcing bars remained elastic through out the test.

At 4 in. below the interface, as shown in the figures, the strain gauges in South rebar in DS-1 were broken before testing. Up to 0.7% drift, the force-strain relationships in specimens DS-1 and DS-2 were similar. When the effective force reached 40 kips, the strains in the North, South and East reinforcing bars were about 25, 0 and $200\mu\epsilon$ respectively in both specimens. This illustrates that, in both specimens, the South bars were subjected to more compression when the effective force increased and the North reinforcing bars were subjected to more compression when the effective force decreased. The relationships had a line of symmetry through effective force Feff = 0. At Feff = 0, all the bar strains were about $-25\mu\epsilon$. Same as column rebar behavior, this suggested that the friction between the column surface and the shaft was still good. When the cyclic drift went from 0.7% to 4.6%, the relationships in DS-1 and DS-2 were also similar. As illustrated in figures, the comression strain in North rebar in specimen DS-1 and North and South rebar in DS-2 decreased while the tension strain increased after each cycle. This suggestted that at this time the shaft concrete was cracked in the top of the shaft, so the tensile force transferred to reinforcing bars.

At 16 in. below the column-shaft interface position, the behaviors were nearly the same as at the previous position. Until 1.5% drift the relationships in both specimens were similar. The North and South reinforcing bars were still transferred more compression. It can be recognized that the friction between the column surface and the shaft were still good in both specimen because the strain values at Feff = 0 were nearly $-50\mu\epsilon$. When drift went from 1.5% to 6.9% drift, the behavior in DS-1 and DS-2 were different. In DS-1, the strain values when Feff = 0 were increase a little bit indicated that the friction was decreased but still good. Therefore the compression strain in reinforcing bars were decreased gradually. The maximum effective forces remained about 60 kips. However, in DS-2, effective force decresed from about 50 kips to 35 kips. The strain value when Feff = 0 were not zero and increased after each cycle. It illustrated that At this period, concrete was cracked and cannot be subjected tension force. Therefore most of tension transferred to spirals. Thus, when the strain in spiral increased over yielding point, it would have residual strain. Consequently, there would have some force in reinforcing bars and spirals when the horizontal load was released to zero.

61

At 28 in. below the interface position, the relationships were plot up to 6.9% drift. As shown in the figures, the friction was still good and the reinforcing bars were still in the elastic ramge in DS-1. In DS-2, before 4.6% drift, the behavior was similar to in DS-1 specimen. The friction was good and reinforcing bars worked in elastic. However, after 4.6% drift, the friction was lost and spirals were broken, and the strains in rebar decreased dramatically.
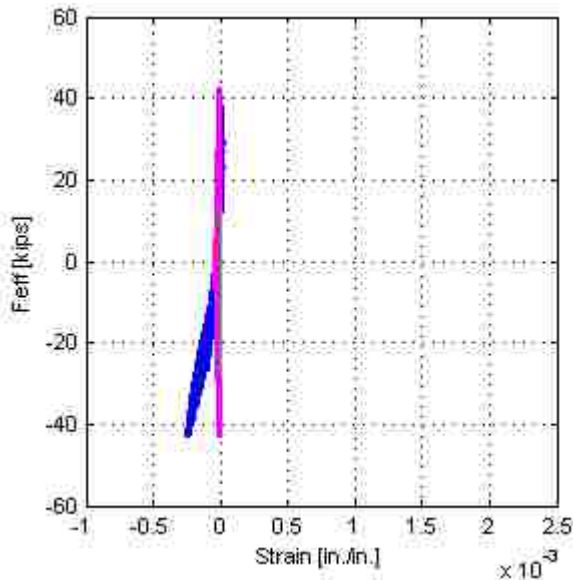
a).DS-1 – Top position (until 0.7% drift)
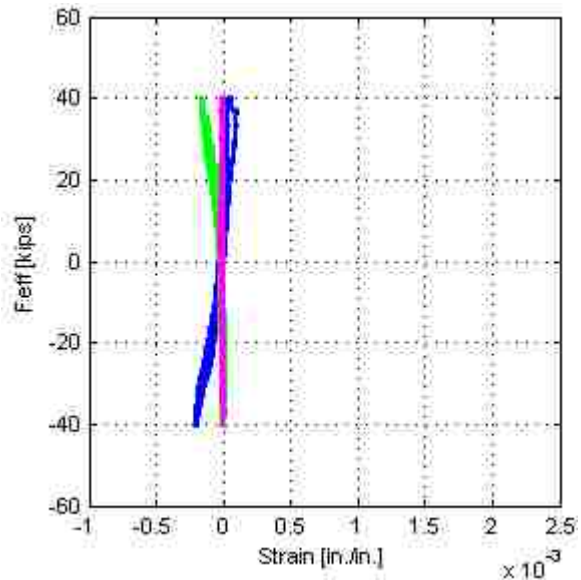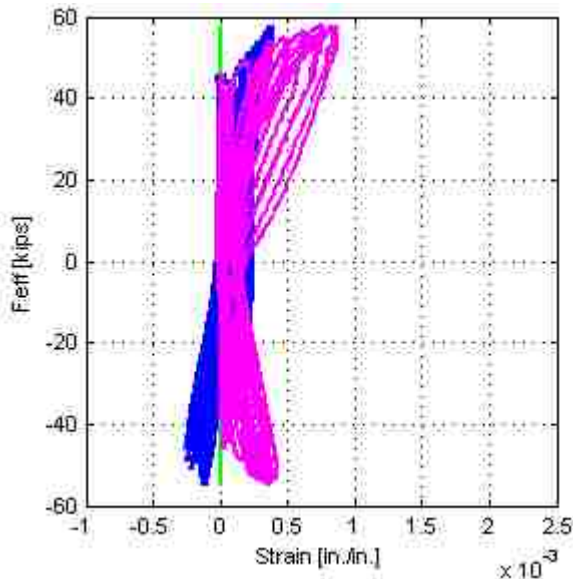
b).DS-2 – Top position (until 0.7% drift)

c).DS-1 – Top position (0.7%-4.6% drift)
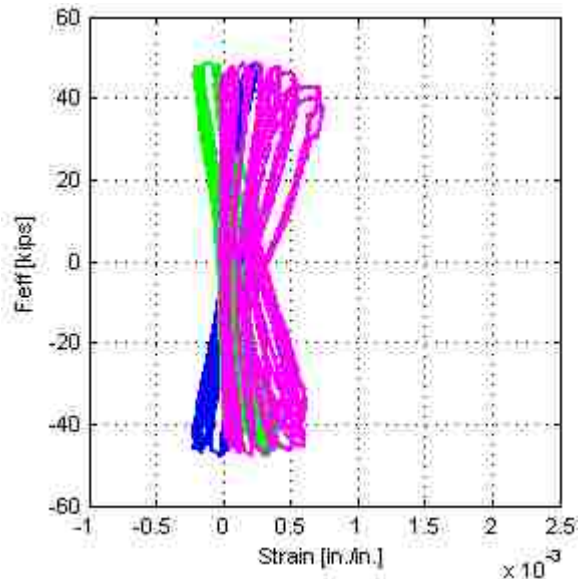
d).DS-2 – Top position (0.7%-4.6% drift)
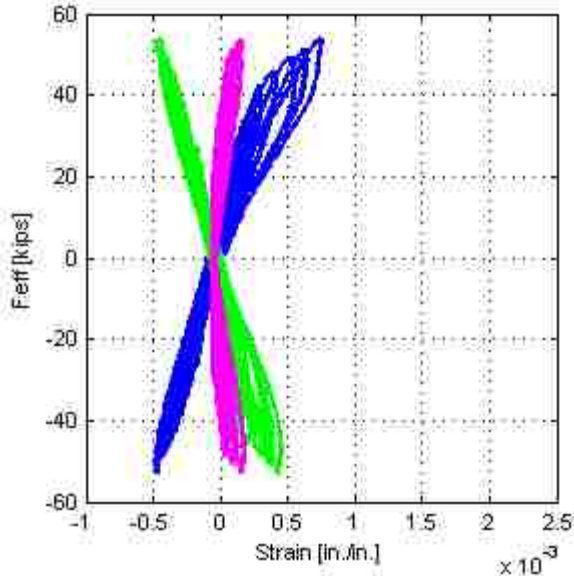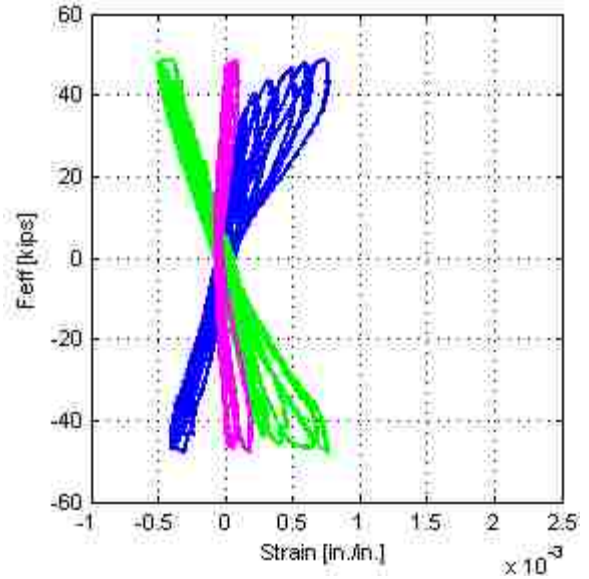
e).DS-1 – Middle position (until 1.5% drift)   f).DS-2 – Middle position (until 1.5% drift)
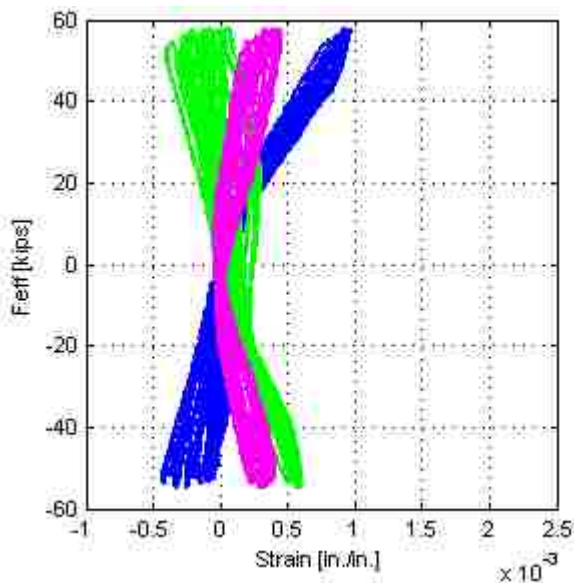
g).DS-1 – Middle position (1.5%-6.9% drift)   h).DS-2 – Middle position (1.5%-6.9% drift)

63

i).DS-1 – Bottom position (until 6.9% drift)   j).DS-2 – Bottom position (until 6.9% drift)

N-rebar   S-rebar   E-rebar
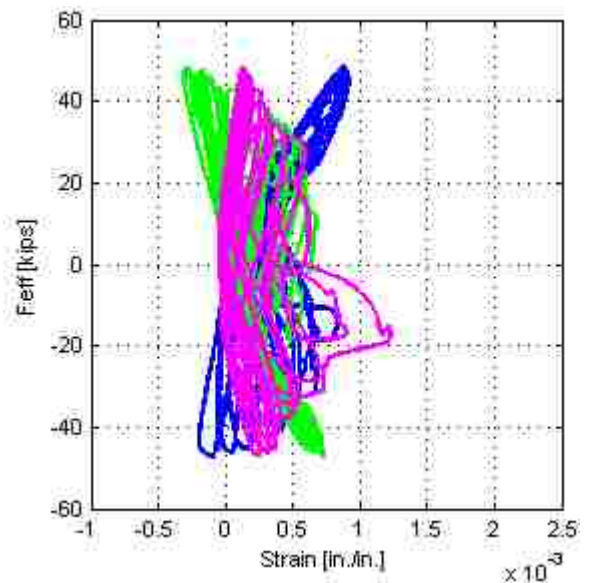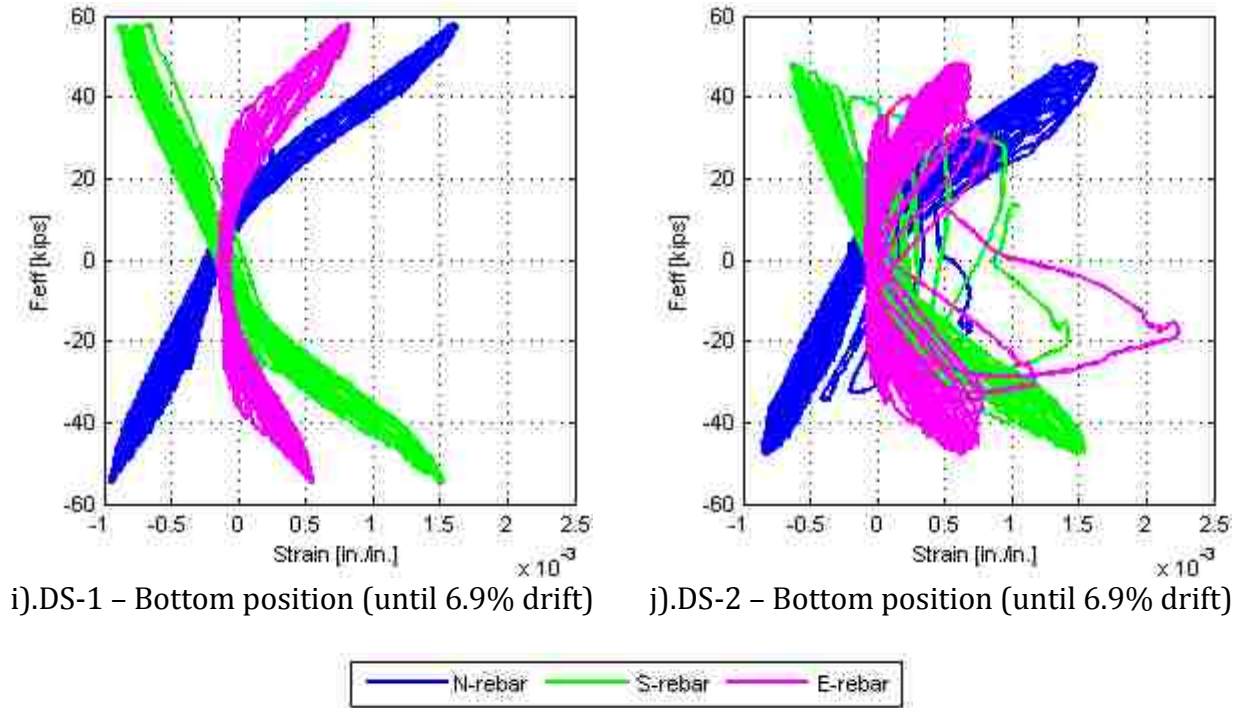
Figure 5-23. Strain-Effective force relationship of the shaft reinforcing bars

5.7 Strains in Shaft Spirals

The shaft spirals were gauged as described in Figure 5-19. Because of the symmetry of the column longitudinal bars, only the East and South sides were gauged. In both specimens, gauges were attached on the spirals at three locations close to those of the gauges on the vertical bars, 4 in., 16 in. and 28 in. below the interface of the shaft and column. At each place, only 1 strain gauge was used.

The strains in the shaft spiral are shown in Figure 5-24. Because all three gauges on the South side of Specimen DS-1 were broken before testing, only the spiral strains on the East side in DS-1 and on the East and South sides in DS-2 were plotted.

The overall trends were:

- In both specimens, the strains in the spiral were tensile regardless of the direction of loading.
- In both specimens, the strains were much larger at the top of the shaft than in the middle or bottom.

64

- The spiral in specimen DS-1 just reached the yield point. However, in specimen DS-2, the spiral first yielded at the top at 3% drift and fractured at 6.9% drift.
- The strain was slightly larger at the South gauge than at the East gauge, at any drift ratio, in Specimen DS-2. That comparison was not possible in Specimen DS-1 because no data were available from the South gauges.

The fact that the strains in specimen DS-2 were higher than those in specimen DS-1 is consistent with the lower spiral steel ratio in specimen DS-2.

As illustrated in figures, up to 3.0% drift, in specimen DS-1, tension strain increased at the top position after each cycle and reach 0.002 at 3.0% drift. Whereas, at the middle position, strain were in compression and increased a little until 3.0% drift. At the bottom position, strain were nearly zero. However, spiral strain in specimen DS-2 were different. All strain value were in tension at 3.0% drift. At the top position, the strain were in tension and increased after each cycle like in DS-1. But the value were higher. The max strain on East side was about 3.4e-3 and on South side was 4.7e-3. At middle position, until 2.0% drift, strain was nearly zero on East side and increased to 0.4e-3 at 3.0% drift. On the South side, strains increased in tension after each cycle and reached 1.25e-3 at 3.0% drift. At the bottom position, max strains were about 0.2e-3. This different behavior between specimens DS-1 and DS-2 suggested that until 3.0% drift, friction between column and shaft was lost from the interface position to some position above the mid-position (16 in. below the interface) in DS-1. However, in specimen DS-2, friction was lost at position below the mid-position.
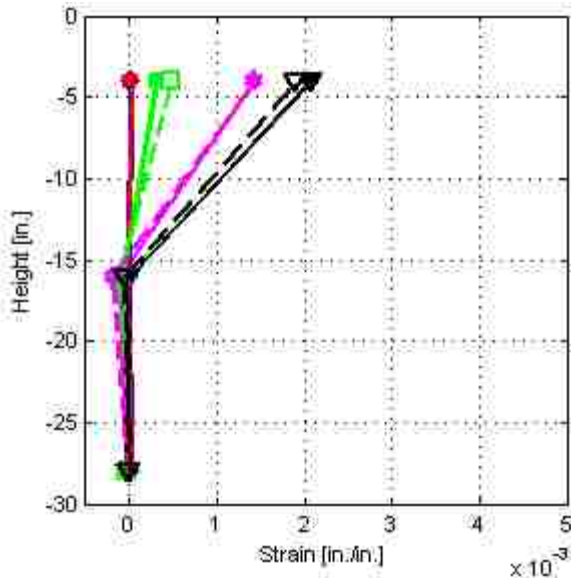
a). DS-1 – East side
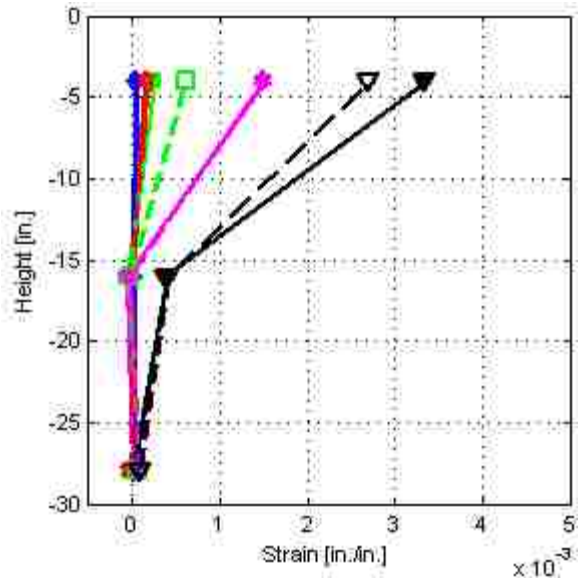
b). DS-2 – East side
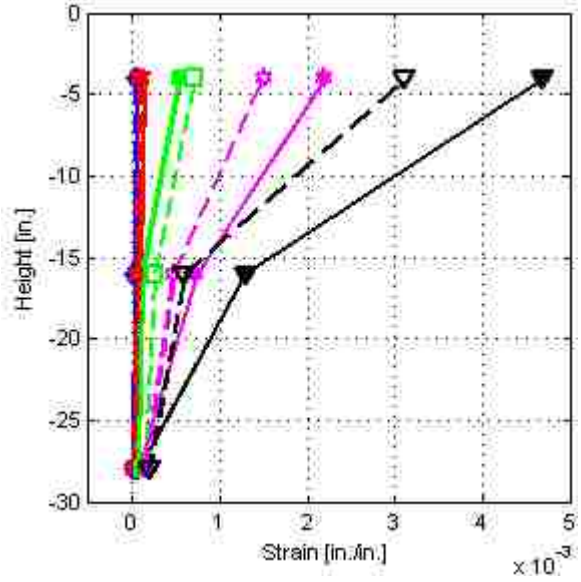
c). DS-2 – South side
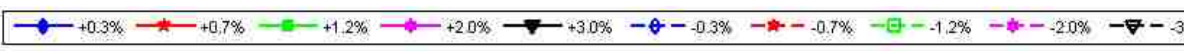
Figure 5-24. Strain in shaft spiral

66

www.manaraa.com

6 DATA ANALYSIS

In bridges designed by WSDOT, the diameter of a drilled shaft is larger than that of the column that it supports. The splices between the longitudinal bars in the transition region are therefore non-contact splices, and special design requirements are necessary. McLean et al. (1997) proposed a model for such a splice, and a modified version of it has been incorporated by WSDOT into the Bridge Design Manual (BDM). However, the predictions of the modified model are not consistent with the test results from specimens DS-1 and DS-2. Therefore, a new conceptual model was developed to describe the observed behavior of the column-to-shaft "socket" connection.

First, the overall statically determinate test assembly is analyzed to give some guidance on parameters for design. Then a simple strut-and-tie model is proposed to determine the amount of lateral reinforcement required in the connection. The proposed model is simple, easy to use in design, and consistent with the data from the two tests. However, because it is based on evidence from only two tests (DS1 and DS2), it cannot be guaranteed to provide correct predictions in all cases, and further testing is needed to support its use on a wider basis.

6.1 Non-contact lap splices models

McLean et al. (1997) proposed both two-dimensional and three-dimensional models. These models are based on the truss analogy to represent the force transfer mechanism within a splice.

Figure 6-1 illustrates a 2-dimential representation of the force transfer between non-contact longitudinal bars. The transverse reinforcement is determined from the following equation:

$$\frac{A_{tr}}{s_{tr}} = \frac{A_l f_{ul}}{f_{yt} l_s \tan \theta} \tag{6-1}$$

where,

A_{tr} =   area of shaft transverse reinforcement or spiral (in.^{2})

A_l = total area of longitudinal column reinforcement (in.^{2})

f_{yt} = specified minimum yield strength of shaft transverse reinforcement (ksi)

f_{ul} = specified minimum tensile strength of column longitudinal reinforcement (ksi), 90 ksi for A615 and 80 ksi for A706

l_s = Class C tension lap splice length of the column longitudinal reinforcement (in.)

s_{tr} = spacing of shaft transverse reinforcement (in.)

θ = inclination angle of the strut (degree or rad)

Equation (6-1) indicates that a longer splice requires less spiral and vice versa. For the special case of the case $\theta = 45°$, the equation becomes:

$$\frac{A_{tr}}{s_{tr}} = \frac{A_l f_{ul}}{f_{yt} l_s} \tag{6-2}$$
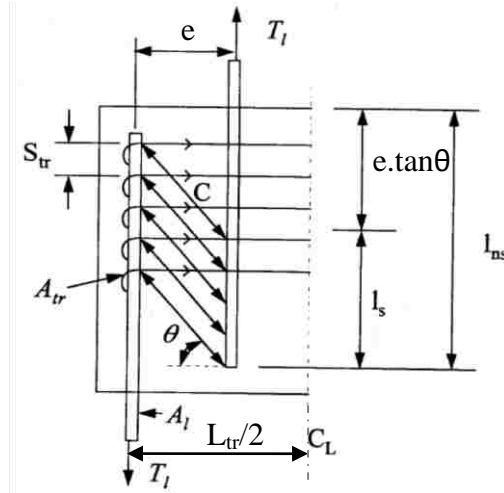
Figure 6-1. Proposed two-dimensional behavioral model for non-contact lap splices.

There is no unique definition for the optimum value of θ to be used. One possible criterion is to use the θ that minimizes the total volume of steel, including both longitudinal and transverse, required in the splice. It is given by:

$$VOL_s = 2A_l l_{ns} + \frac{A_{tr} l_s}{s_{tr}} L_{tr} \tag{6-3}$$

68

where,

$$l_{ns} \quad = \quad \text{total noncontact lap splice length}$$

$$= \quad l_{ns} = l_s + e.\tan\theta$$

$$L_{tr} \quad = \quad \text{distance between the outer bars}$$

Substituting eq. (6-2) into eq. (6-3), we obtain:

$$VOL_s = 2A_l(l_s + e.\tan\theta) + \frac{A_l f_{ul}}{f_{yt}\tan\theta}L_{tr} \tag{6-4}$$

The value of V_s can be minimized by differentiating with respect to θ and setting the result to zero:

$$VOL'_s(\theta) = 2A_l e(1 + \tan^2\theta) + \frac{A_l f_{ul} L_{tr}}{f_{yt}}\left(-1 - \frac{1}{\tan^2\theta}\right) = 0$$

$$2A_l e \tan^4\theta + \left(2A_l e - A_l L_{tr}\frac{f_{ul}}{f_{yt}}\right)\tan^2\theta - A_l L_{tr}\frac{f_{ul}}{f_{yt}} = 0$$

$$\tan\theta = \sqrt{\frac{L_{tr}}{2e}\frac{f_{ul}}{f_{yt}}} \qquad with\ \theta \in (0°, 90°) \tag{6-5}$$

$$VOL_{s,min} = 2A_l\left(l_s + \sqrt{2eL_{tr}\frac{f_{ul}}{f_{yt}}}\right) \tag{6-6}$$

The relationship of the total volume of steel used in the splice, VOL_s, and the inclination angle of the strut, θ, is illustrated in Figure 6-2 using the nominal properties of the splice in the test specimens:

$$f_{ul} = 90\ ksi \qquad\qquad f_{yt} = 60\ ksi \qquad\qquad A_l = 10 \times 0.31 = 3.1\ in.^2$$

$$l_s = 22\ in. \qquad\qquad e = 4\ in. \qquad\qquad L_{tr} = 26\ in.$$

69
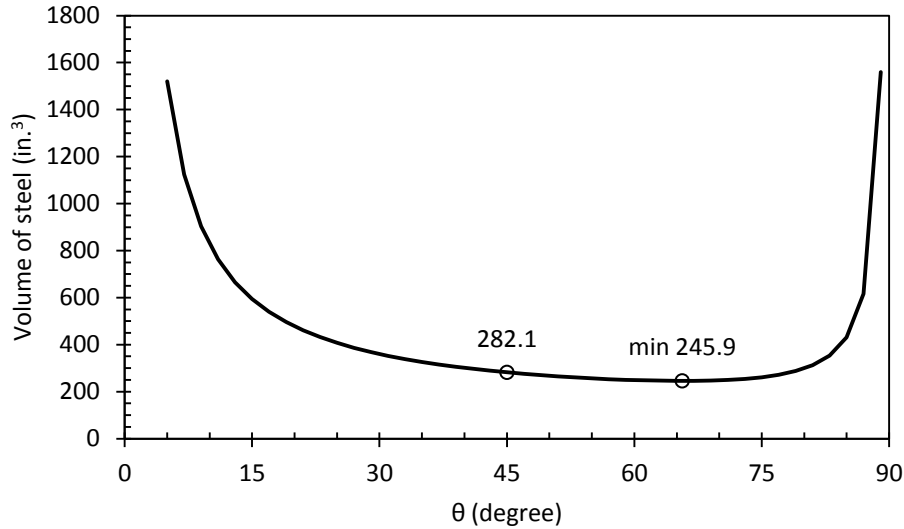
Figure 6-2. (Total steel volume in a splice vs. inclined angle of struts) relationship

At $\theta = 45°$, the volume of steel in the splice is given as:

$$V_{s,45} = 2A_l \left(l_s + e + \frac{L_{tr}}{2} \frac{f_{ul}}{f_{tr}} \right) = 282.1 \; in.^3$$

$$V_{s,min} = 245.9 \; in^3 \quad at \quad \theta = 65.6°$$

$$\frac{V_{s,45}}{V_{s,min}} = \frac{282.1}{245.9} = 1.15$$

This analysis and Figure 6-2 show that the minimum is very flat; even quite a large change in θ makes little difference to the total steel volume.

The foregoing model of a non-contact splice is two-dimensional and applies to rectangular tied columns. For a circular column, a three-dimensional model is needed, and one is illustrated in Figure 6-3.

It, too, is taken from MacLean et al. (1997), and addresses loading in pure tension, rather than bending.

70
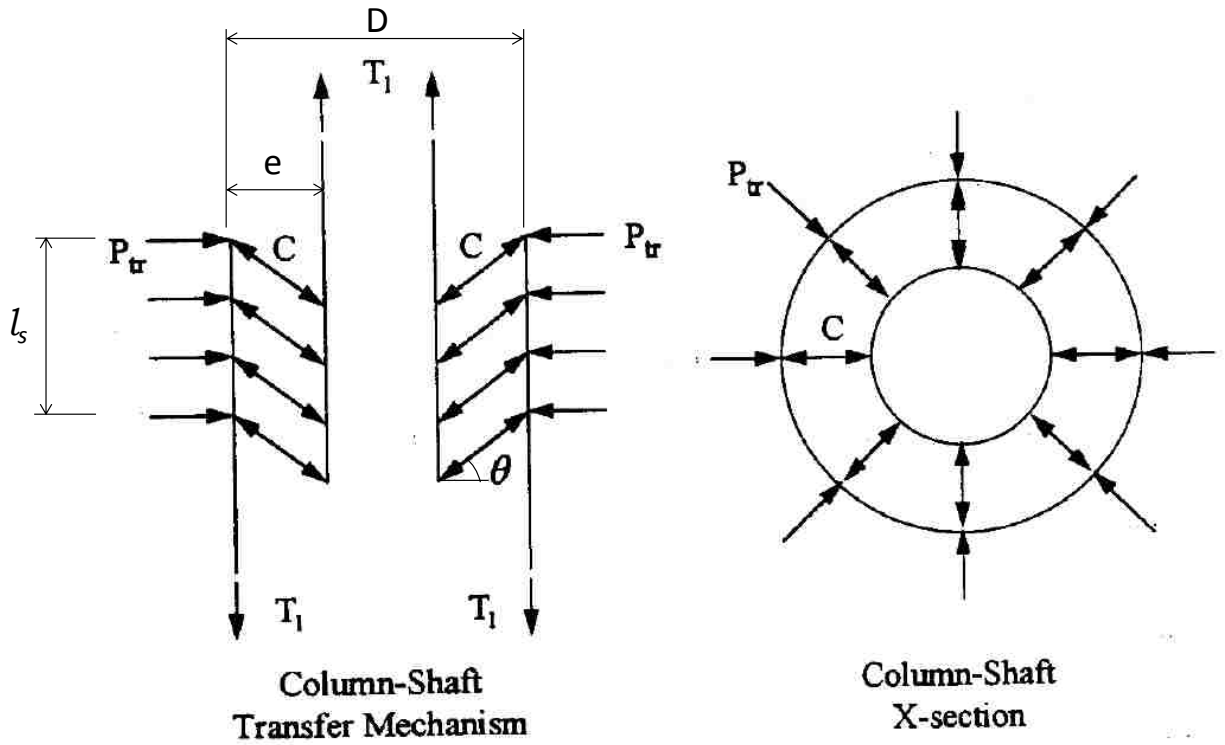
Figure 6-3. Proposed three-dimensional behavioral model for non-contact lap splices (McLean et al. 1997)

The area of spiral reinforcement required in the transition region of the column-to-shaft connection, in order to fully develop the column reinforcing bars, is determined as:

$$\frac{A_{tr}}{s_{tr}} = \frac{A_l f_{ul}}{2\pi f_{yt} l_s \tan\theta} \tag{6-7}$$

The total volume of steel, including both longitudinal and transverse, used in the splice is determined as:

$$VOL_s = 2A_l l_{ns} + \frac{A_{tr} l_s}{s_{tr}}\pi D \tag{6-8}$$

Substituting eq. (6-7) into eq. (6-8), we obtain:

71

$$VOL_s = 2A_l(l_s + e.\tan\theta) + \frac{A_l f_{ul}}{2\pi f_{yt}\tan\theta}\pi D$$

$$= 2A_l(l_s + e.\tan\theta) + \frac{A_l f_{ul}}{f_{yt}\tan\theta}\frac{D}{2} \tag{6-9}$$

where,

D = diameter of shaft spiral (in.)

The minimum steel volume VOL$_s$ is given by:

$$VOL_{s,min} = 2A_l\left(l_s + \sqrt{eD\frac{f_{ul}}{f_{yt}}}\right) \tag{6-10}$$

$$at \qquad \tan\theta = \sqrt{\frac{D}{e}\frac{f_{ul}}{f_{yt}}} \qquad with\ \theta \in (0°, 90°) \tag{6-11}$$

For properties of

$f_{ul} = 90\ ksi$ $\qquad\qquad$ $f_{yt} = 60\ ksi$ $\qquad\qquad$ $A_l = 10 \times 0.31 = 3.1\ in^2$

$l_s = 22\ in.$ $\qquad\qquad$ $e = 4\ in.$ $\qquad\qquad$ $D = 26\ in.$

θ becomes

$$\theta_{min} = 57.4°$$

At $\theta = 45°$, the volume of steel in the splice is given as:

$$VOL_{s,45} = 221.7\ in^3$$

$$VOL_{s,min} = 213.8\ in^3$$

$$\frac{VOL_{s,45}}{VOL_{s,min}} = \frac{221.7}{213.8} = 1.04$$

72

The 3-dimensional model was developed for a column in pure tension, in which all the bars are subjected to equal tension stress. In a column subjected to combined compression and bending, only some of the bars are in tension. Therefore, the model was modified by WSDOT before inclusion in to the WSDOT BDM as follows:

$$\frac{A_{tr}}{s_{tr,max}} = \frac{kA_l f_{ul}}{2\pi f_{yt} l_s} \qquad (6\text{-}12)$$

where:

k = factor representing the ratio of column tensile reinforcement to total column reinforcement at the nominal resistance.

The ratio, k, is to be determined from column moment-curvature analysis or, as a default, taken as k = 0.5.

In tests DS-1 and DS-2, the length of splices was chosen as 28 in. The spiral used in the splices was designed using the above eq. (6-12) in Specimen DS-1 and was reduced by half in Specimen DS-2. However, the measured strains from the gauges on the spirals of Specimen DS-1, shown in Figure 5-24a, showed that the spirals at mid-height and the bottom of the transition experienced almost no stress. Most of the transverse strain was concentrated in the top part of transition region. Figures 5-24b and c also provide the same information for Specimen DS-2, in which the spiral strain was much the largest at the top and almost zero at the bottom. These data are inconsistent with the predictions of the models based on MacLean et al., because they depend on the assumption that the spirals are fully stressed over the entire length of the splice.

6.2 Column moment-curvature analysis

To develop a method for column-shaft connection design, the distribution of longitudinal bar stresses round the column was needed. It was found using moment-curvature analysis. The validity of the analysis was confirmed by comparing the predicted and measured moments. Moment-curvature analysis was conducted using an in–house University of Washington program (Stanton 2010). Two analyses were conducted, each with different material properties, and compared with test data from Specimen DS-1.

The concrete model used in the program is based on the one proposed Kent and Park (1971) and is illustrated in Figure 6-4. Note that tension stress and strain are positive. It consists of a parabolic rising curve, followed by a linear falling segment, then a constant stress extending to infinite strain. In the program, the initial parabolic curve is replaced by a cubic, which allows the user to specify E_{c0}, ε_{c0} and f'_c independently. It defaults to the original parabolic curve if E_{c0} is chosen to be $f'_c/(2\varepsilon_{co})$. The strain at peak stress, $\epsilon_{cc} = 0.002$. However, here the values of the confined concrete strength, $f_{cc} = 8\ ksi$, and the ultimate compression strain, $\epsilon_{cu} = 0.009$, were generated from the properties of the confinement reinforcement using Mander's formula (Mander et al. 1988; Priestley et al. 1996), rather than using the values recommended by Kent and Park.

The steel model in the program contains three regions: elastic, a yield plateau, and a curved strain-hardening region. In the first analysis the expected steel reinforcement properties were used, in accordance with the *AASHTO Guide Specifications for LRFD Seismic Bridge Design (2009)*. These recommendations ($f_y = 68\ ksi; \epsilon_{sh} = 0.015; f_u = 95\ ksi$) are based on data collected by Caltrans. The steel properties in the second analysis were based on the measured reinforcement properties for these tests ($f_y = 68\ ksi; \epsilon_{sh} = 0.0027; f_u = 106\ ksi$). The stress-strain curves for the reinforcing steel and concrete, and resulting moment-curvature relationships, are shown in Figure 6-4 and Figure 6-5. The flexural strengths from the two analyses and Specimen DS-1 are shown in Table 6-1.

Table 6-1. Comparision of peak column moment

Analysis 1 (expected properties) [kip-in.]	Analysis 2 (measured properties) [kip-in.]	Measured (Specimen DS-1) [kip-in.]
3507	3530	3476

The moments predicted by both analyses give values close to the measured peak moment. These results suggest that the differences in longitudinal reinforcement properties do not affect the flexural strength of the column. Both analyses give the ultimate flexural strength at the curvature value of 0.0065. However, when curvature increases from about 0.0005 to 0.002, the moments in two analyses are different. This occurs because, at those curvatures, the reinforcement strain in analysis 1 reaches the yield plateau region, whereas, the reinforcement

74

strain in analysis 2 starts going to the strain-hardening region. Thus, the tension force in reinforcement in analysis 2 is larger than in analysis 1, so the moment in analysis 2 is higher. Later, when the reinforcement strain reaches the fracture point, the difference in stress between in analysis 1 and 2 is small. Therefore the moments of column are equal in both analysis.
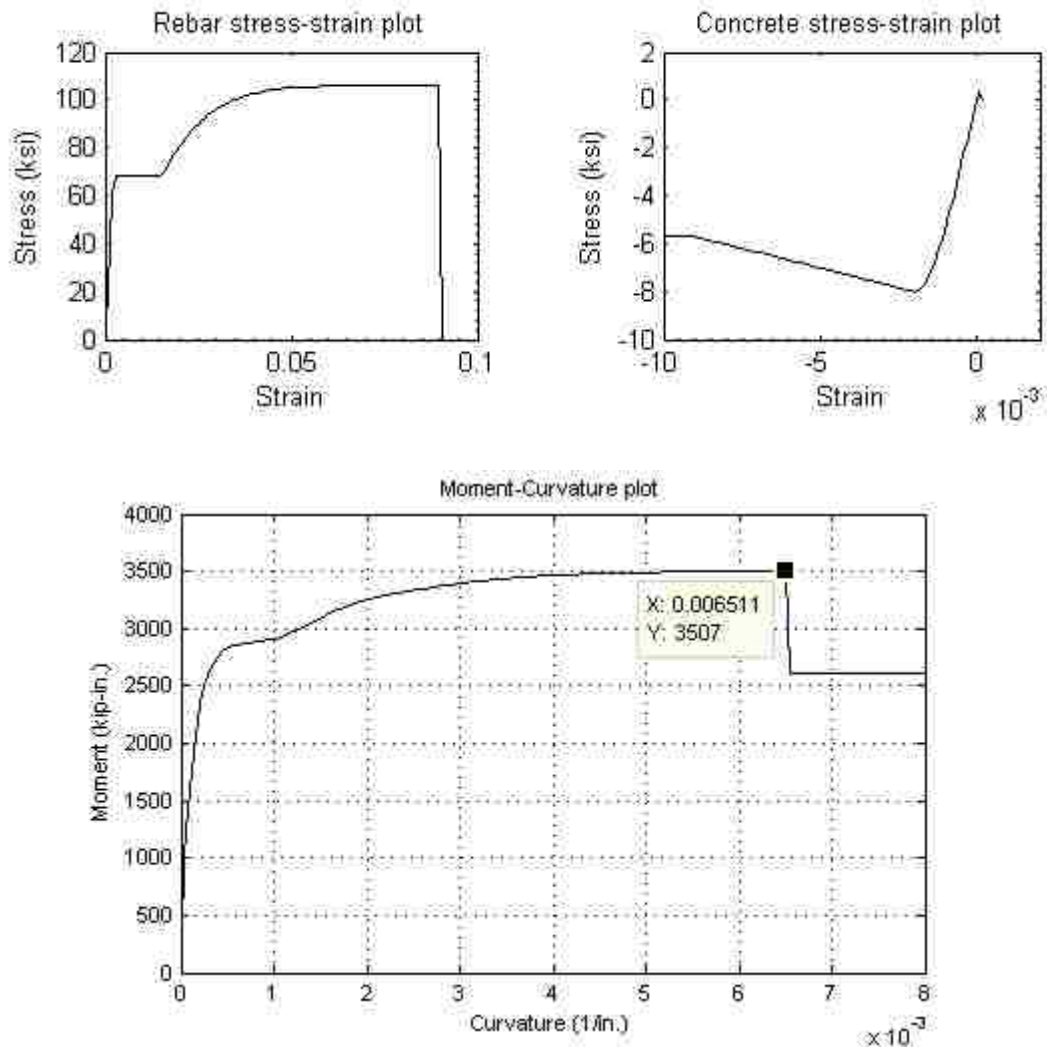
Figure 6-4. Moment-curvature analysis (based on expected material properties)
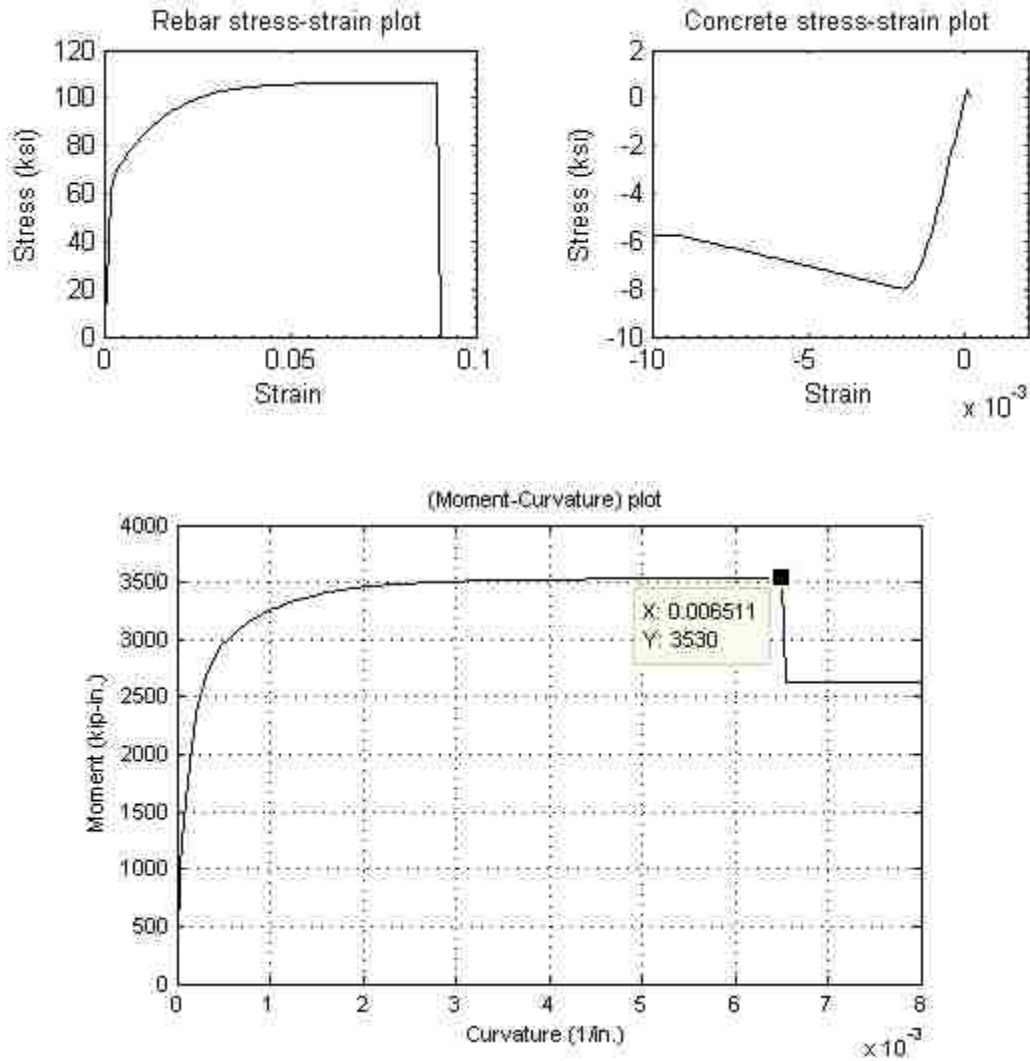
Figure 6-5. Moment-curvature analysis (based on measured material properties)

Table 6-1 compares the measured and predicted peak moments. For a more detailed comparison, Figure 6-6 and Figure 6-7 show a plot of moment vs. strain in the extreme tensile reinforcement, and gives the measured values for specimens DS-1 and DS-2 and the values predicted by the moment-curvature analyses. The curves were plotted up to the peak strain measured in the tests, of about 0.011 (At larger strains, the gages continue to read but the data acquisition system saturates, and simply displays the saturation strain). All curves include two regions: an elastic region and a curved post-yield region.

76
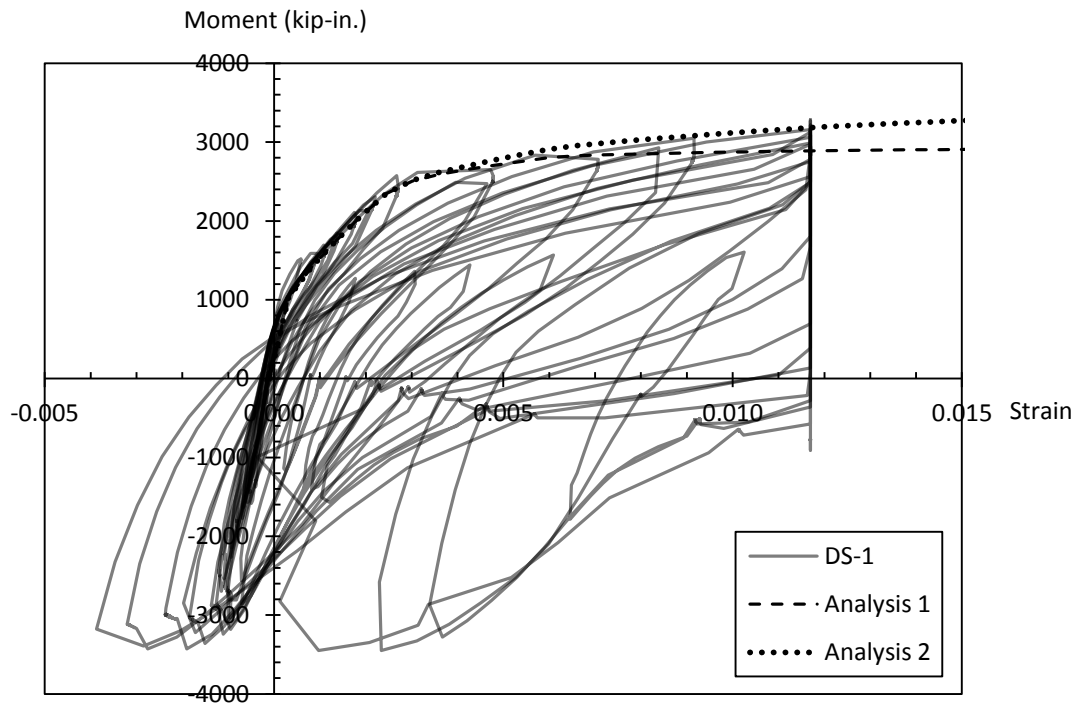
Figure 6-6. Moment-extreme reinforcement tensile strain relationship for column (in DS-1)
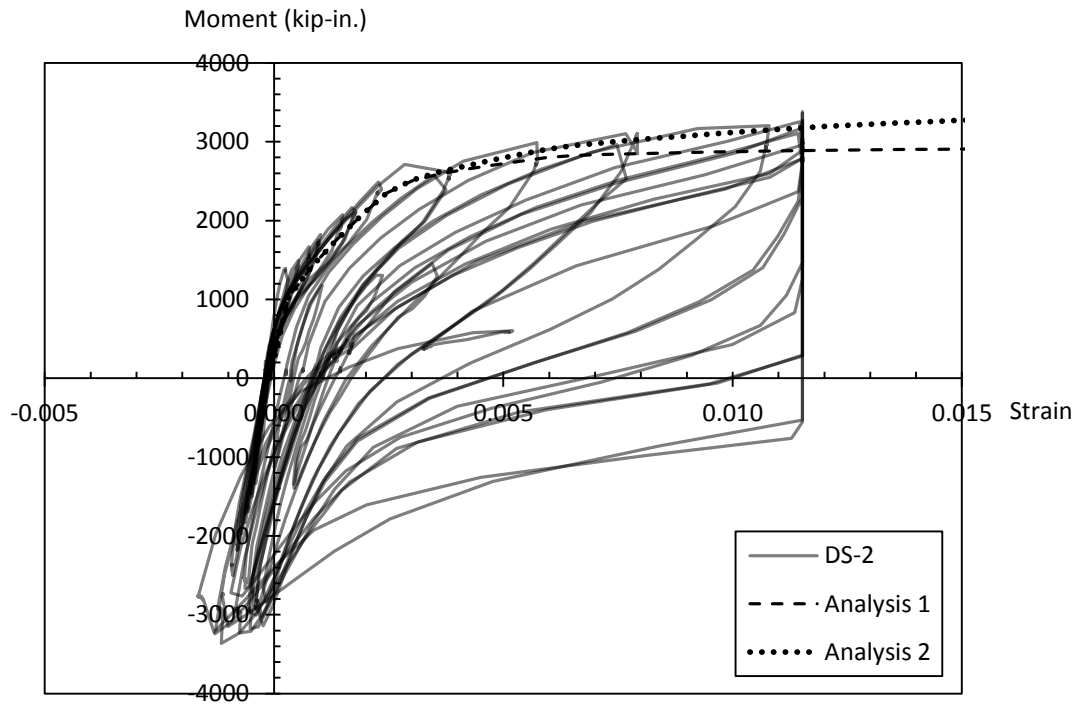
Figure 6-7. Moment-extreme reinforcement tensile strain relationship for column (in DS-2)

77

The measured moments for a given strain in both specimens DS-1 and DS-2 are remarkably similar to the ones predicted by analysis 2, which used measured reinforcement properties. The moments in the post-yield region in analysis 1, using expected reinforcement properties, are smaller than the measured ones. At a strain of 0.0115, the measured moment is approximately 10% higher than the predicted one in analysis 1. The cause of discrepancy, as mentioned above, is because of the yield plateau region of the expected steel model. In the confined concrete model, the strain at peak stress, ϵ_{cc} is given as 0.002 instead of 0.0034 as in Mander's formula. If Mander's formular is used here, the predicted moments in the yield region in analysis 1 and 2 are approximately 10% and 20% smaller than the measured ones, respectively. It suggests that Mander's confined concrete model is inconsistent with these tests DS-1 and DS-2.

The shaft longitudinal reinforcement strain was smaller than 0.002 during the testing, so the shaft remained elastic. Figure 6-8 shows the relationship between moment at the base of the shaft and tensile strain in the extreme longitudinal reinforcement in the shaft at three different levels. The figure includes measured data from specimens DS-1 and DS-2 and moments predicted using measured material properties and strains at the bottom of the shaft. The analysis is comparable to Analysis 2 for the column, but used the shaft geometry. Note that the jump in the predicted curve at about 2400 in-kips indicates first cracking.

Several features are evident.

For a given moment at the base of the shaft, the strains in the longitudinal shaft bars are largest at the bottom and smallest at the top. This is as expected because it follows the trend of the moment diagram.

The measured strains from specimens DS-1 and DS-2 are remarkably similar. This similarity reflects the fact that, early in the load sequence, the load-deflection curve of the two specimens were very similar.

The measured strains are smaller than the predicted ones. This is the opposite of what might be expected, for several reasons. First, application of a strain gage involves some grinding and sanding of the bar, which inevitably reduces its area. For a given bar force, the measured strain is therefore likely to be *higher* than that obtained by dividing the nominal stress by E.

78

Second, reinforcing bars tend to have areas that are, on average, less than the nominal value, but they have a higher true f_y to compensate. But, because the Young's modulus is essentially unchanged, this tendency should be expected to lead to measured strains that are, again, higher than those predicted from the nominal material properties. Last, the bars are elastic, so increases in the yield strength cannot explain the difference.
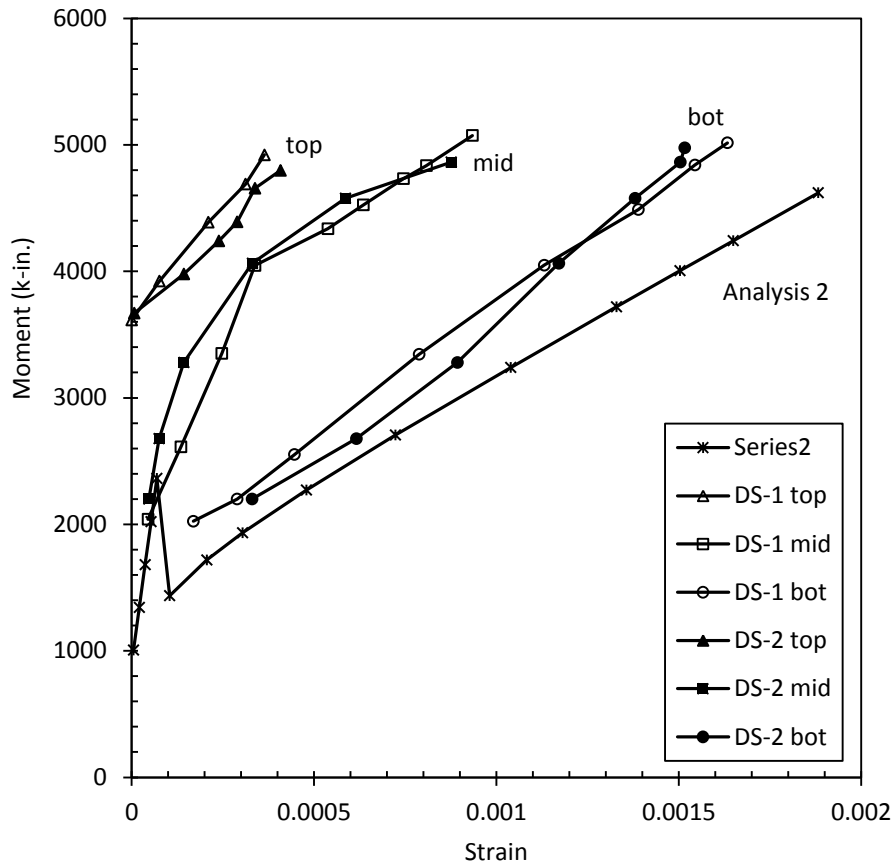
Figure 6-8. Relationship of moment at the base and extreme reinforcement tensile strain for shaft

6.3 The Strut-and-Tie model and shaft spiral design

The geometry of the transition region defines it as a "Disturbed Region" in which Engineering Beam Theory is not applicable. Other methods, such as the strut-and-tie method (STM), must be used to model the behavior of the column-shaft connection. Schlaich et al. (1991) proposed two models for a socket footing. One has smooth surfaces and the other has rough surfaces between the column and the walls of the socket (Figure 6-9).

79

For the geometry used in specimens DS-1 and DS-2, the model for the column-shaft connection with a smooth surface leads to a horizontal force T_2 of approximately150 kips when V = 50 kips, and an additional tensile force T_4 of approximately 100 kips at the bottom of the transition. To resist these forces, 55 turns of spiral of the size used in the tests would be needed at the top and 36 turns at the bottom of the transition, whereas Specimen DS-1 had a total of only 24 turns and Specimen DS-2 had 12. Thus, when the specimens reached their peak loads, the distribution of internal forces cannot have been the same as in the smooth surface model. However, at the very end of the Specimen DS-2 test, when contact between the column surface and shaft surface was lost and friction was no longer possible, the specimen is believed to have behaved like the smooth surface model. At that stage, the loads were much smaller, and the low capacity of the spiral was consistent with the low load.

In the tests on Specimen DS-1, no vertical slip at the interface was observed. The tie forces in the test were much smaller than those needed for the smooth model. Thus, the rough surface model for the column-shaft connection appears to be the one that is more consistent with the observed behavior. However, Schlaich's model is for a 2-dimensional system, so it was necessary to perform a 3-dimensional analysis for the circular column used in the tests. Figure 6-10 illustrates the model.

80
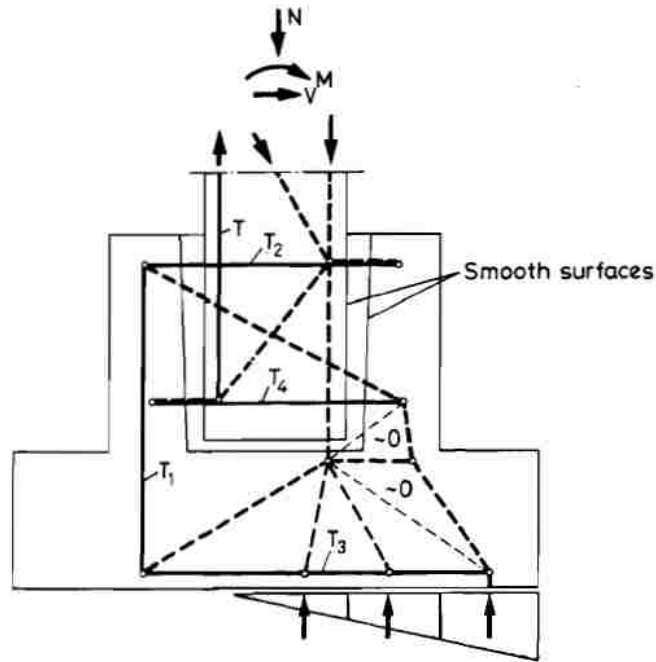
a)Model for a footing with smooth surfaces
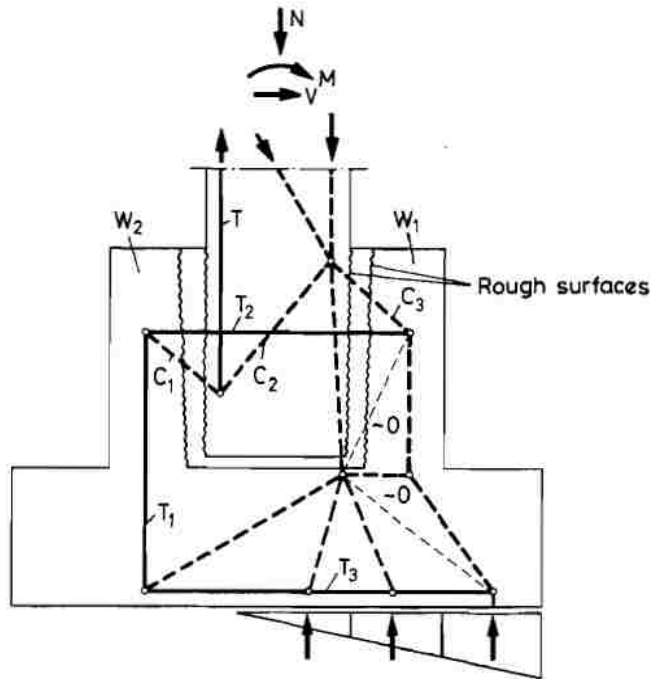
b)Model for a footing with rough surfaces

Figure 6-9. STM model proposed by Schlaich et al. (1991)
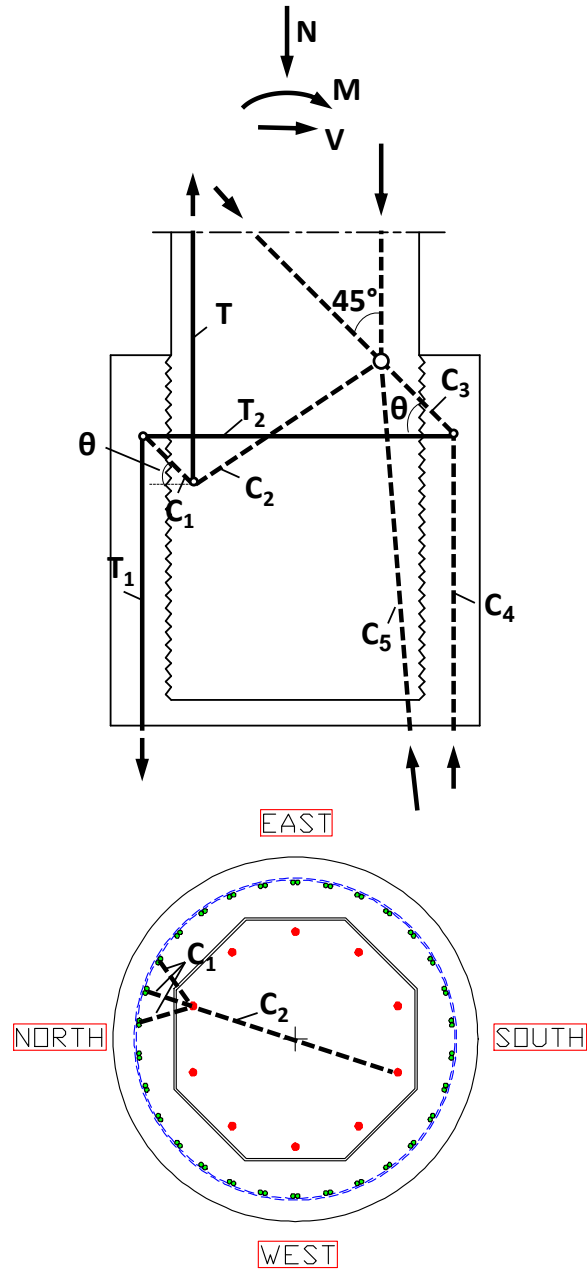
Figure 6-10. Elevation and Plan of STM model for load transmitting from one column reinforcing bar to the three nearest shaft bundles bars

The column contained ten #5 bars and the shaft contained thirty pairs of #3 bars. Thus, the tension force, T, in any column bar is assumed to transfer to the three nearest bar pairs of shaft reinforcement as indicated in Figure 6-10. The angle of inclination between struts C_1 and C_3 and the horizontal is taken to be θ. To simplify the analysis, the longitudinal reinforcement in the column and shaft was assumed to be distributed continuously round the perimeter, rather than as discrete bars,

and the struts C_1 directions are radial as shown in Figure 6-11. The horizontal component of the strut force C_1 is $T_1/\tan\theta$, and this is therefore the radial force per unit length applied to the shaft spiral. The distribution of tension T_1 in the shaft longitudinal bars is calculated by using moment-curvature analysis proposed above.
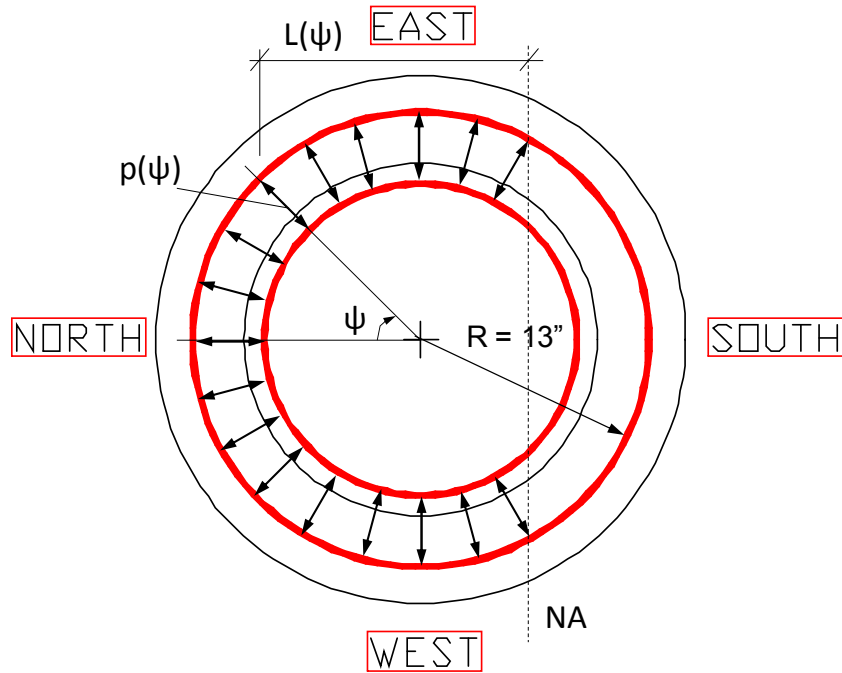
Figure 6-11. Tension transfer from column to shaft longitudinal reinforcement

As indicated in Figure 6-11, the distributed load p applied around the circumference of the shaft spiral is given by

$$p(\psi) = \frac{T_1(\psi)}{\tan\theta} \tag{6-13}$$

The distribution of tension in shaft reinforcement is obtained by

$$\begin{aligned}
T_1(\psi) &= \frac{A_{l,sh}}{2\pi R} f_s(\psi) \\
&= \frac{A_{l,sh}}{2\pi R} E_s \epsilon_s(\psi) \\
&= \frac{A_{l,sh}}{2\pi R} E_s \Phi L(\psi)
\end{aligned} \tag{6-14}$$

83

where,

$A_{l,sh}$ = total area of longitudinal shaft reinforcement (in.^{2})

f_s = tensile stress in shaft reinforcement (ksi)

ϵ_s = tensile strain in shaft reinforcement

$L(\psi)$ = distance from the neutral axis to the tension longitudinal reinforcement

E_s = modulus of elasticity of reinforcement (ksi)

R = radius of shaft spiral (in.)

Φ = curvature (1/in.)

ψ = angular coordinate (rad)

From the strain distribution in Figure 6-12, we have

$$L(\psi) = (d - c) - R(1 - \cos \psi)$$

where,

d = distance from the extreme compression fiber to the extreme tension longitudinal reinforcement

c = depth to the neutral axis

Substituting $L(\psi)$ in Eq. 6-14, we obtain

$$T_1(\psi) = \frac{A_{l,sh}}{2\pi R} E_s \Phi . [(d - c) - R(1 - \cos \psi)]$$

$$= \frac{A_{l,sh}}{2\pi} E_s \Phi . \left[\frac{(d - c)}{R} - (1 - \cos \psi) \right] \qquad (6\text{-}15)$$

Substituting $T_1(\psi)$ in Eq. (6-13), we obtain

$$p(\psi) = \frac{\Phi A_{l,sh} E_s}{2\pi \tan \theta} . \left[\frac{(d - c)}{R} - (1 - \cos \psi) \right] \qquad (6\text{-}16)$$

Summing North-South horizontal forces leads to

$$\sin(\alpha) . T_2(\alpha) = \int_0^\alpha R . p(\psi) . \cos \psi . d\psi \qquad (6\text{-}17)$$

Where α is an angular coordinate measured from the North.

84

Substituting Eq. (6-16) in Eq. (6-17), yields

$$\sin(\alpha) \, . \, T_2(\alpha) = \int_0^\alpha R \, . \, \frac{\Phi A_{l,sh} E_s}{2\pi \tan\theta} \, . \, \left[\frac{(d-c)}{R} - (1 - \cos\psi) \right] . \cos\psi \, . \, d\psi$$

$$= \frac{R\Phi A_{l,sh} E_s}{2\pi \tan\theta} \int_0^\alpha \left[\frac{(d-c) - R}{R} \cos\psi + \cos^2\psi \right] d\psi$$

$$= \frac{R\Phi A_{l,sh} E_s}{2\pi \tan\theta} \left[\frac{(d-c) - R}{R} \sin\alpha + \left(\frac{\sin 2\alpha}{4} + \frac{\alpha}{2} \right) \right]$$

Then

$$T_2(\alpha) = \frac{R\Phi A_{l,sh} E_s}{2\pi \tan\theta} \left[\frac{(d-c) - R}{R} + \left(\frac{\cos\alpha}{2} + \frac{\alpha}{2\sin\alpha} \right) \right] \tag{6-18}$$
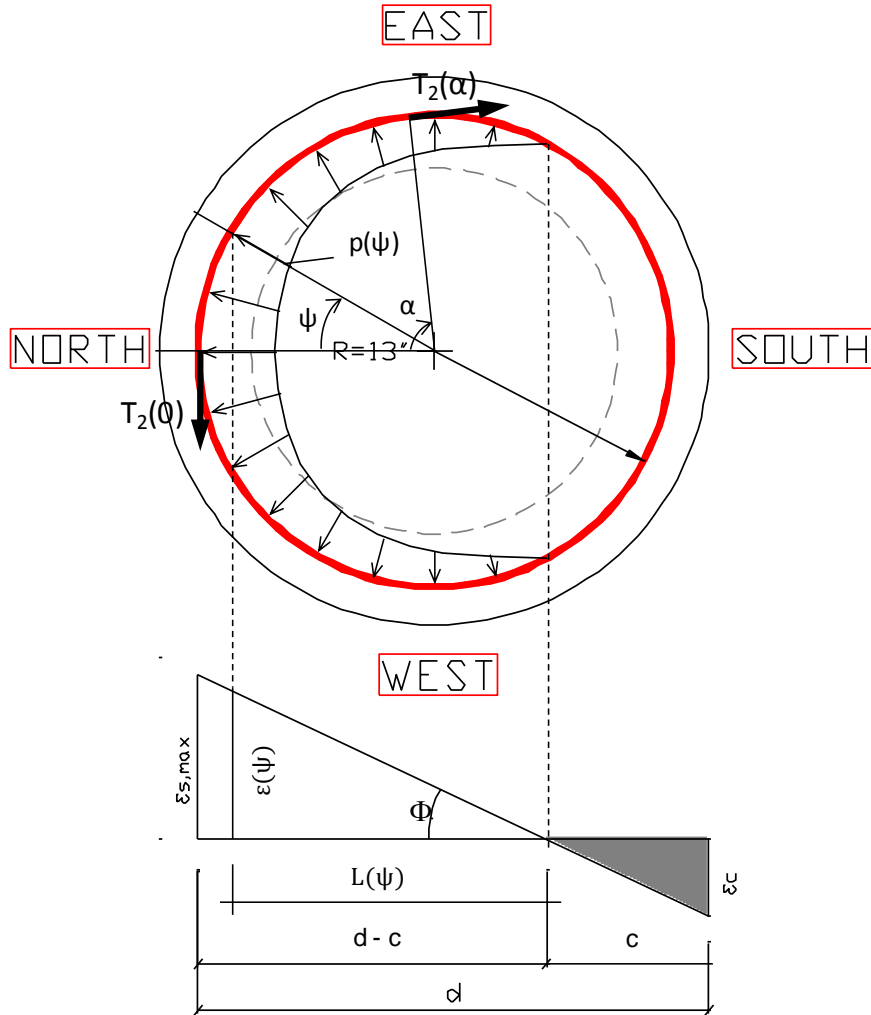
Figure 6-12. Distributed load applied to shaft spirals

85

www.manaraa.com

The parameters used in the tests were:

R = 13 in. $A_l = 30*0.22 = 6.6$ in.^{2} Es = 29000 ksi

d = 28 in.   c = 9 in.

If θ is assumed to be 45^0, and the curvature is taken when the predicted moment is equal to the peak measured moment ($\Phi = 106.11$ e-6 in.$^{-1}$), the distribution of the tensile force, T_2, in the shaft spirals is shown in Figure 6-13.
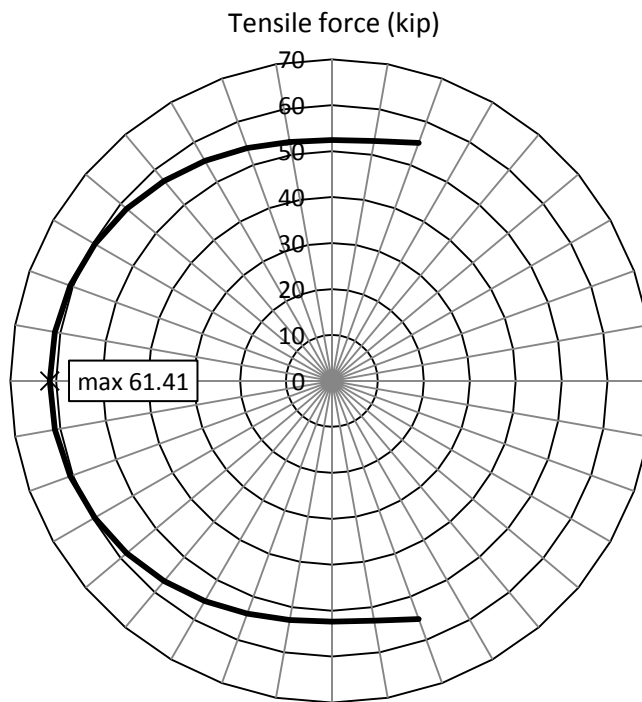
Figure 6-13. Tensile force distribution in tie T_2 in tension area

The maximum tensile force in the tie, T_2, occurs at $\alpha = 0.0$, and is

$$T_{2,max} = \frac{R\Phi A_{l,sh}E_s}{2\pi \tan\theta}\left[\frac{(d-c)-R}{R} + \left(\frac{1}{2}+\frac{1}{2}\right)\right]$$
$$= \frac{\Phi A_{l,sh}E_s}{2\pi \tan\theta}(d-c) \tag{6-19}$$

86

The relationship between the maximum spiral force, $T_{2,max}$, and the assumed strut inclination angle, θ, is shown in Figure 6-14. As might be expected, steeper strut angles lead to lower spiral forces.

The strut angle can be estimated by equating the spiral capacity and demand. The yield strength of a single spiral wire is

$$f_{yt}A_{tr} = 80 \times \left(\pi \times \frac{0.148^2}{4} \right) = 1.376 \ k/wire$$

If, in Specimen DS-1, all 24 turns of spiral were to be active in the load transfer, the total spiral capacity would be 24*1.376 = 33.0 kips, for which Figure 6-14 shows a corresponding strut angle of 62 degrees. However, the measured strains in Specimen DS-1 showed that only the spiral in the top of the transition region was stressed significantly. If only the spiral at the 15-in. upper transition (i.e. 16 turns) was active, the force would have been 22.0 kips and the angle, close to 70 degrees. The assumed 16 active spirals is probably too high, given the strain distribution in the spiral shown in Figure 5-24. However if less spiral is assumed to be active, the strut angle becomes steeper. This 70 degrees angle is sufficiently steep that it is improbable, both because the space for such a strut is not available and because it implies a low ratio of radial force to shear force being transferred across the column-to-shaft interface. The latter implies a friction coefficient significantly greater than 1.0.
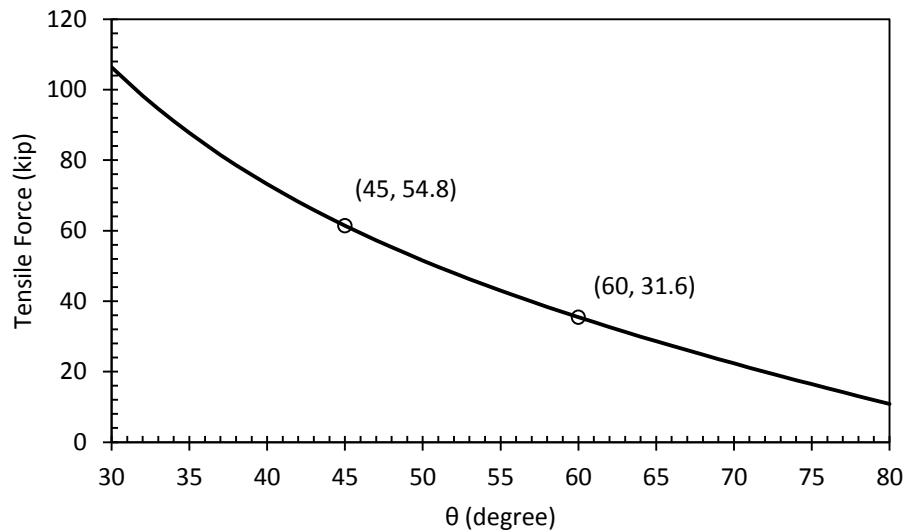
Figure 6-14. (T_2max vs. θ) relationship

In fact, the concrete may have provided some of the hoop tension force. If the concrete surrounding each spiral is taken into account, and the concrete width is taken as the thickness of the concrete annulus outside column, 5 in., the strength of the surrounding concrete per unit length is

$$f_r A_c = 0.63 \times (5 \times 1) = 3.15 \text{ kips/in.}$$

where,

$$f_r \quad = \quad \text{concrete modulus of rupture}$$

$$= \quad 7.5\sqrt{f_c'} = (7.5\sqrt{7000})/1000 = 0.63 \; ksi$$

If the strut angle is taken as $\theta = 45$ degrees, which implies a friction coefficient equal to 1.0, Figure 6-14 shows a maximum tensile force of 54.8 kips. At the upper transition, the strength of spirals is 22 kips as mentioned above. Thus, the necessary length of concrete is

$$l = \frac{54.8 - 22}{3.15} = 10.4 \; in.$$

The necessary length of concrete is smaller than the assumed length of upper transition (15 in.), so this assumption seems to be plausible. If the designers do not want to rely on the concrete tensile strength, they can increase the number of spiral 2.5 times to get the strength of 55 kips.

This suggests that the spiral was at yield stress (80 ksi, $\epsilon = 0.003$) while the concrete was still uncracked ($f_r = 630$ psi, $\epsilon = 0.630/5000 = 0.00012$). So, it is likely that the strength of spiral was active at the upper transition and concrete tensile strength was active at the lower stransition.

7   SUMMARY AND CONCLUSIONS

7.1   Summary

A new system is proposed for connecting drilled shafts to precast columns in bridge bents. It is adapted from the column-to-footing "socket" connection proposed for spread footing by Haraldsson et al. (2011), and consists of embedding a precast column into the cast-in-place transition region of the drilled shaft. The purpose is to facilitate rapid on-site construction through the use of pre-fabricated elements. The system is suitable for use in seismic regions.

Two drilled shaft specimens were fabricated and tested at the University of Washington. This section of the document summarizes the construction procedure, the design methodology, the test specimens and performance, and analytical models used to study the connection.

7.1.1   Construction sequence

The field construction sequence is as follow:

- A precast column is cast. The surface is roughened in the region where the column will be embedded in the cast-in-place drilled shaft.
- The hole for the shaft is bored, the reinforcing cage is placed, and the shaft is cast up to the bottom of the transition region (approximately ten feet below grade).
- The precast column is positioned, leveled and braced in the drilled shaft.
- The transition region (approximately the top ten feet of the shaft) is cast around the precast column.

7.1.2   Connection design

A shaft and column system prototype was designed according to the *AASHTO Load Resistant Factor Design 2009, AASHTO Guide Specifications for LRFD Seismic Design 2009, and WSDOT Bridge Design Manual (2012).* Reduced scale test specimens were then developed from the prototype

The prototype-precast column was designed to have a reinforcement ratio of approximately 1%. The transverse reinforcement in the column was defined by requirements for shear and confinement of the concrete core.

89

The column longitudinal reinforcement was equipped with anchor heads, instead of using the conventional detail of bending the longitudinal bars outwards into the foundation. This configuration has several benefits. It reduces the development length of the reinforcement and thus indirectly reduces the embedment length of the column in the shaft. It has better seismic performance, because the force transfer between the column and shaft is more direct. Lastly, this design makes fabrication, transportation, and erection safer and easier.

The surface of the column was roughened where it was to be embedded in the drilled shaft. The details of the roughening were the same as those used by the WSDOT BDM for roughening the ends of prestressed concrete girders. Load transfer at the interface was designed using AASHTO LRFD's shear-friction design procedure. In the embedded region, the column section was an octagon, circumscribed within the circular section of the main column. This was done to facilitate the forming of the roughened surface, which used wooden strips.

The embedment length of the column in the drilled shaft was defined by requirements for splicing the shaft and column bars. The splice is by definition a non-contact splice, for which the WSDOT BDM provides design requirements. The column bars were larger than the shaft bars (Pang et al. 2008), so they would normally control the splice length. However, the heads on the column bars improve their anchorage so that the shaft bars, which had no such heads, in fact controlled the splice length.

The shaft was designed as a capacity-protected element to ensure that the hinge would form in the column and not in the shaft. The scale of the system was chosen so that the ratio of shaft diameter/column diameter was as small as possible according to WSDOT BDM, so that test specimens represented the most critical conditions. That choice led to a prototype system of a 6 ft diameter column and a 9 ft diameter shaft, which were represented at 28% scale in the laboratory specimens by a 20-inch diameter column and a 30-inch diameter shaft.

The shaft spiral was designed according to WSDOT BDM requirements for non-contact lap splices in conventional cast-in-place drilled shafts. The spiral was terminated by three turns of spiral.

7.1.3 Test specimens

Two test specimens were built. The scale factor (1/3.6, or 28%) was chosen in order to match the 20-in. diameter of column specimens tested by previous researchers (e.g., Haraldsson et al. 2011, and Janes et al. 2011).

The only difference between specimens DS-1 and DS-2 was the amount of spiral in the column-to-shaft transition region, which was reduced by half in DS-2. The goal was to promote failure in the shaft transition region in Specimen DS-2, in order to develop an understanding of the load transfer mechanism there.

In both specimens, a cast-in-place base was built monolithically with the transition region in order to attach the specimen to the testing rig. The specimens were heavily instrumented.

7.1.4 Test performance

Quasi-static, cyclic lateral load tests were performed to evaluate the seismic performance of the two specimens.

In each test, the specimen was subjected to a constant, unfactored axial dead load value of 159 kips, accompanied by a cyclic displacement-controlled lateral excitation. The displacement history was a modification of a loading history for precast structural walls recommended in NEHRP.

The response and mode of failure of each specimen was the same as had been anticipated during design. Specimen DS-1 was controlled by column behavior. Failure occurred by plastic hinging in the column while the connection region in the shaft remained largely undamaged. Testing was stopped when almost all the column longitudinal reinforcement had fractured. By contrast, Specimen DS-2 was dominated by deformations of the shaft. The failure mode was prying action of the shaft in the transition region. Testing was stopped when all the spiral reinforcement in the shaft had broken.

91

7.1.5 Response Data

The measured data included loads and displacements, deflection and rotation of column and shaft, strain in the column and shaft longitudinal reinforcement, and strain in the shaft spiral. The measured data confirmed the observed responses and modes of failure.

7.1.6 Analytical model

The load transfer within the transition region was modeled using a three-dimensional strut and tie mechanism. This model is necessarily a simplification of the true behavior but it provides reasonable agreement with the experimental results and helps to identify the probable load paths.

7.2 Conclusions

From the results obtained in these tests, the following conclusions can be drawn for the behavior of the column-to-shaft connection.

(1) Provision in the precast system of the amount of spiral reinforcement required for conventional drilled shafts of the same dimensions protects the shaft and causes failure to occur by plastic hinging of the precast column, as desired. Because the test specimens had the smallest possible shaft/column diameter ratio, and the shortest possible embedment length, this conclusion will hold for all permissible shaft and column combinations.

(2) Use of half of the conventional amount of shaft spiral causes failure to occur in the shaft, by prying action of the concrete shell surrounding the precast column. Note that the test specimens contain no external confining steel shell. If one were used, it might provide some of the benefits of additional spiral, and force the failure back into the column.

(3) Mechanical anchor heads are needed at the ends of the column longitudinal reinforcement to ensure hinging in the column without anchorage failure, especially if the large bar system proposed by Pang et al. (2008) is used. The need for heads on the shaft bars is apparent from the strut and tie model, but was not clear from the test results.

(4) The spiral at the very top of the shaft is subjected to high tension during lateral loading. The strut and tie model shows that the spiral resists prying failure of the shaft, and that conclusion is supported by the high strains recorded in the spiral in Specimen DS-1 and the fractured spiral in Specimen DS-2. However, the spiral was in both cases distributed

92

uniformly up the transition region, with additional turns at the termination point at the top. Further testing is needed to determine whether a non-uniform distribution of the spiral, with the majority at the top, would provide better response.

(5)   The WSDOT requirements for non-contact lap splices do not provide satisfactory agreement with the experimental results.

(6)   Two questions are raised to obtain a consistent strut-and-tie model. One question is what is the value of inclined angle θ of struts which transfer tensile force from column reinforcement to shaft reinforcement. This value has a large effect on the amount of spirals required in the splice. A bigger value of θ leads to a smaller amount of spirals. However the size of these struts is limited by the small space between the column reinforcement and shaft reinforcement. Thus, a large θ is not plausible. The second question concerns the role, if any, that the tensile strength of shaft concrete plays in the confinement of the splices. It appears to have played an important role in the tests.

(7)   If the tension strength of the shaft concrete is excluded, the analytical model shows that the amount of spiral steel must be increased by a factor of 2.5.

7.3   Recommendations for Further Research

The study demonstrated the fundamental behavior of the column-to-shaft socket connection. However, further work is needed in the flowing areas:

(1)   Two more tests are recommended to determine the optimal distribution of the transverse reinforcement at the top of the shaft. One test specimen should be the same as Specimen DS-1 except that the shaft spiral should be anchored in such a way that additional spiral turns are not used. Welding is a possibility. The other test specimen should be designed with no distributed spiral in the shaft and a concentrated ring of spiral at the top of the shaft. If the first specimen fails in the shaft and the second one fails in the column, the top of the shaft will have been proven to be the optimal location for the spiral.

(2)   Experiments should be conducted to determine the need for mechanical anchorages or hooks on the top of the longitudinal shaft bars. The strut-and-tie model suggests the need for anchorage devices of some struts, but the test specimens performed well without them.

(3)   The WSDOT requirements for confinement of non-contact splices in drilled shafts should be re-examined. In particular, the k - factor of 0.5 should be evaluated critically

93

(4) The contribution of the tensile strength of concrete in the confinement of non-contact splices should be examined. One test specimen should be the same as Specimen DS-1 except that the transition concrete is separated in two parts. Two plastic pieces can be place in the North and South side to isolate two parts of transition concrete. So the confinement would be based on only spirals.

(5) Experiments should be conducted to determine the 3-dimensional force transfer mechanism between reinforcing bars in the splice. The bars should be heavily gauged. Based on the force transfer mechanism, a consistent value of inclination angle, θ, of the struts should be proposed for design.

ACKNOWLEDGEMENTS

A debt of gratitude is due to professors John F. Stanton and Marc O. Eberhard, for their inspiration, friendship and guidance. Thanks to Vietnamese Education Foundation (VEF) for giving me a great chance in my life. Thanks to my friends Todd Janes, Olafur Haraldsson, Bo-Shiuan Wang, Po-Chien Hsio, Patricia Clayton, and Tu Nguyen for making graduate school an enjoyable experience. Thanks to my family for always being so supportive and encouraging. Finally, thanks to my wife, Hang, for everything she has done for me, and I apologize for the many long nights and lost weekends.

REFERENCES

AASHTO (2009). "*LRFD Bridge Design Specifications*" 4th ed., American Association of State Highway and Transportation Officials, Washington, DC.

"*AASHTO Guide Specification for LRFD Seismic Bridge Design*" (2009). AASHTO, Washington DC.

ACI Committee 318 (2008). "*Building Code Requirements for Structural Concrete and Commentary.*" *ACI 318-08*, American Concrete Institute, Farming Hills, MI.

Berry, Mike P., and Eberhard, Marc O. (2004). "*PEER Structural Performance Database User's Manual.*" Pacific Earthquake Engineering Research Center Report 2004, <www.ce.washington.edu/~peeral>, University of California, Berkeley, CA.

Brown, W. (2008). "*Bar Buckling in Reinforced Concrete Bridge Columns.*" Master's Thesis, University of Washington, Seattle, WA.

Building Seismic Safety Council for the FEMA. (2004) "*NEHRP Recommended Provisions for Seismic Regulations and for New Buildings and Other Structures (FEMA 450) 2003 Ed.*," Washington D.C.

Caltrans (2006). "*Seismic Design Criteria Version 1.4*". Caltrans, Sacramento, CA.

Cohagen, L.S. Pang, J.B.K., Steuck, K.P., Eberhard, M.O. and Stanton, J.F. (2008), "*A Precast Concrete Bridge Bent Designed to Re-center after an Earthquake,*" Washington State Department of Transportation Report, WA-RD 684.3, Olympia, Washington, October, 184 pp.

FHWA (2006). "*2006 Condition and Performance Report.*" U.S. Department of Transportation, Federal Highway Administration.

Getty Center Tram Guideway. http://www.cement.org/transit/tr_cs_gettycenter.asp

Haraldsson, O. (2011). "*Spread Footing Socket Connections for Precast Columns.*" Master's Thesis, University of Washington, Seattle, WA.

Hieber, D.G., Wacker, J.M., Eberhard, M.O. and Stanton, J.F. (2005), "*Precast Concrete Pier Systems for Rapid Construction of Bridges in Seismic Regions*," Washington State Department of Transportation Report WA-RD 611.1, Olympia, Washington, March, 312 pp.

Hieber, D.G., Wacker, J.M., Eberhard, M.O. and Stanton, J.F. (2005), "*State-of-the-Art Report on Precast Concrete Systems for Rapid Construction of Bridges*," Washington State Department of Transportation Report WA-RD 594.1, Olympia, Washington, March, 112 pp.

Janes, T. (2011). "*Precast Column Socket Connections for Thin Spread Footings*." Master's Thesis, University of Washington, Seattle, WA.

Kent, D.C., and R. Park (1971). *"Flexural Members with Confined Concrete,"* Journal of the Structural Division, ASCE, Vol. 97, No. 7, July, pp. 1969-1990.

Mander, J.B., M.J.N. Priestley, and R. Park (1988). *"Theoretical Stress-Strain Model for Confined Concrete,"* Journal of the Structural Division, ASCE, Vol. 114, No. 8, August, pp. 1804-1826.

Marsh, L. (2009). Personal communication with J. Stanton.

Matsumoto, E., Waggoner, M., Sumen, G., Kreger, M., Wood, S., and Breen, J. (2001). *"Development of a Precast Bent Cap System,"* Center for Transportation Research, Research Project 0-1748, University of Texas at Austin.

McLean, D.I. and Smith C.L. (1997), "*Noncontact Lab Splices in Bridge Column-Shaft Connections*," Washington State Department of Transportation Report WA-RD 417.1, Olympia, Washington, July.

Moustafa, S., (1989). "*Ductile Pullout Connections*". Concrete Technology Associates, CTA Bulletin 74B11. Now available from the Precast and Prestressed Concrete Institute, Chicago, IL.

Nakaki, S.D., Stanton, J.F., Sritharan, S. (1999). "*Overview of the PRESSS Five Story Precast Test Building*," *PCI Jo.*, 44(2), March-April 1999, pp 26-39.

Osanai, Y., Watanabe, F. and Okamoto, S., (1996). "*Stress Transfer Mechanism of Socket Base Connections with Precast Concrete Columns*". ACI Structural Journal, ACI, Chicago. IL. May-June, pp. 266-276.

Pang, B.K., Eberhard, M.O., and Stanton, J.F. (2010), "*Large-Bar Connection for Precast Bridge Bents in Seismic Regions*," Journal of Bridge Engineering, ASCE, May-June, pp 231-239.

Pang, J.B.K., Steuck, K.P., Cohagen, L.S., Eberhard, M.O. and Stanton, J.F. (2008), "*Rapidly Constructible Large-Bar Precast Bridge-Bent Connection*," Washington State Department of Transportation Draft Report, WA-RD 684.2, Olympia, Washington, October, 184 pp.

Precast/Prestressed Concrete Institute (2004). "*PCI Design Handbook*". 6th ed. Chicago, IL.

Priestley, M. J. N., Seible, F. and Calvi, G. M. (1996), " *Seismic Design and Retrofit of Bridges*," John Wiley & Sons, Inc., Hoboken, NJ, USA.

Raynor, D.J., Lehman, D.L. and Stanton, J.F. (2002). "*Bond-Slip Response of Reinforcing Bars Grouted in Ducts*". *ACI Str. Jo.* 99(5), Sept. pp 568-576.

Schlaich, J., Schäfer, K., and Jennewein, M. (1987). "*Toward a Consistent Design of Structural Concrete*". *PCI Journal,* V. 32, No. 3, May-June, pp. 74-150.

Schlaich, J. and Schäfer, K., "*Design and Detailing of Structural Concrete Using Strut-and-Tie Models,*" The Structural Engineer, Vol. 69, No. 6, March 1991, pp. 113-125.

Stanton, J.F. (2010), Moment-curvature program, University of Washington, Seattle, WA.

Steuck, K.P., Pang, J.B.K., Eberhard, M.O. and Stanton, J.F. (2008), "*Anchorage of Large-Diameter Reinforcing Bars Grouted into Ducts*," Washington State Department of Transportation Report, WA-RD 684.1, Olympia, Washington, July, 148 pp.

Steuck, K., Stanton, J.F. and Eberhard, M.O. (2009) "*Anchorage of Large-Diameter Reinforcing Bars in Ducts*," *ACI Str. Jo.,* July-August, pp 506-513.

Wacker, J.M, Hieber, D.G., Eberhard, M.O. and Stanton, J.F. (2005), "*Design of Precast Concrete Piers for Rapid Construction in Seismic Regions*," Washington State Department of Transportation Report, WA-RD 629., Olympia, Washington.

Xiao, Y., Priestley, M.J.N., and Seible, F. (1996). "*Seismic Assessment and Retrofit of Bridge Column Footings*". *ACI Str. Jo.,* ACI, Farmington Hills, MI. Jan-Feb., pp. 79-94.
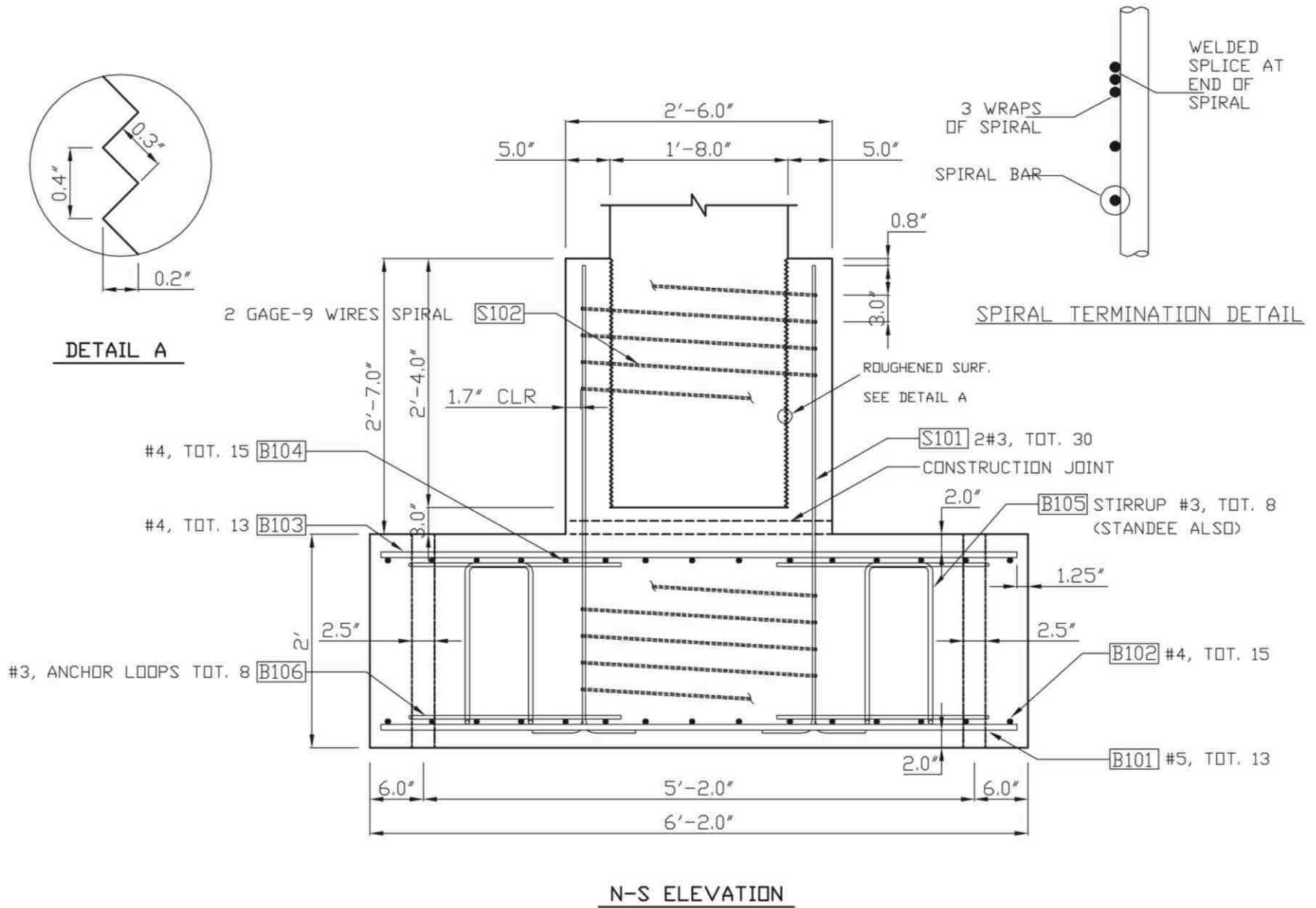
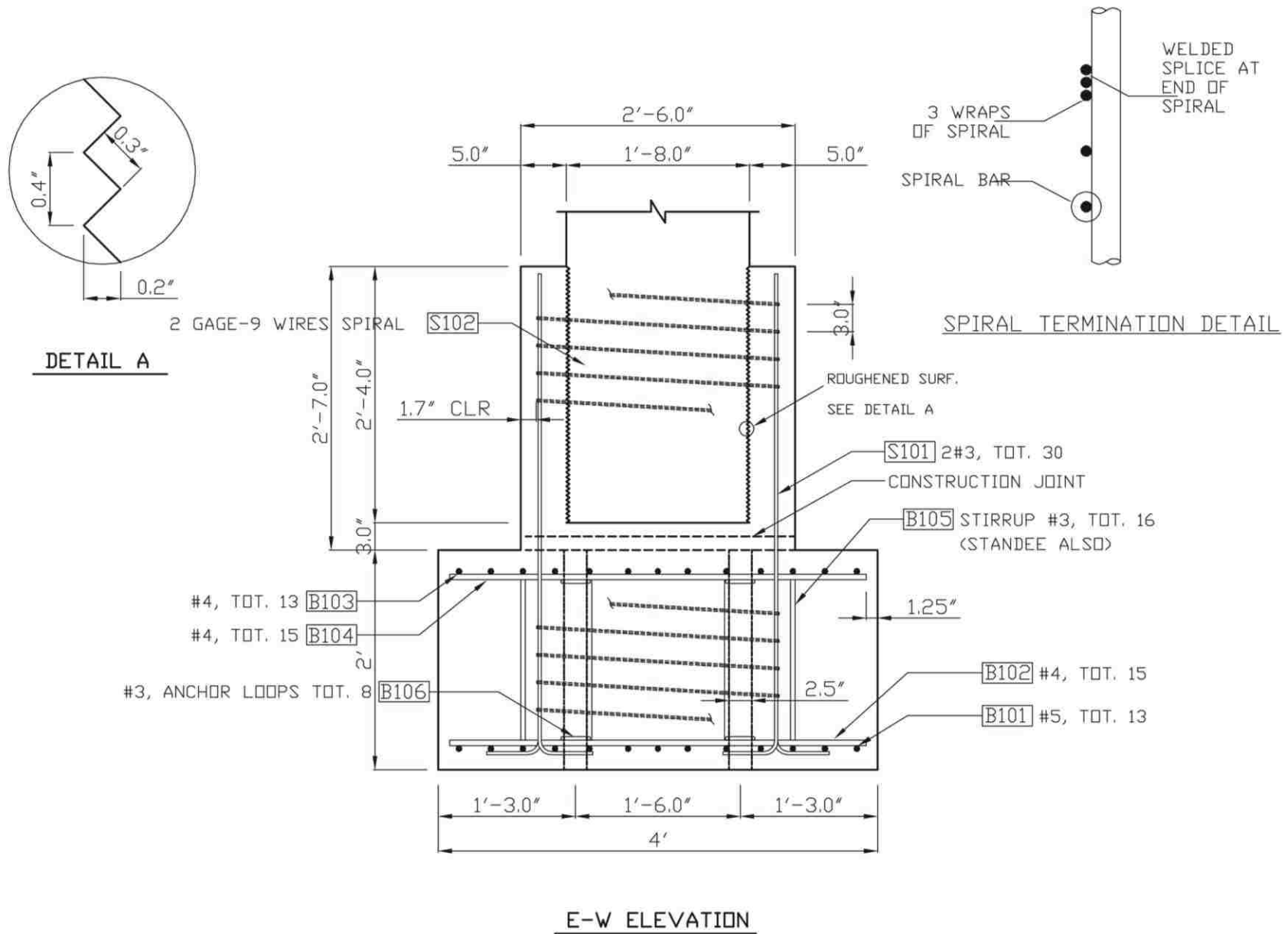# APPENDIX A: SPECIMEN CONSTRUCTION DRAWINGS

Figure A-0-1.Column Elevation

Figure A-0-2.Column Sections

101

Figure A-0-3.Shaft & Base – Longitudinal Section

102

www.manaraa.com

Figure A-0-4.Shaft & Base – Transverse Section

103
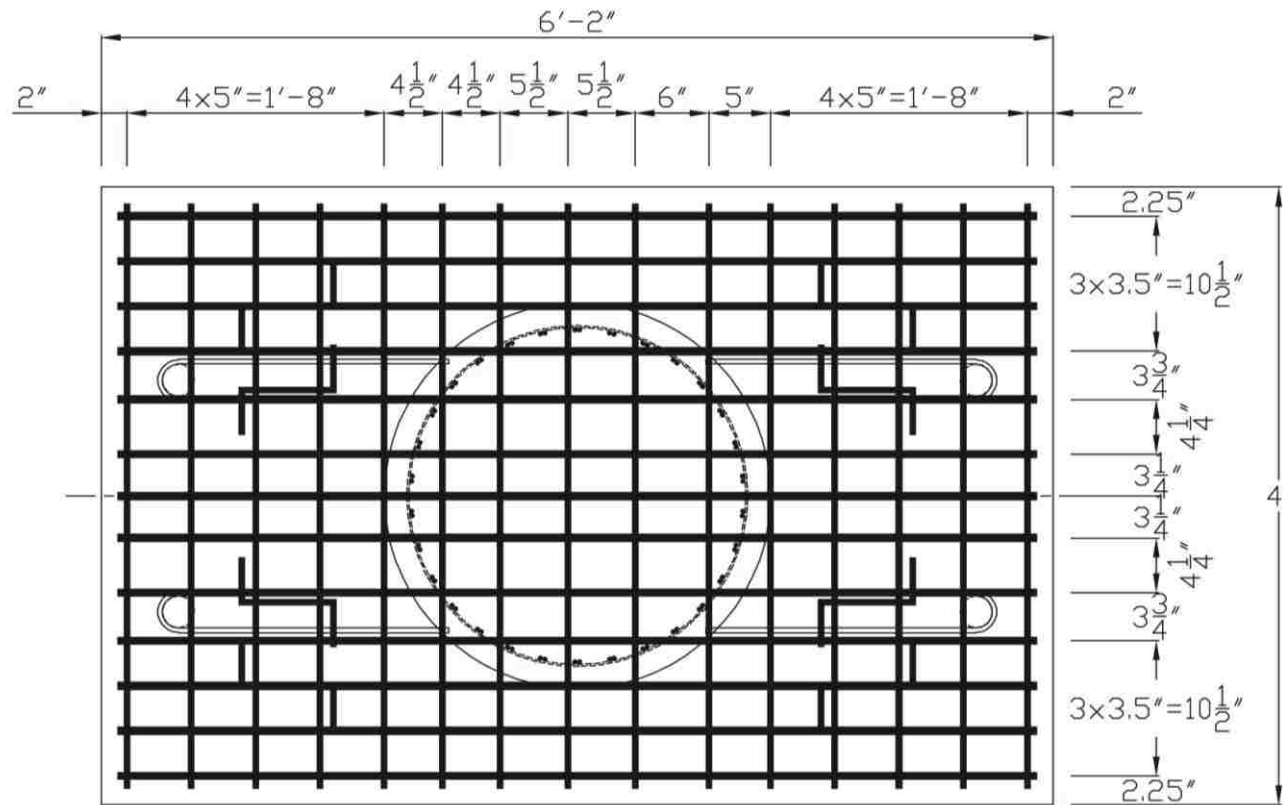
Figure A-0-5.Shaft & Base Reinforcement Arrangement

104

APPENDIX B: MATERIAL TESTS

B.1 Concrete Strengths

Both specimen DS-1 and DS-2 used the common concrete mix with code 09468 provided by Calportland Company. The concrete design strength was 6000 psi. It used 3/8-in aggregate pea gravel and had a specified slump of 5-in.

The concrete compressive strength at 7, 14, 28 day are provided in the following table.

Table B-0-1. Concrete strengths for Specimen DS-1 and DS-2

Time	7 Day (psi)	14 Day (psi)	28 Day (psi)	Day of Test (psi)
DS1 Column	5130	5820	6250	7770
DS1 Shaft	5320	6350	6600	7360
DS2 Column	4780	6350	6600	7170
DS2 Shaft	5270	5790	6400	6450

B. 2 Reinforcement

Reinforcement used in the footing and column conformed to ASTM Standard 706. The column spiral used the 3-gauge wire (0.244-in dia.), which was the same as that used by Haraldsson et al. (2011) and Janes et al. (2011). The shaft spiral used the 9-gauge wire (0.148-in dia.). All spirals conformed to ASTM Standard A82.

The tension tests were performed using MTS system machine and the elongation was measured by an extensometer. The tension specimen was loaded slowly until the load reached its maximum and started reducing. The extensometer was then removed to prevent damage to the equipment. The specimen was then loaded until failure, after which the length was measured to obtain a strain at failure.
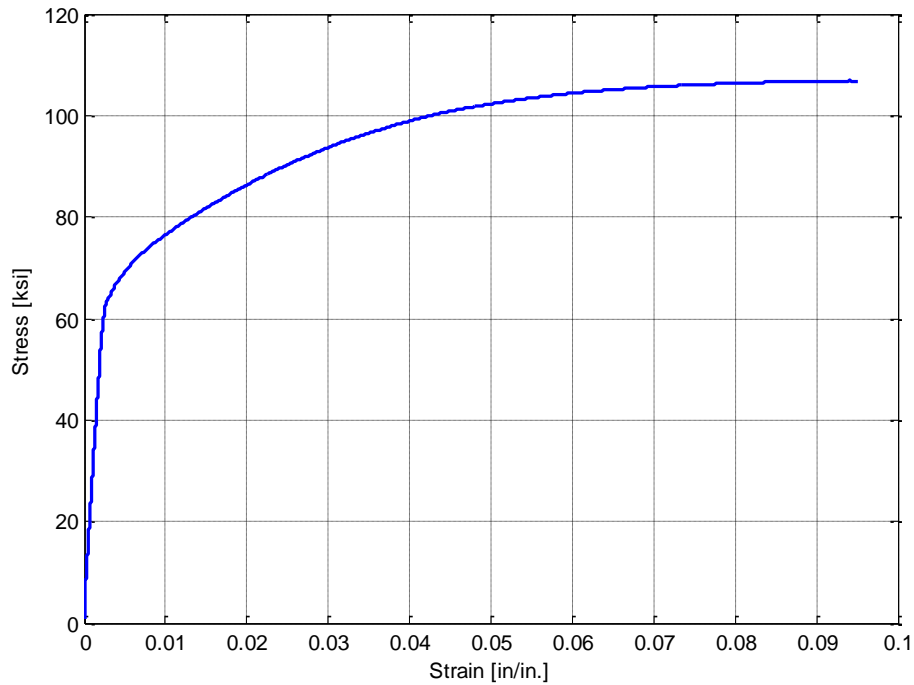
Results of the tension tests for bars #3 and #5 are shown in Figure B-0-1 and Figure B-0-2. Because the spirals were too small and extensometer cannot be used to measure the elongation, only the ultimate stress of spirals were found.

Table B-0-2. Tensile strength of spiral

9-gauge wire (psi)	3-gauge wire (psi)
109,860	95,050

106
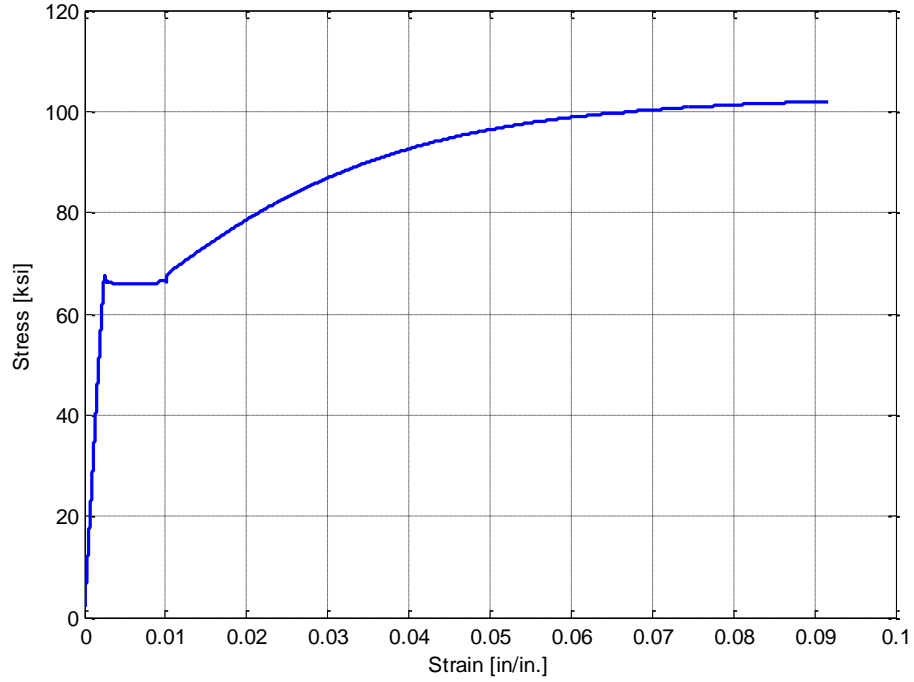
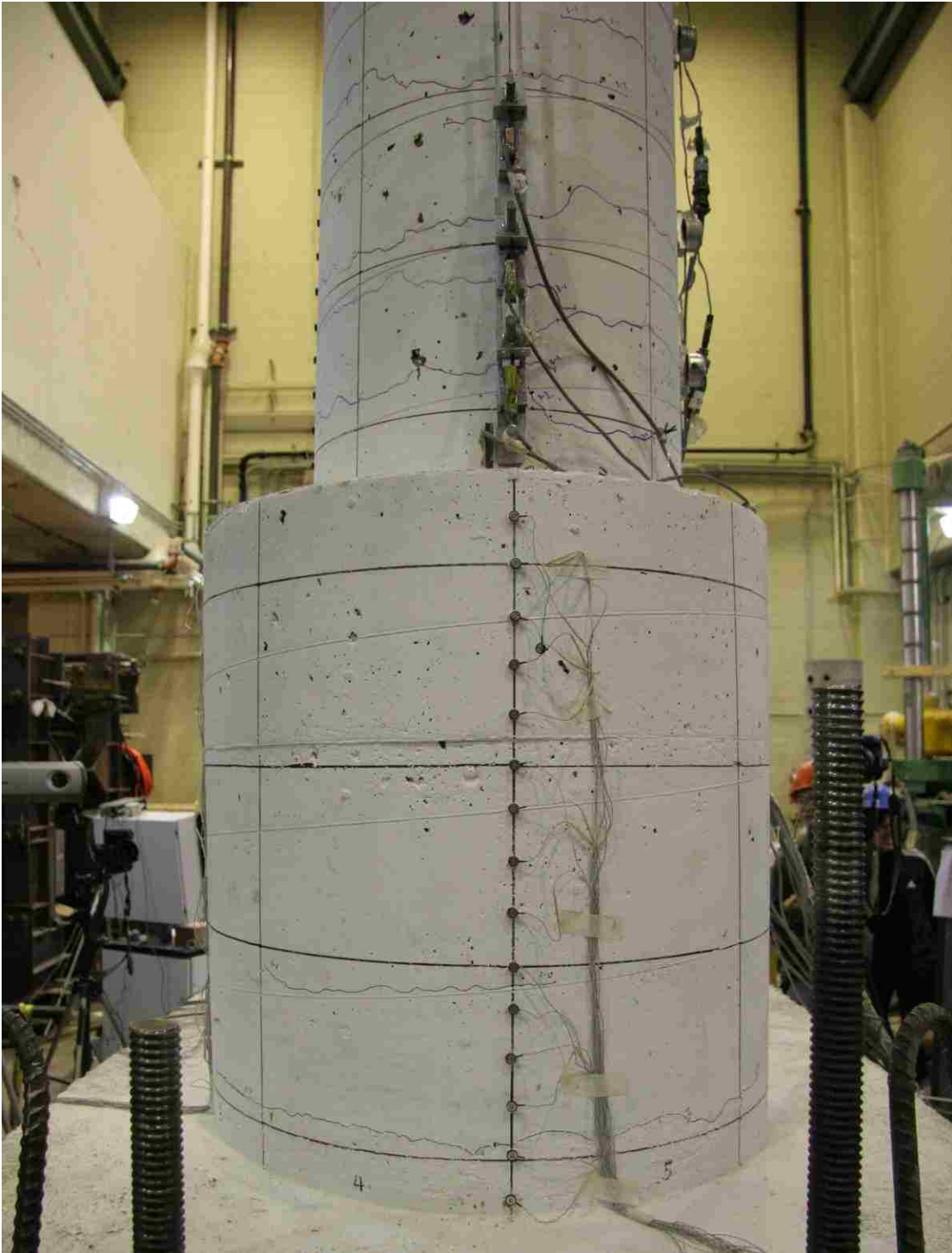**Figure B-0-1.Stress-strain curve for No. 3 bar**

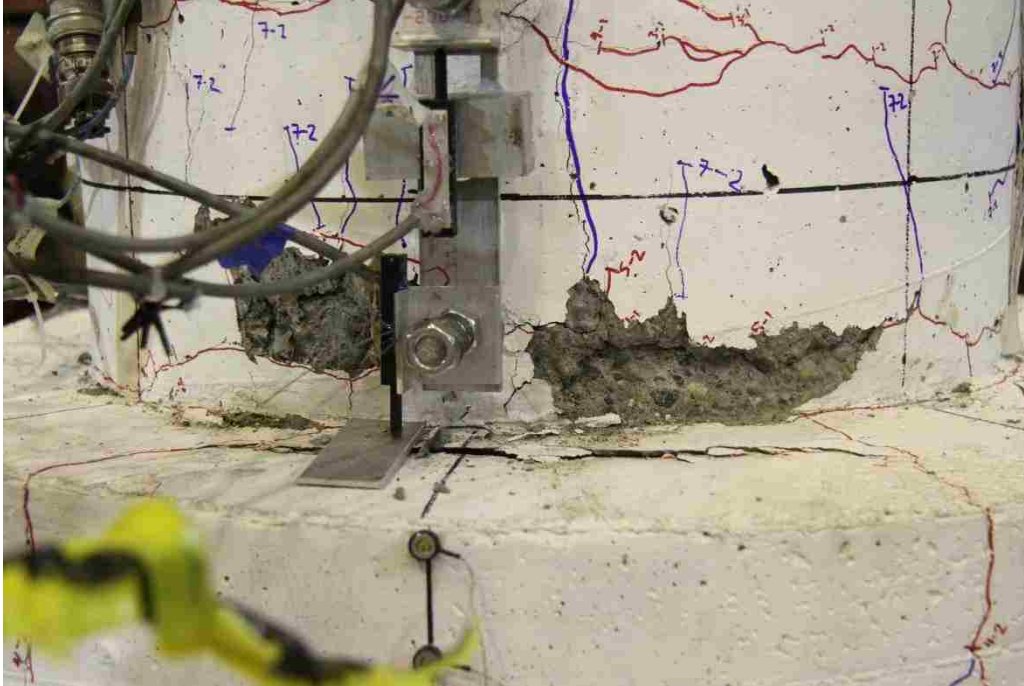**Figure B-0-2.Stress-strain curve for No. 5 bar**
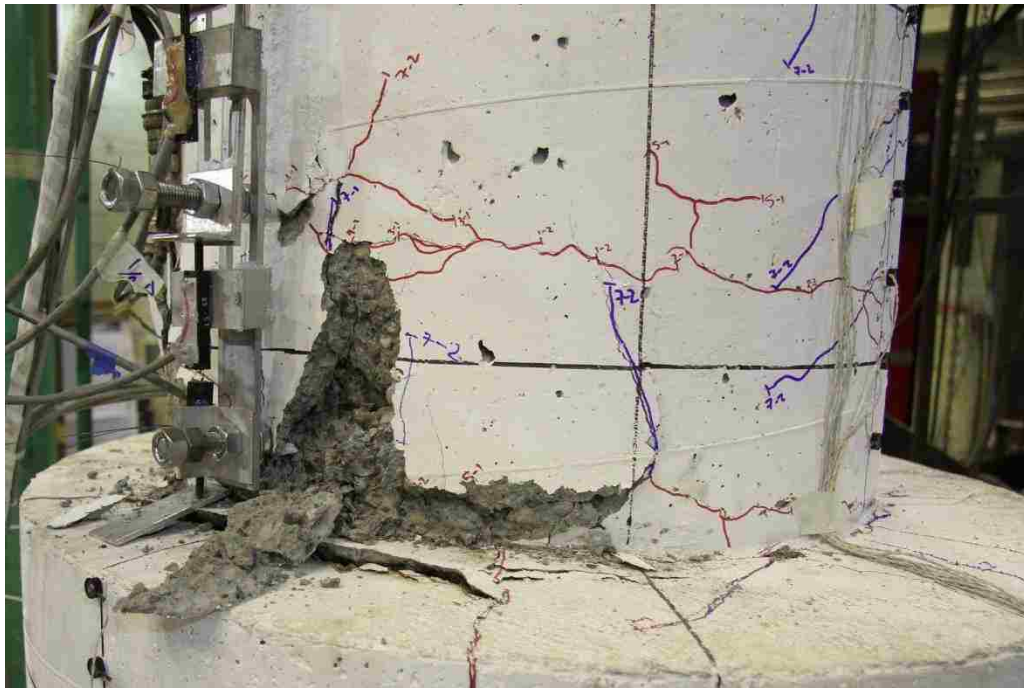
107

APPENDIX C: DAMAGE PROGESSION

C.1 Specimen DS-1

**Figure C-0-1. DS-1 – Significant horizontal crack in Cycle 4-1
(0.56/-0.75 percent drift)**

Figure C-0-2. DS-1 – First significant spalling occurred in the column in Cycle 7-2 (3.00/-3.14 percent drift)

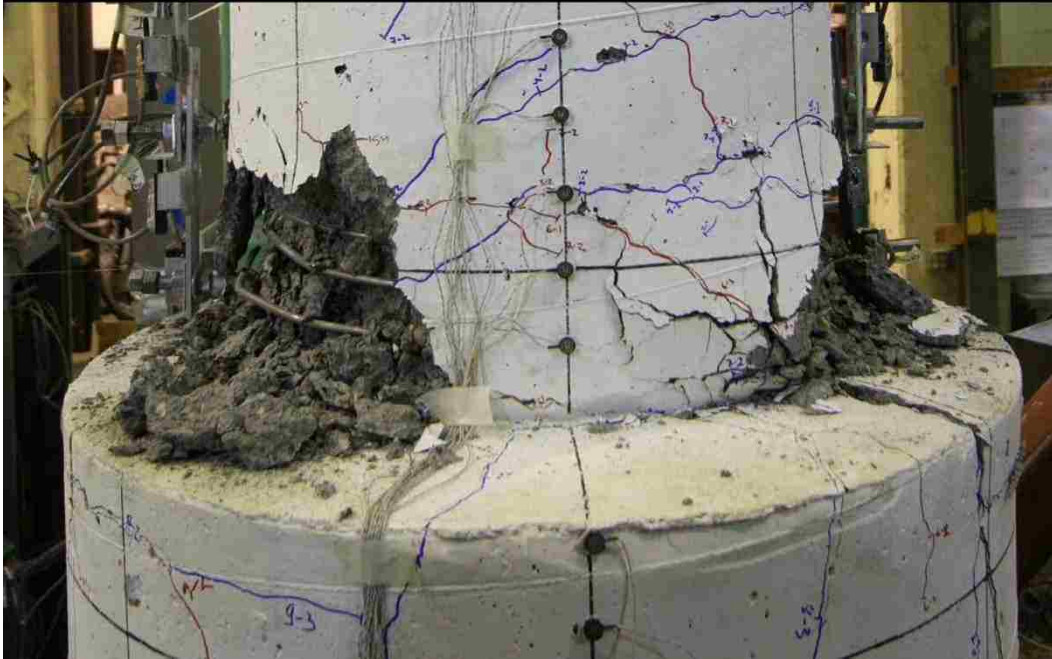**Figure C-0-3. DS-1 – Plastic hinge formed in the column in Cycle 8-3 (4.60/-4.68 percent drift)**

**Figure C-0-4. DS-1 – First noticeable bar buckling in the column in Cycle 9-3
(6.90/-6.81 percent drift)**

**Figure C-0-5. DS-1 – First column spiral fractured in Cycle 10-1
(8.43/-8.27 percent drift)**

111

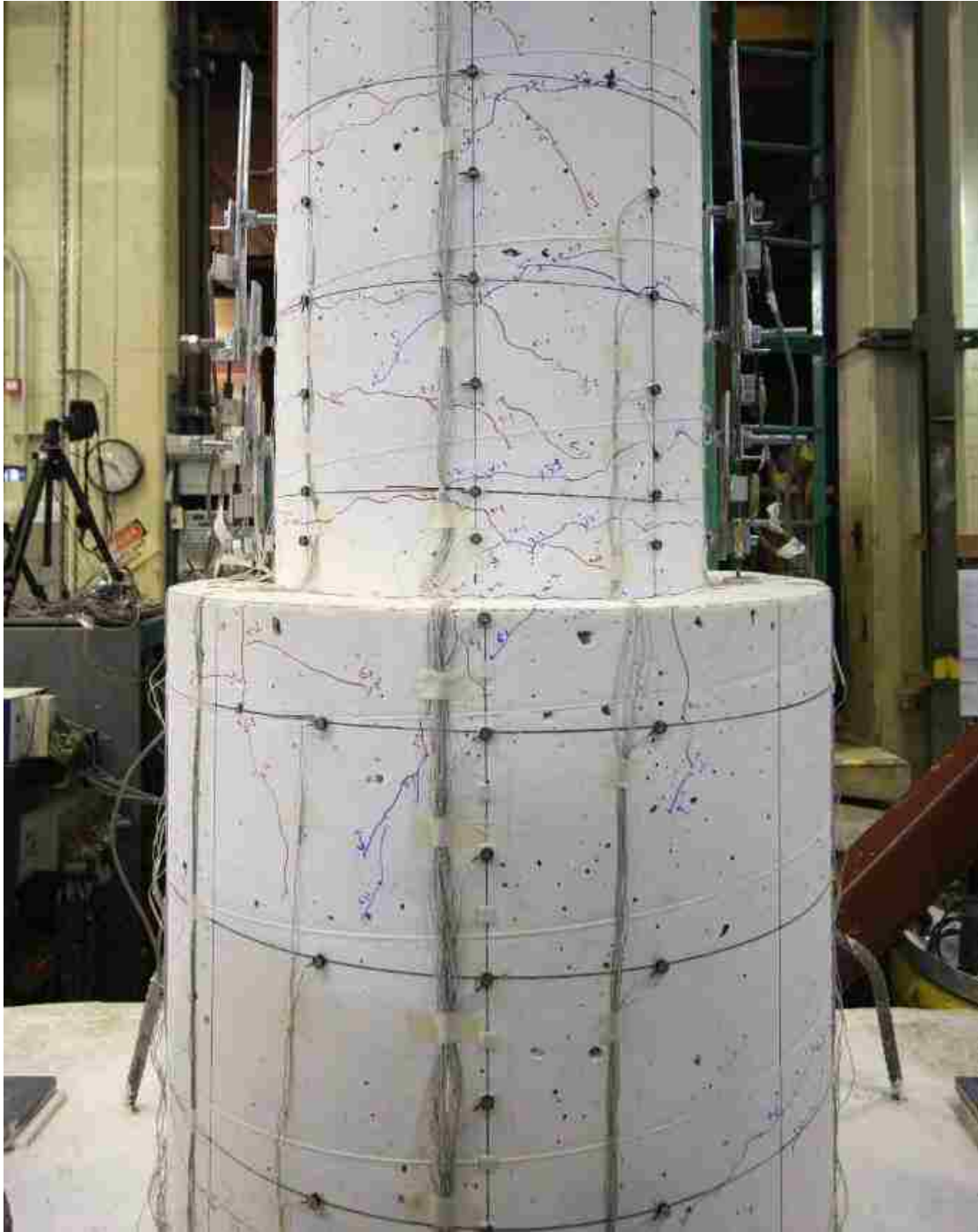**Figure C-0-6. DS-1 – Column damage after cyclic testing**
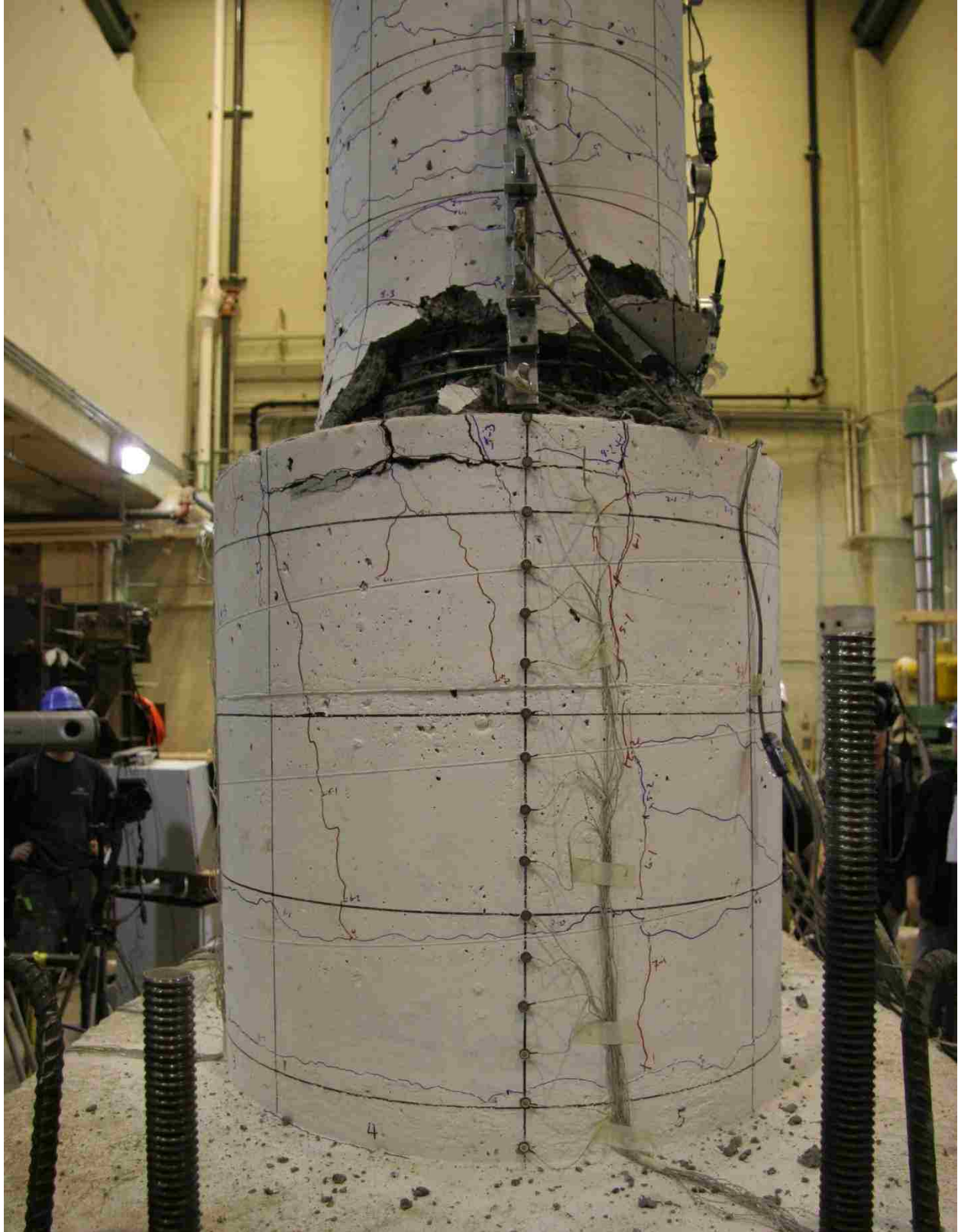
Figure C-0-7. DS-1 – Shaft damage after cyclic testing
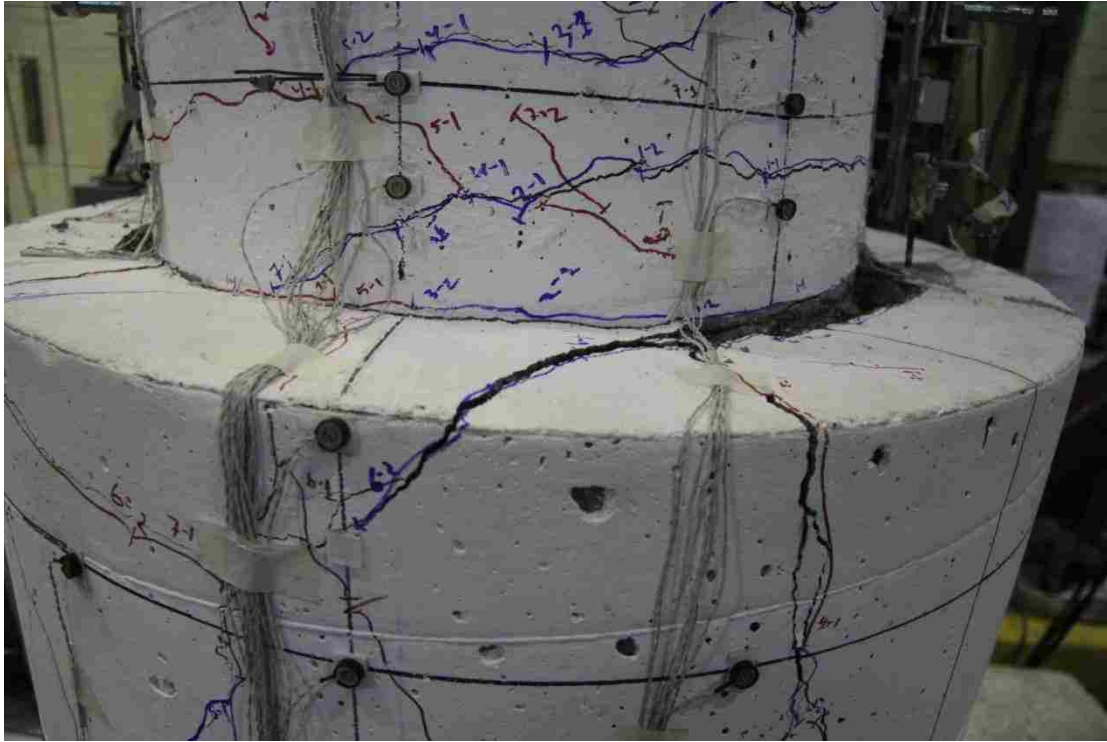
C.2 Specimen DS-2
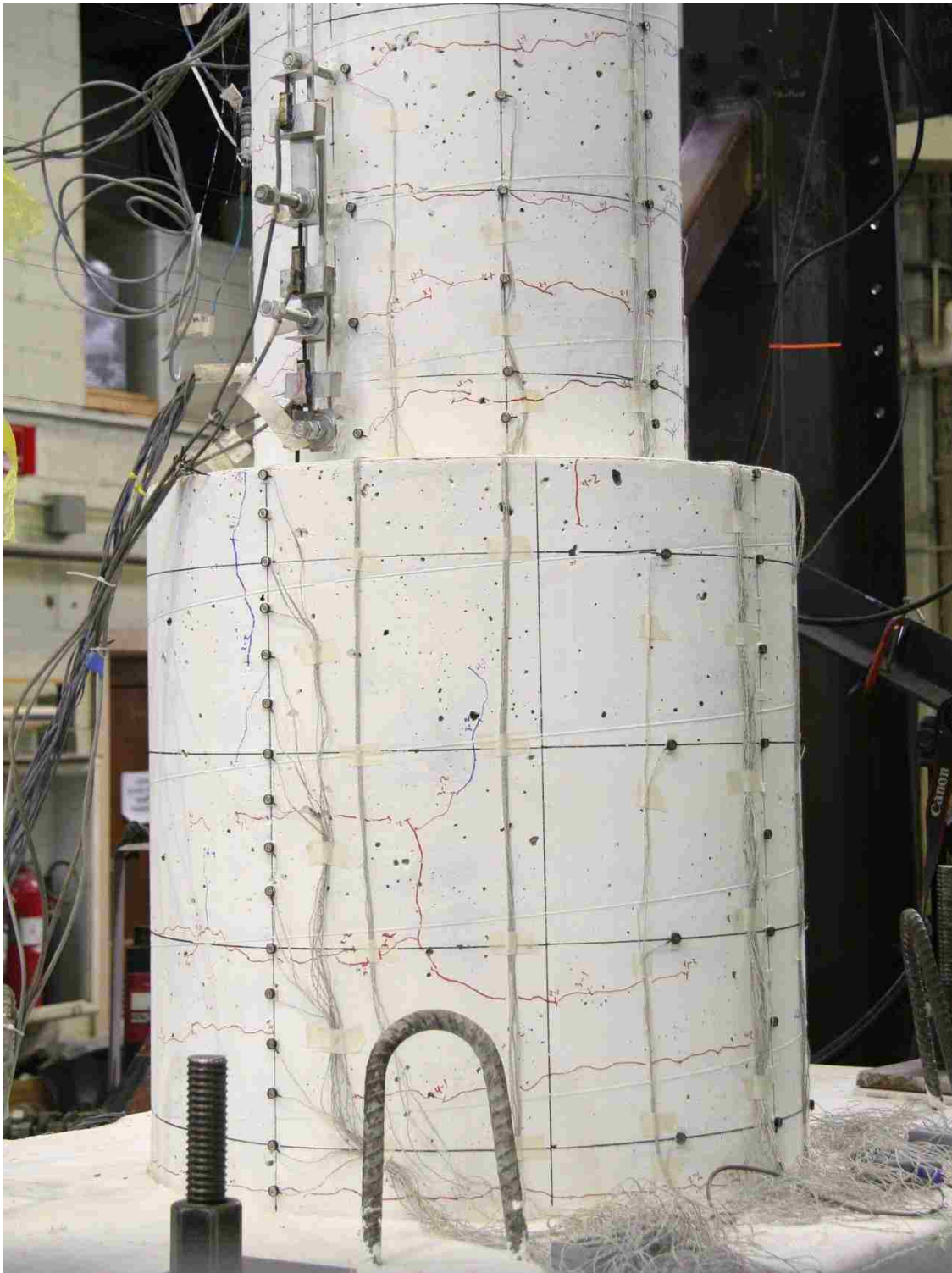
**Figure C-0-8. DS-2 – Significant horizontal crack in Cycle 4-2
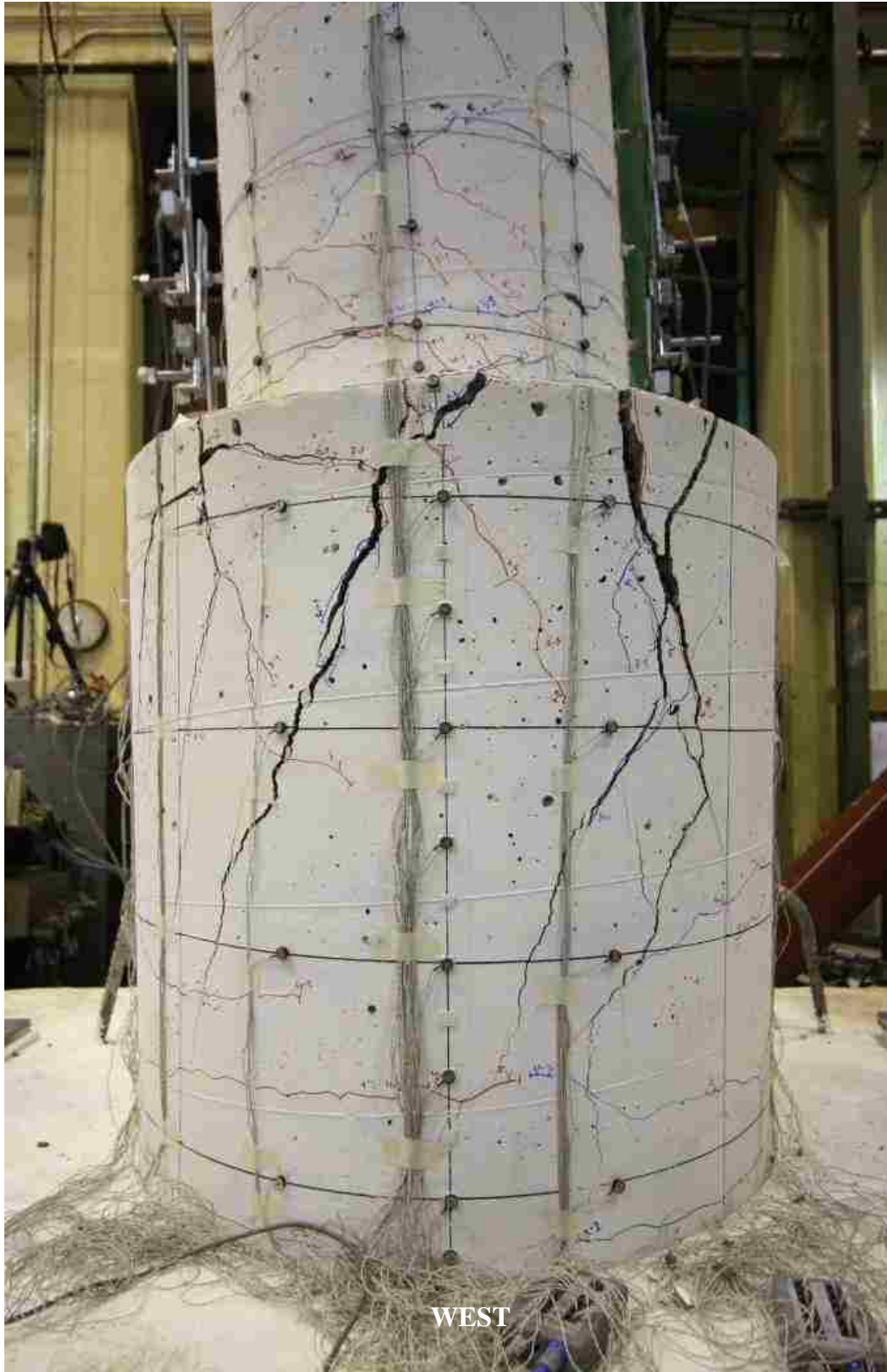(0.73/-0.87 percent drift)**

**Figure C-0-9. DS-2 – First diagonal crack in the shaft in Cycle 6-2
(1.87/-2.02 percent drift)**

Figure C-0-10. DS-2 – Shaft damage when first shaft spiral fractured in Cycle 8-2 (4.59/-4.59 percent drift)

Figure C-0-11. DS-2 – First noticeable prying action in shaft in Cycle 9-2 (6.72/-6.83 percent drift)
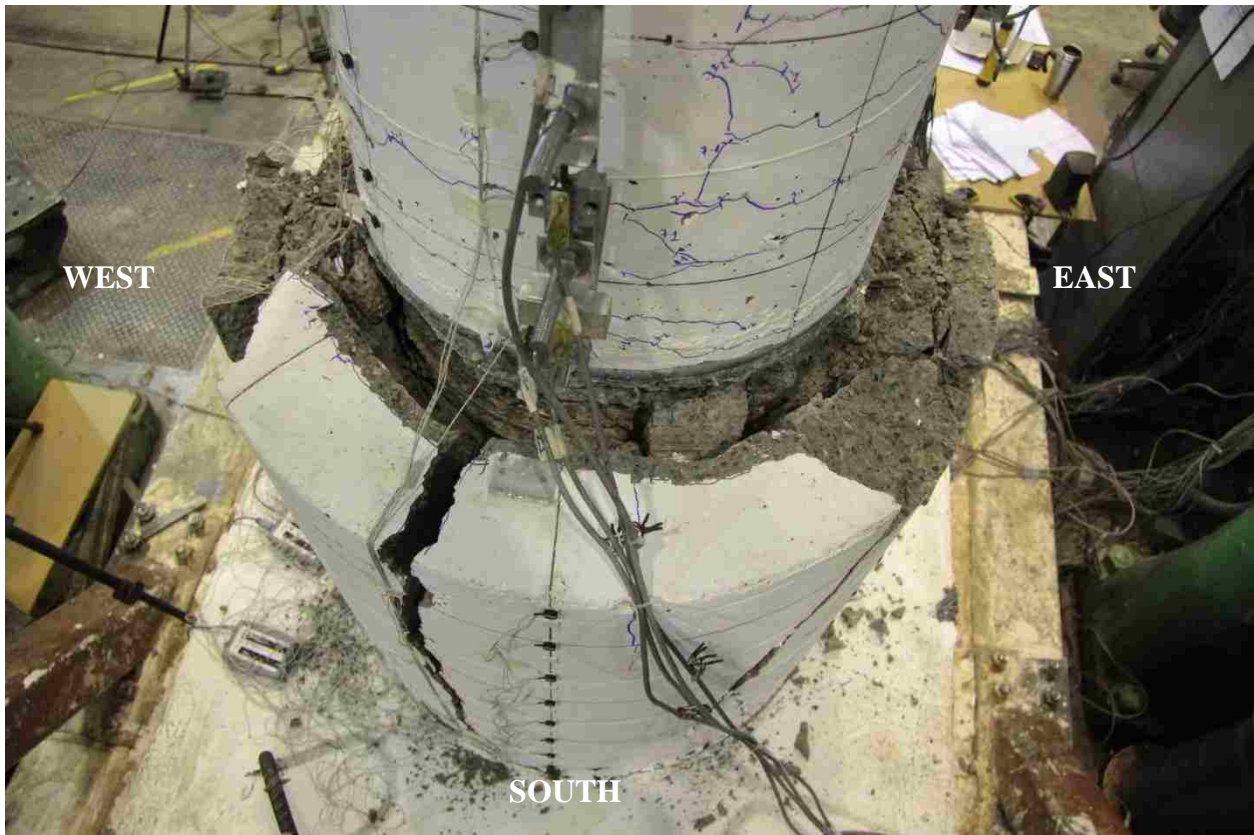
117

Figure C-0-12. DS-2 – Shaft damage after cyclic testing

Figure C-0-13. DS-2 – Column damage after cyclic testing